# A Study on Molecular Mechanisms underlying Force Generation in Neuronal Growth Cones using Optical Tweezers

Thesis submitted for the degree of
"*Doctor Philosophiæ*"

SISSA
Neurobiology Sector
October 2012

CANDIDATE
Ladan Amin

SUPERVISOR
Prof. Vincent Torre

SISSA, Via Bonomea 265, TRIESTE, ITALY

*To my parents and Houman*

# DECLARATION

The work described in this thesis was carried out at the International School for Advanced Studies, Trieste, between September 2008 and October 2012, under the supervision of Professor Vincent Torre.

This thesis led to following published and unpublished articles:

1. R. Shahapure, F. Difato, A. Laio, G. Bisson, E. Ercolini, L. Amin, E. Ferrari, V. Torre, "Force generation in lamellipodia is a probabilistic process with fast growth and retraction events" Biophysical journal 98 (6), 979-988 (2010)

2. L. Amin*****, E. Ercolini*****, R. Shahapure*****, G. Bisson, V. Torre, "The elementary events underlying force generation in neuronal lamellipodia" Sci. Rep. 1, 153; DIO:10.1038/srep00153 (2011)
(***** Equally contributed)

3. L. Amin, E. Ercolini, R. Shahapure, E. Migliorini, V. Torre, "Multiple role of membrane stiffness and actin turnover on the force exerted by DRG lamellipodia" Biophysical journal, (2012) DIO: 10.1016/j.bpj.2012.04.036

4. L. Amin, W. Sayyad, E. Ercolini, J. Ban, P. Fabris, A. Valbuena & V. Torre "Multiple role of myosin II in force generation in DRG growth cones" (in preparation)

5. L. Amin, E. Ercolini, J. Ban, and V. Torre "Comparison of the force exerted by hippocampal and DRG growth cones" (in preparation)

# CONTENTS

# ABSTRACT

Understanding the dynamical and molecular properties of force generation in neuronal growth cones is fundamental in elucidating how neurons sense the environment and process mechanical information. In this study and in order to address this issue, I used optical tweezers to measure the force exerted by filopodia and lamellipodia of Dorsal Root Ganglia (DRG) and hippocampal neurons. I have investigated in detail the roles of several important players in force generation such as actin turnover, membrane stiffness and myosin II. Therefore, my PhD thesis provides precise characterization of the molecular mechanism underlying force generation in growth cones.

In the first chapter of my result dynamical properties of force generation in neuronal lamellipodia are presented. Force-velocity (Fv) relationship has been measured with millisecond (ms) temporal resolution and picoNewton (pN) sensitivity. My results show that force generation is a probabilistic process and the fast growth of lamellipodia leading edge alternates with local retractions.

The results of the second part of this study show that force generation in neuronal lamellipodia of DRG neurons is composed of elementary events corresponding to forward and backward jumps of bead displacement. These jumps have an amplitude ranging from 2 to 20 nm suggesting that force generation occurs at different rates. A detailed statistical analysis of these jumps and their importance in characterizing the force generation are discussed.

In order to understand the role of actin turnover and membrane stiffness on force generation, I analyzed the effect of jasplakinolide and cyclodextrin on force exerted by neuronal growth cones. I found that 25 nM of jasplakinolide, which slows down the actin filament turnover, reduced both the maximal exerted force and the maximal velocity during lamellipodia leading edge protrusion. On the contrary, lamellipodia treated with 2.5 mM of cyclodextrin could advance with a higher velocity. The amplitude and frequency of elementary jumps underlying force generation were reduced by jasplakinolide but not by cyclodextrin. Using atomic force microscopy, I verified that cyclodextrin decreases the membrane stiffness of DRG neurons. The results of this part of my thesis indicate that membrane stiffness provides a selective pressure that shapes force generation and confirm the fundamental role of actin turnover during protrusion.

Studying the details of the inhibition of myosin II and its effect on the morphology, kinetics and dynamics of lamellipodia and filopodia emerging from the growth cones of DRG neurons is the subject of next part of my thesis. Treatment with Blebbistatin, inhibitor of myosin II, had the opposite effect on the force generated by lamellipodia and filopodia. My results suggest a possible role of myosin II in force generation and in particular during lamellipodia retractions and confirm a coupling between actin and microtubule dynamics.

At the end, the comparison of force generation in growth cones of the central nervous system (hippocampal) and peripheral nervous system (DRG) are presented. I found that filopodia and lamellipodia of DRG and hippocampal growth cones can exert forces with amplitudes varying from 1 to 20 pN developing with a similar time course. At a more quantitative level two main differences appear: firstly, filopodia from hippocampal growth cones exert a force larger than from DRG growth cones; secondly, lamellipodia from DRG growth cones exert a larger force and can move up at a higher speed in axial direction.

# 1
# INTRODUCTION

Neurons are among the most specialized cells in living organisms and are capable of self-organization in complex networks. During the development of mammalian nervous system, neuronal cells migrate to their final destination within the embryonic brain and body. Once at the specific location, neurons project neurites in order to explore the environment in search of appropriate chemical cues necessary for the formation of correct synaptic connections (Gallo and Letourneau, 2000; Ghashghaei et al., 2007; Solecki et al., 2006; Song and Poo, 2001). Understanding the overall dynamics regulating this process is an important question in neurobiology which has been addressed with different theoretical models and experimental approaches but the molecular mechanisms underlying force generation in neuronal growth cones (GCs) are not completely understood. The main object of the present work is to characterize the molecular mechanisms underlying force generation in neuronal GCs from dorsal root ganglia (DRG).

In this introduction I review the state of art of the field to set the background of my PhD work. Therefore I will initially describe the growth cone structure, then the role of individual cytoskeletal elements and of myosin II in force generation and motility will be discuss. At the end I will briefly review some theoretical models proposed for force generation.

## 1.1 Neuronal growth cone

Growth cones are highly motile sensory structures at the tips of developing and regenerating neurites and they regulate the rate and direction of neurite growth during neuronal development and nerve regeneration (Burnette et al., 2008). GCs actively explore the surroundings and respond to different chemical cues in the vicinity and play a critical role in the formation of appropriate neuronal connections (Ghashghaei et al., 2007; Solecki et al., 2006). The size, morphology and motility of GC can vary widely between different cell types. However most of the GCs have a broadly common structure. They are composed of two distinct cytoplasmic regions: Peripheral and central domain (P and C domain). (Fig. 1.1 a and b).

The P domain has a flat shape consisting of filopodia and lamellipodia. Filopodia are formed by bundles of actin filaments playing an important role in sensing guidance cues while lamellipodia are dense meshwork of actin filaments and are responsible for the advancement of the growth cone (Forscher et al., 1987). The central domain of the growth cone is the thickest region containing dense microtubule (MT) arrays (Fig. 1 d). It is enriched in cellular organelles such as mitochondria and exocytotic vesicles. Although actin filaments are primarily present in the peripheral region of growth cone and microtubules mostly terminate in the central region (Fig. 1 c and d), these two cytoskeletal elements overlap at the interface of the P domain and the C domain called transition domain of the growth cone. (Lowery and Van Vactor, 2009)(Fig. 1 b).

Guidance molecules activate receptors present on the growth cone surface which induces intracellular signalling events directing the GCs to turn toward (attraction) or away from (repulsion) the guidance cue (Goodman, 1996). Both microtubules and actin are highly dynamic structures in the GC and their interactions are very important for GC motility involving their coordinated polymerization and depolymerization (Dent and Kalil, 2001). Actin cytoskeleton which is mainly located at the leading edge of the GC is responsible for directing GC, whereas microtubules support the new extensions initiated by the actin (Mitchison and Kirschner, 1988; Smith, 1988).

Moreover membrane recycling in the form of exocytosis and endocytosis occurs in neuronal GC and may regulate the motility. It has been shown that during neurite outgrowth,

plasma membrane must be expanded rapidly to provide the sufficient surface area (Meldolesi, 2011). The exocytosis within the growth cone provide the majority of plasma membrane expansion in this process. It is also observed that the rate of endocytosis in the early developmental stages of outgrowth is significantly higher (Bonanomi et al., 2008; Vitriol and Zheng, 2012).

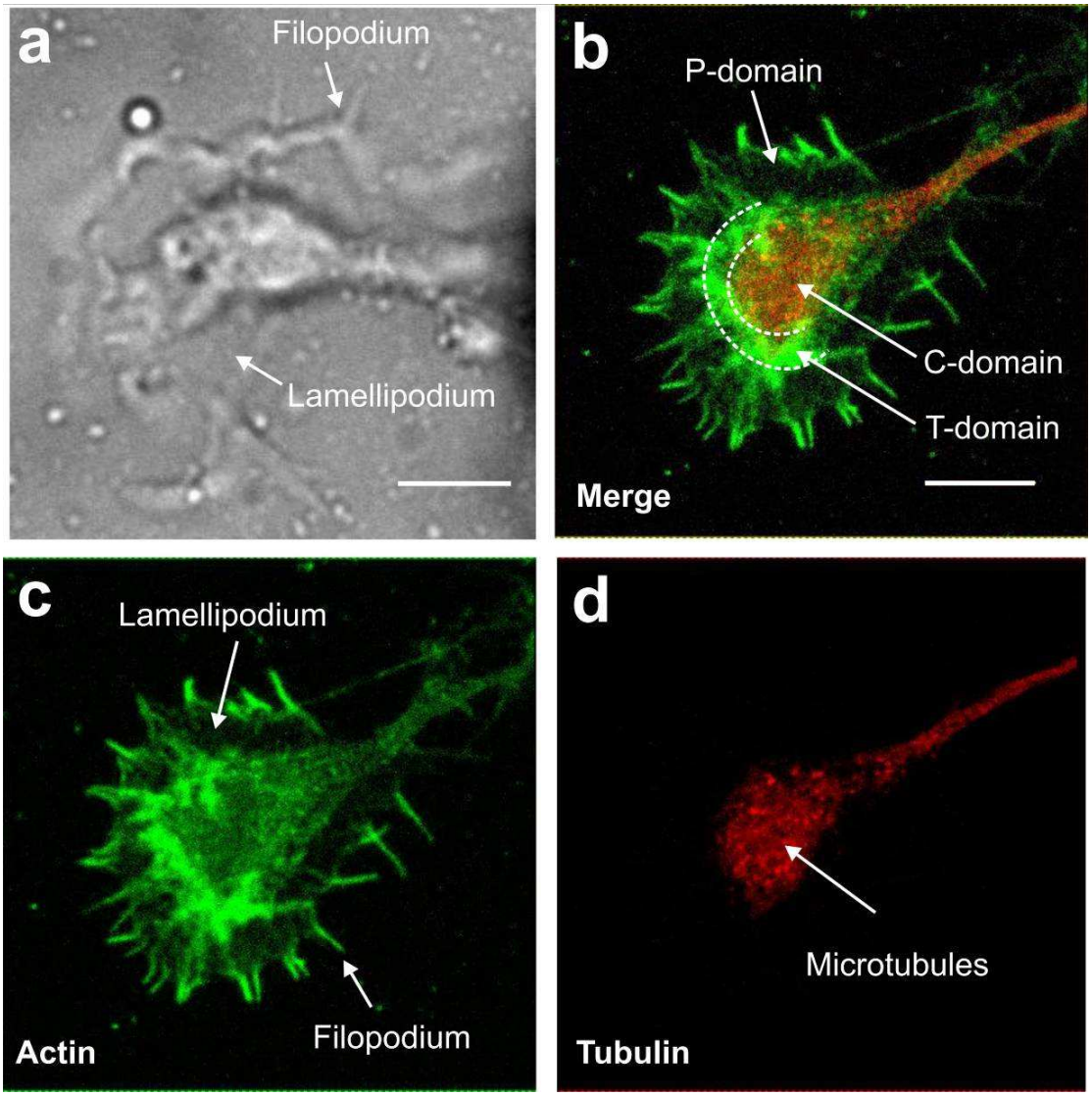


**Figure 1**: **Growth Cone structure**. (a) Images of Lamellipodia and filopodia emerging from a DRG GC. (b-d) . confocal fluorescence images of a DRG GC for Actin (c), tubulin (d) and merge of the both staining (b). Panels show the different domains of the growth cone; the peripheral, transition and central regions, and the different structural components of the growth cone such as the filopodia, lamellipodia and microtubules.

## 1.2 Force generation by neuronal growth cone

The force necessary for growth cone motility which cause the neurite to explore the environment, grow, retract, turn and branch is generated as the result of various processes such as actin and microtubule dynamics coupled with myosin-based retrograde actin flow and also selective adhesion to extracellular substrate (Dent and Gertler, 2003; Lin et al., 1994; Lowery and Van Vactor, 2009; Suter and Forscher, 1998; Vitriol and Zheng, 2012). In this study, we used optical tweezers as the appropriate experimental tool to obtain accurate force measurements on living neurons without causing any damage. Quantitative characterization of the force exerted by lamellipodia and filopodia during neuronal differentiation and migration enabled us to understand the dynamical properties of force generation. In the next sections, the role of individual cytoskeletal elements and molecular motors in force generation and growth cone motility will be briefly discussed.

### 1.2.1 Cytoskeleton

The cytoskeleton is an elaborate array of protein that provides architectural support and mechanical strength and also mediates cell motility and guidance (Suter and Forscher, 1998). In the nervous system, it has a fundamental role in axon and dendrite formation which allows neurons to establish their complex morphology. There are three main elements in cytoskeleton: actin, intermediate filaments and microtubule. Intermediate filaments are the most rigid filaments and are fundamental for structural rigidity of cells and the overall cell shape (Howard, 2001). Actin and microtubule are essential components in many cellular processes and their dynamics regulate the GC motility. In the following section some of the most significant findings about these two elements will be summarized.

### 1.2.2 Actin dynamics and actin regulating proteins

Actin is the most abundant protein in most cells and is involved in a variety of cellular processes such as: membrane protrusion, cell division and morphogenesis. In developing neurons, actin cytoskeleton is essential in neurite formation, extension and branching. At the leading edge of GC, actin is organized into filopodia and lamellipodia and their polymerization drives protrusion of the plasma membrane (Pantaloni et al., 2001; Pollard and Borisy, 2003).

Actin filaments are ~7 nm diameter, semi-flexible polymers with persistence length ~17 µm (Gittes et al., 1993). Under physiological conditions, Actin filaments are made up of dimer pairs of globular actin monomers (length ~2.7 nm). The actin filament is polar because the subunits are arranged head-to-tail in the filament and its ends are structurally different. This polarity has an important consequence which is the asymmetry in the polymerization rate along the filament, mainly the polymerization is faster at one end than the other. (Howard, 2001). The fast-growing end is called the barbed or plus end, whereas the slow-growing end is called the pointed or minus end.

Critical actin monomer concentration of the plus end of an actin filament is approximately six times less than that of minus end. When the concentration of actin monomer is greater than its critical concentration, the filament polymerizes and grows by binding the new monomers to the filament. On the contrary, while the monomer concentration is below the critical concentration, monomers detach from the filament end and the filament depolymerizes. When the concentration lies between the two values, only the plus end grows while the minus end shrinks. The state in which actin monomers or small oligomers are added to the barbed end of actin filaments (polymerization) and removed from the other end (depolymerization) is called “treadmilling”. The cyclical polymerization and depolymerisation of actin near the plasma membrane pushes the cellular membrane forward and exerts a protrusive force (Howard, 2001; Mogilner and Oster, 1996; Pollard and Borisy, 2003).

On the other hand, actin filaments also draw the growth cone membrane rearward during retrograde actin flow and are involved in growth cone retraction. Retrograde actin flow regulates the rate of neurite outgrowth and avoids microtubules from entering into the peripheral domain of the growth cone (Zhou and Cohan, 2004). The arrangement of F-actin polymerization, depolymerization, and retrograde flow is responsible for the behavior of lamellipodia and filopodia. The net protrusion of lamellipodia and filopodia is largely determined by the rates of F-actin treadmilling and retrograde flow.

The actin turnover is controlled by variety of regulatory proteins. Generally these proteins can be divided into several categories base upon their function such as filament nucleation, end capping, crosslinking and severing as well as monomer sequestering (Pak et al., 2008). Also molecular motors seem to participate to the overall process by controlling

several aspects of this process. In the model proposed in (Pollard and Borisy, 2003) the actin polymerization is activated by proteins such as profilin, Wasp, or Arp2/3 in response to external guidance cues. Capping proteins bind to barbed ends and prevent addition of actin subunits to filaments. Severing and depolymerizing proteins such as ADF/cofilin break down the existing filaments in to small fragments for disassembly and increasing the pool of free actin monomer. Profilin catalyzes the exchange of ADP for ATP on monomeric actin molecules which become available for new polymerization at barbed ends. Crosslinking proteins link filaments together to create complex structure (Pollard and Borisy, 2003).

### 1.2.3 Microtubule dynamics and microtubule associated proteins

Microtubules (MTs) are major cytoskeletal elements that support growth cone stability and axonal and dendritic extension. Moreover, they control various aspects of the regeneration and repair processes in the nervous system (Hur et al., 2012). In addition, MTs provide platforms for intracellular transport.

Microtubules made up of 13 protofilaments and are assembled from αβ tubulin heterodimers in a polarized manner with polymerization occurring mostly on plus end of the microtubules. The plus ends of MTs exhibit cycles of growing and shortening, a process called ‘‘dynamic instability’’ in which their polymerization is interrupted by rapid depolymerization and shrinkage. It is believed that dynamical instability enables MTs to quickly remodel their organization and selectively grow in response to extracellular signals.

Typically Microtubules are located in the central domain of the growth cone, from which small number of them protrude into the periphery domain and even penetrate into filopodia (Dent and Kalil, 2001; Schaefer et al., 2002). These individual MTs are highly dynamic and play an important role in guidance decisions and migration (Dent et al., 2011; Schaefer et al., 2002; Vitriol and Zheng, 2012). MTs in P domain of GC undergo cycles of growth and catastrophe due to “dynamic instability” of MTs. Therefore, they have direct effect on membrane protrusion (Buck and Zheng, 2002; Mack et al., 2000; Rochlin et al., 1999). Recent studies show that blocking MTs dynamics inhibits growth cone turning in response to guidance cues (Dent et al., 2011; Lowery and Van Vactor, 2009; Vitriol and Zheng, 2012) indicating that MTs are sensitive to extracellular signals. This shows that they

play an instructive role in growth cone guidance. Moreover dynamical instability of MTs may activate Rac1 and RhoA signaling which controls actin dynamics (Hur et al., 2011).

Similar to the actin cytoskeleton, there are a variety of microtubule associated proteins (MAPs) that bind to MTs and regulate MT polymerization and depolymerization, stability, crosslinking, severing, and transport (Hirokawa et al., 2010; Maccioni and Cambiazo, 1995).

### 1.2.4 Non-muscle myosin II

Myosin molecules, like all motor proteins, are molecular machines that convert chemical energy into mechanical work. In this way by hydrolyzing ATP, the energy used to generate the force and power cellular motility is released (Howard, 2001).

Non-muscle myosins II (NMII) have been shown to play important roles in a variety of cellular processes such as growth cone motility, cellular locomotion, cellular morphology, adhesion, cytokinesis and cell division (Conti et al., 2004; Forscher and Smith, 1988; Vicente-Manzanares et al., 2009; Wylie and Chantler, 2008).

In neuronal GC, the balance between the rate of polymerization and myosin base retrograde flow of actin determines growth cone protrusion or retracting. If the polymerization rate is balanced with the rate of actin retrograde flow, then the membrane remains stationary. Indeed, the motor protein myosin II controls the retrograde flow of actin by severing the actin filaments at their minus end (Medeiros et al., 2006). Recent studies show that myosin II does not sever actin filaments directly, but it binds into actin filaments, forming the actomyosin complex which are able to exert contractile force on anti parallel actin filaments that contracts the actin meshwork and breaks the filaments. Moreover, NMII mediates adhesion by acting indirectly through actin to bring adhesion-related proteins such as integrins or signal transduction molecules into close proximity. NMII bundles actin filaments, therefore adhesion proteins at the ends of these actin filaments are clustered.

NM II molecules are composed of three pairs of peptides: two heavy chains of 230 kDa, two 20 kDa regulatory light chains (RLCs) that regulate NMII activity and two 17 kDa essential light chains (ELCs) that stabilize the heavy chain structure (Vicente-Manzanares et

al., 2009). In Neuronal cells, there are three different isoforms of non-muscle myosin II (A, B, and C). They have similar structural and dynamical properties but they also have slightly different localizations and functions. Differential localization of myosin isoforms depends on the cellular specificity and possibly also on the developmental stage of the cell (Betapudi, 2010; Conti and Adelstein, 2008; Vicente-Manzanares et al., 2009; Wylie and Chantler, 2008). In neurons, NMIIB is required for the outgrowth of neuritic processes (Bridgman et al., 2001; Wylie and Chantler, 2008), while NMIIA is an important regulator of retraction and promotes the adhesion with formation of focal contact sites (Conti et al., 2004; Wylie and Chantler, 2001; Yu et al., 2012). NMIIC, which is thought to regulate cell membrane extension and the formation of focal contacts shows separate but coupled activities with NMIIA and NMIIB (Wylie and Chantler, 2008). There are two important kinetic properties that differ among the NMII isoforms: The rate of ATP hydrolysis by myosin when bound to actin and the time that myosin is bound to actin and generate force (duty ratio). NMIIA has the highest rate of ATP hydrolysis and it moves more rapidly along the actin filaments than the other isoforms but NMIIB has higher duty ratio (Vicente-Manzanares et al., 2009).

However, it is clear that actin dependent processes, such as actin and MTs dynamics, adhesion, membrane trafficking, and endo/exocytosis, play important roles in growth cone formation, motility, and guidance responses and there are fundamental crosstalks among them (Hines et al., 2010; Kolpak et al., 2009; Tojima et al., 2007; Tojima et al., 2010). The existence of a coupling between actin and MT dynamics is confirmed by the observation that inhibition of myosin II with Blebbistatin markedly accelerates neurite growth and promote the reorganization of both actin and MTs in GCs (Hur et al., 2011).

## 1.3 Theoretical models for force generation

The protrusion of the leading edge is a complex process however the actin filaments treadmilling and their interaction with the motor protein myosin II are the major responsible for force generation. The overall dynamics regulating this process is not yet completely clear, but mathematical modeling as a fundamental investigation technique provides a way to link known molecular events to force generation processes. A key outcome of these models is represented by the Fv relationships, describing how the force (F) exerted by the actin filament network is related to the velocity (v) of their growing ends (Carlsson, 2001; Carlsson, 2003; Mogilner, 2009; Mogilner and Oster, 1996; Mogilner and Oster, 2003; Peskin et al., 1993).

Various theoretical models for understanding the force generation have been developed. Earlier models of force generation were considering only a single actin filament but more modern models such as tethered ratchet, autocatalytic branching, helped to understand the dynamics and forces in complex actin networks. Two main theoretical models have been proposed to explain force generation by actin polymerization are ratchet model (Mogilner and Oster, 1996; Mogilner and Oster, 2003) and autocatalytic model (Carlsson, 2001; Carlsson, 2003). Fluctuations of contact between the tips of actin filaments and the surrounding membrane is an essential feature of Brownian ratchet models (Mogilner and Oster, 2003; Peskin et al., 1993) leading to Fv relationships in which v decreases exponentially with increasing values of F. On the other hand, in autocatalytic models (Carlsson, 2001; Carlsson, 2003) when an obstacle is encountered, the actin network - due to the activity of controlling proteins - originates new branches, so that the velocity v remains constant for increasing values of F. A brief review of these two models is presented in the following subsesions.

### 1.3.1 Ratchet model

A ‘Brownian ratchet’ model (Peskin et al., 1993) explains how force is generated when a resisting force is applied to the object in front of the filament’s tip, the object can still diffuse away, creating a gap sufficient for monomers to insert and assemble onto the tip. Experimental observations indicate that actin filament is not an unbending rod, but it is an elastic filament that can bend in response to the load. Therefore an ‘elastic ratchet’ model suggested that thermal fluctuation of filamens create a gap between their tips and the load (Mogilner and Oster 1996) and an actin monomer can easily insert itself between the filament and membrane. Monomer assembly increases the filament’s length so that when the tip contacts the load, the polymer is bent. So the extended filament consequently applies an elastic force on the membrane and moves it forward. These models, explain force generation by considering a single polymerizing actin filament but they are not able to properly describe the complex geometry of the actin network at the leading edge. Therefore, extended models such as tethered ratchet was proposed which considers the transient attachment of actin filaments to the membrane (Mogilner and Oster, 2003). In this extended model the filaments are attached to the membrane by protein complexes. However, they can dissociate and grow and exert a force until capped.

### 1.3.2 Autocatalytic Model

Autocatalytic model assumes that the new actin branches are generated from existing branches (Carlsson, 2003). In this model the rate of filament branching is proportional to the density of the existing filaments. Autocatalytic model predicates that the protrusion rate should not depend on opposing force exerted by the obstacle. Greater load force causes faster branching and therefore this implies greater actin density. This means that the load per filament remains constant.

Spontaneous oscillations of the lamellipodia leading edge which have been seen in several cell types including DRG neurons (Amin et al., 2012) enable cells to explore the extracellular environment. These oscillations could be based on actin polymerization exerting forces on the cell membrane and cause the cell protrusion (Carlsson, 2010a). It has been suggested that the essential mechanisms which make actin waves are actin filament positive feedback, actin filament spreading and delayed negative feedback (Carlsson, 2010b). Actin filament positive feedback is the mechanism in which actin filament feeds back its assembly and thus regulating itself (Carlsson, 2012). Actin filament spreading can be interpreted as the direct nature of branching from existing filament. Both Actin filament positive feedback and actin filament spreading are direct predictions of autocatalytic model. On the other hand, indirect feedbacks can occur because of possible interactions between actin filament and nucleation-promoting factors (Carlsson, 2012). Because of the nature of these interactions, they effect after some delay with respect to the positive feedback which this can lead to oscillatory behavior (Carlsson, 2012). Therefore, the combination of these mechanisms provides a mechanism for actin dynamic.

The role of myosin II in producing force in nonmuscle cells have been explored by simulation of myosin mini filament motion through a random two dimensional actin network (Dasanayake et al., 2011). Using the mentioned numerical simulations, extremely contractile stresses have been observed as a result of directional movement of myosin mini filament along the actin network filaments in order to reach more stable configurations.

In addition to the classical plasma membrane (PM) protrusions, cells display structures referred to as plasma membrane blebs which are bulky rounded morphology expanding up to 2 μm from the PM. (Fackler and Grosse 2008).

Cell internal hydrostatic pressure can lead to rapid protrusion of the PM as a result of the initiation of events that involve local disruption of membrane – actin cortex interactions (Charras et al., 2005), which is named as blebbing. This effect can also be caused by a local increase in cortical contractility of the actomyosin gel (Paluch et al., 2006). Importantly, initial powering of bleb expansion does not involve actin polymerization events, which distinguishes PM blebs from all other known cell protrusions.

Recently, several other mathematical models have been developed to increase our understanding about polymerization force and their underlying molecular mechanism in which some of them were reviewed in (Mogilner, 2009). Moreover, recently (Allard and Mogilner, 2012) reviewed some advanced experimental and theoretical studies of actin waves and discussed mechanisms of wavy protrusions. Because of the complexity of cellular processes neither models has been precisely described three dimensional cell motility and coupling between self-organization and force generation. However, these studies are essential for complementing experimental data and provide useful estimates of the polymerization forces.

# 2

# RESULTS

## 2.1

## Force generation in lamellipodia is a probabilistic process with fast growth and retraction events

R. Shahapure, F. Difato, A. Laio, G. Bisson, E. Ercolini, L. Amin, E. Ferrari, V. Torre,
Biophysical journal 98 (6), 979-988 (2010)

# Force Generation in Lamellipodia Is a Probabilistic Process with Fast Growth and Retraction Events

Rajesh Shahapure,[†] Francesco Difato,[†‡] Alessandro Laio,[†] Giacomo Bisson,[†] Erika Ercolini,[†§] Ladan Amin,[†] Enrico Ferrari,[¶] and Vincent Torre[†‡*]

[†]International School for Advanced Studies (SISSA-ISAS), Trieste, Italy; [‡]Italian Institute of Technology, ISAS Unit, Trieste, Italy; [§]Cluster in Biomedicine (CBM), Trieste, Italy; and [¶]National Research Council, Istituto Nazionale per la Fisica della Materia, Laboratorio Nazionale TASC, Trieste, Italy

ABSTRACT Polymerization of actin filaments is the primary source of motility in lamellipodia and it is controlled by a variety of regulatory proteins. The underlying molecular mechanisms are only partially understood and a precise determination of dynamical properties of force generation is necessary. Using optical tweezers, we have measured with millisecond (ms) temporal resolution and picoNewton (pN) sensitivity the force-velocity (*Fv*) relationship and the power dissipated by lamellipodia of dorsal root ganglia neurons. When force and velocity are averaged over 3–5 s, the *Fv* relationships can be flat. On a finer timescale, random occurrence of fast growth and subsecond retractions become predominant. The maximal power dissipated by lamellipodia over a silica bead with a diameter of 1 $\mu$m is $10^{-16}$ W. Our results clarify the dynamical properties of force generation: i), force generation is a probabilistic process; ii), underlying biological events have a bandwidth up to at least 10 Hz; and iii), fast growth of lamellipodia leading edge alternates with local retractions.

## INTRODUCTION

Neurons are among the most specialized cells in living organisms and are capable of self-organization in complex networks. To self-organize, neurons protrude neurites, highly motile structures that explore the environment in search of appropriate chemical cues necessary for the formation of correct synaptic connections (1,2). Neurite exploration is guided by the growth cone located at the neurite tip (3–5) that is formed by an extended lamellipodium from which thin filopodia emerge (6). Filopodia tips can move at a velocity that can reach 0.8–1 $\mu$m/s and their motility is at the basis of the efficient formation of neural networks. The primary source of motility in growth cones is the polymerization of actin filaments (7–9), a process controlled by a variety of regulatory proteins (10). The addition of actin polymers to actin filaments in close contact with the membrane pushes the cellular membrane forward exerting a protrusive force (11,12).

The overall dynamics regulating this process is not yet clear, and mathematical modeling provides a way to link known molecular events to force generation (13). A key outcome of these models is represented by the *Fv* relationships, describing how the force ($F$) exerted by the actin filament network is related to the velocity ($v$) of their growing ends (7,14–19). Fluctuations of contact between the tips of actin filaments and the surrounding membrane is an essential feature of Brownian ratchet models (7,15,16) leading to *Fv* relationships in which $v$ decreases exponentially with increasing values of $F$. In autocatalytic models (14,16,17), when an obstacle is encountered, the actin network—due to the activity of controlling proteins—originates new branches, so that the velocity $v$ remains constant for increasing values of $F$.

Previous determinations of the *Fv* relationships (20) with an atomic force microscope (AFM) cantilever (21,22) had a limited time resolution and were obtained either in vitro or in migrating keratocytes exerting forces in the nanoNewton range. In this work, using optical tweezers (23–25), we provide an experimental characterization of *Fv* relationships in neuronal growth cones with millisecond resolution and picoNewton sensitivity. Bold notations $\mathbf{x}$, $\mathbf{v}$, and $\mathbf{F}$ indicate vectorial quantities, and $x$, $v$, and $F$ indicate either the modulus or a component of these vectors. This experimental technique enabled us to determine the three components of the force exerted by a lamellipodium, $\mathbf{F} = (F_x, F_y, F_z)$, from rat dorsal root ganglia (DRG) and of the velocity of its leading edge, $\mathbf{v} = (v_x, v_y, v_z)$. From these vectorial quantities, we have derived properties of force generation in lamellipodia, with important biological consequences. We found that force generation in lamellipodia is an intrinsically multiscale process. At a temporal resolution of 3–5 s, the exerted force can increase, maintaining a constant velocity. At a millisecond resolution, a much more complex behavior is observed, with random occurrence of fast growths and subsecond retractions. Our results show that autocatalytic models (14,16,17) of force generation are correct in a mean or average approximation. At a higher temporal resolution, the network of actin filaments evolves in a much more complex manner that can be characterized only probabilistically.

*Submitted August 27, 2009, and accepted for publication November 20, 2009.*

*Correspondence: torre@sissa.it

Vincent Torre's present address is International School for Advanced Studies (SISSA), Area Science Park, S.S.14, Q1 Bldg., Basovizza, Trieste-34149, Italy.

Editor: Jason M. Haugh.



0006-3495/10/03/0979/10 $2.00

doi: 10.1016/j.bpj.2009.11.041

## MATERIALS AND METHODS

### Neuron preparation

Wistar rats at postnatal days 10–12 (P10–P12) were sacrificed by decapitation after anesthesia with $CO_2$ in accordance with the Italian Animal Welfare Act. After dissection, DRGs were incubated with trypsin (0.5 mg/ml; Sigma Aldrich, Milan, Italy), collagenase (1 mg/ml; Sigma Aldrich), and DNase (0.1 mg/ml; Sigma Aldrich) in 5 ml Neurobasal medium (Gibco, Invitrogen, Milan, Italy) in a shaking bath (37°C for 35–40 min). After mechanical dissociation, they were centrifuged at 300 rpm, resuspended in culture medium, and plated on poly-L-lysine-coated (0.5 $\mu$g/ml; Sigma Aldrich) coverslips. Neurons were incubated for 24–48 h and nerve growth factor (50 ng/ml; Alomone Labs, Jerusalem, Israel) was added before performing the measurements.

### Optical tweezers setup

The optical tweezers set-up was built as described by Cojoc et al. (25). Briefly, the trapping source was an ytterbium fiber laser operating at 1064 nm (IPG Laser GmbH, Burbach, Germany), which was sent onto an inverted microscope (IX81, Olympus, Milan, Italy) to the focusing objective (Olympus 100× oil, NA 1.4), as shown in the schematic diagram of Fig. S1 in the Supporting Material. The dish containing the differentiating neurons and the beads (PSI-1.0NH2, G. Kisker GbR, Steinfurt, Germany) was placed on the microscope stage, which could be moved by a three-axis piezoelectric nanocube (17 MAX 301, Melles Griot, Albuquerque, NM). The temperature of the dish was kept at 37°C by a Peltier device. The dish was maintained in an environment with a controlled level of $CO_2$ (5%) and moisture (95%). The bead position $\mathbf{x} = (x, y, z)$ was determined along all the axes with an accuracy of 2 nm using back focal plane detection, which relies on the interference between forward scattered light from the bead and unscattered light (24,26,27). The back focal plane of the condenser was imaged onto a quadrant photodiode (QPD) (C5460SPL 6041, Hamamatsu, Milan, Italy), and the light intensity was converted to differential outputs digitized at 20 kHz and low-pass filtered at 5 kHz. The z position of the bead was determined using the Gouy phase-shift effect (24). The trap stiffness, $\mathbf{K}_{x,y,z} = (k_x, k_y, k_z)$, and the detector sensitivity were calibrated using the power spectrum method (24). Detector sensitivity was also checked by measuring voltage signals originating from displacements of a bead stuck to the coverslip obtained with the three-axis piezoelectric nanocube. The force exerted by the lamellipodium, $\mathbf{F}$, was taken as equal to $-\mathbf{F}_{trap}$. When the displacement of the bead from its equilibrium position inside the trap, $\mathbf{d} = (d_x, d_y, d_z)$, was <400 nm, $\mathbf{F}_{trap} = (F_x, F_y, F_z)$ was calculated as $F_x = d_x k_x$, $F_y = d_y k_y$, and $F_z = d_z k_z$ (24). All experiments of force recordings were monitored by video imaging with a charge-coupled device (CCD) camera at a frame rate of 5 Hz. Visual inspection of recorded images made it possible to discard from the analysis all force recordings during which visible debris interfered with the optical determination of bead position $\mathbf{x}$.

### Bandwidth of biological events underlying force generation

A reliable and accurate computation of *Fv* relationships from the bead displacement $\mathbf{x}$ and force $\mathbf{F}$ requires a careful analysis of time series obtained from digitization of the three components of $\mathbf{x}$. When the velocity, $\mathbf{v} = (v_x, v_y, v_z)$, is derived from the bead displacement $\mathbf{x}$ by numerical differentiation, it is necessary to low-pass filter the original data, as spurious high frequencies amplify noise (28). To find the appropriate cut-off frequency, we investigated the bandwidth of biological events underlying force generation. We computed and compared the power spectrum density of forces measured far from any neuron ($PSD_{noise}(f)$; Fig. 1 *a*, *red traces*)—originating from Brownian fluctuations and instrumental noise—and the $PSD_{push}(f)$ of forces measured when the leading edge of the lamellipodium pushed the bead (Fig. 1 *a*, *blue traces*). $PSD_{noise}(f)$ and $PSD_{push}(f)$ are very similar, and almost indistinguishable for $f > 30$ Hz, but at frequencies below 1 Hz the energy of $PSD_{push}(f)$ is at least 30 times larger than that caused by Brownian collisions. The analysis of $PSD_{noise}(f)$ and $PSD_{push}(f)$ in 14 experiments indicates that the bandwidth of biological events underlying force generation in DRG lamellipodia extends up to 10 Hz. Therefore, events occurring on a timescale of 100 ms cannot be neglected, and force generation needs to be analyzed at a higher temporal resolution than in previous investigations.

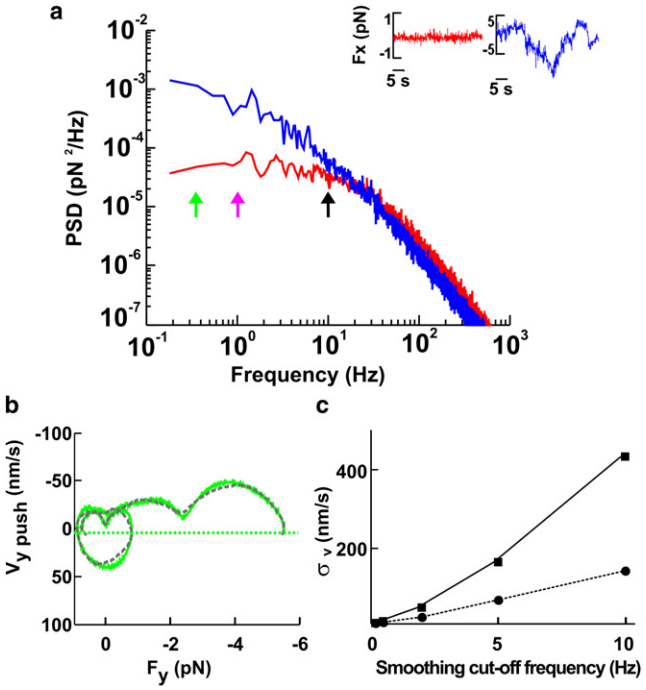


FIGURE 1 Computation of *Fv* relationships. (*a*) Power spectrum density of forces measured far from the lamellipodium (*red trace*) and when the lamellipodium pushed the bead (*blue trace*), computed from the red and blue traces, respectively, shown in the inset. Green, pink, and black arrows indicate 0.2, 1, and 10 Hz, respectively. (*b*) *Fv* relationships computed with Gaussian filtering at 0.2 Hz (*green*) and linear regression with $W = 10{,}000$ (*gray*), as described in Materials and Methods. The green dotted line represents $-3\sigma_v$ at the 0.2-Hz bandwidth (where $\sigma_v$ was calculated from bead fluctuations measured away from the lamellipodia). (*c*) Relationship between the standard deviations of velocity distribution as a function of smoothing for two values of the trap stiffness, 0.005 pN/nm (*squares*) and 0.045 pN/nm (*circles*).

### Computation of *Fv* relationships

The velocity, $\mathbf{v} = (v_x, v_y, v_z)$, of the bead was obtained by numerical differentiation of its sampled position $\mathbf{x} = (x(n), y(n), z(n))$ $n = 1,\ldots N$. Numerical differentiation was computed either by convolution of position components $x(n)$, $y(n)$, and $z(n)$ with the derivative of a Gaussian filter $1/[\sigma(2\pi)^{1/2}]$ $\exp(-t^2/\sigma^2)$ (Gaussian filtering) or by linear regression. Gaussian filters corresponding to cut-off frequencies of 0.2, 1, and 10 Hz were used (see Figs. 4–6). In the linear regression method, the components $v_x(n)$, $v_y(n)$, and $v_z(n)$ of velocity $\mathbf{v}$ were calculated by a linear least-square fit of the equations $x(n) = a_x + v_x(n)\,(i-n)\Delta t$, $y(n) = a_y + v_y(n)\,(i-n)\Delta t$, and $z(n) = a_z + v_z(n)\,(i-n)\Delta t$ with $i = -W,\ldots,W$, where $\Delta t$ was the sampling interval. The two parameters $a_x$ and $v_x(n)$ were determined by minimizing the cost function

$$[v_x, a_x] = \arg\min_{[v,a_x]}\left[\sum_{i=n-W}^{n+W}\left(a_x + v_x(i-n)\Delta t - y(i)\right)^2\right].$$

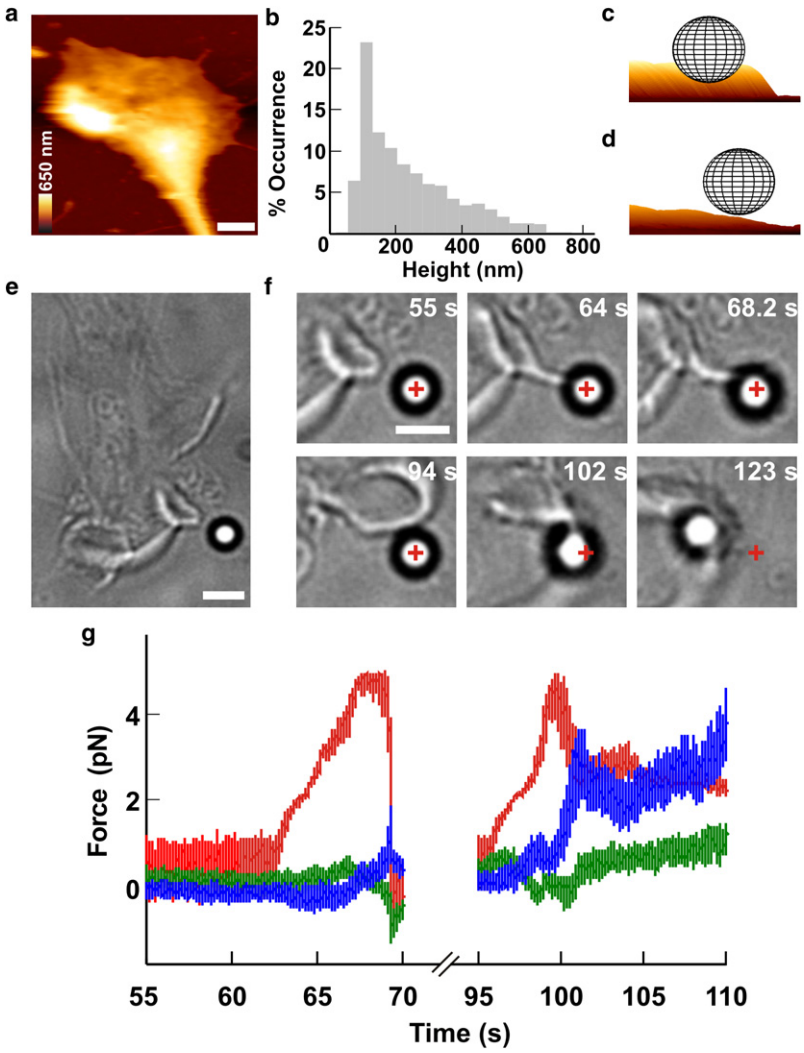


FIGURE 2 Push and retraction by a lamellipodium. (*a*) AFM image of a lamellipodium. The height is coded as in the colored scale bar and horizontal white scale bar, 2 $\mu$m. (*b*) Occurrence histogram of measured height of lamellipodium leading edges from seven growth cones. (*c* and *d*) Three-dimensional representations of a 1-$\mu$m bead in front of a thick (*c*) and a thin (*d*) lamellipodium. (*e*) Low-resolution image of a lamellipodium in front of a bead trapped with an infrared laser. Scale bar, 2 $\mu$m. (*f*) Successive frames showing the lamellipodium (*55 s*) growing toward the bead (*64 s*) and lifting it up (*68.2 s*). Subsequently, the lamellipodium retracted (*94 s*) and grew under the bead pulling it out of the trap during retraction (*102–123 s*). The cross indicates the center of the optical trap. Scale bar, 2 $\mu$m. (*g*) The three components $F_x$ (*blue*), $F_y$ (*green*), and $F_z$ (*red*) of the force when the lamellipodium pushed the bead vertically (55–70 s) and when the lamellipodium lifted up and retracted (95–110 s).

$a_y$ and $v_y(n)$, and $a_z$ and $v_z(n)$, were determined in a similar way. Computation of derivatives with the linear regression method depended on the number of samples, $W$.

$Fv$ relationships computed from vertical and lateral pushes had periods of negative velocity (see Figs. 4 *c* and 5 *f*), corresponding to transient retractions of the lamellipodium leading edge. When the velocity reverses its direction, becoming negative, the same force can be exerted for two different values of the velocity, leading to the appearance of loops in $Fv$ relationships (see Fig. 4 *c*), typical of systems exhibiting hysteresis (21). Because of the limited spatial and temporal resolution of the CCD camera used in this study, these transient retractions could not be confirmed by video imaging. Therefore, we asked whether these loops could originate from numerical artifacts and noise fluctuations. Indeed, the numerical computation of derivatives from noisy data is ill-conditioned (28), and negative velocities could be produced by the specific method used to compute the velocity from the displacement. For this reason, we compared two different methods to obtain the velocity, $v$, from the displacement: Gaussian filtering and linear regression. In these two methods, the timescale is given by the cut-off frequency of the Gaussian function and by the number of points in the window ($W$), respectively. $Fv$ relationships obtained from the same force measurement sampled at 10 kHz with the linear regression method with $W = 10{,}000$ (Fig. 1 *b*, *gray trace*) and obtained by using a Gaussian filter with a cut-off frequency of 0.2 Hz (Fig. 1 *b*, *green trace*) had the same shape and number of loops.

As numerical differentiation is very sensitive to noise and amplifies its high-frequency components, we investigated to what extent loops could be caused by Brownian fluctuations. We computed $Fv$ relationships from force measurements obtained far from lamellipodia. The obtained velocity was Gaussian-distributed around 0, with a standard deviation of $\sigma_v$ increasing with the bandwidth of Gaussian filtering, depending also on the trap stiffness (Fig. 1 *c*). Periods with a negative velocity observed during vertical and lateral pushes, during which $v$ was $<-3\sigma_v$, could not be ascribed to Brownian fluctuations, and all negative velocities exceeding $-3\sigma_v$ lines (Fig. 1 *b*, *horizontal lines*; and see Figs. 4 *d* and 5 *f*,) were caused by transient retractions of the lamellipodium.

## AFM imaging

The three-dimensional (3D) structure of DRG lamellipodia (Fig. 2 *a*) was determined by using AFM, as shown in. Before imaging with AFM, DRG neurons were fixed with glutaraldehyde (Sigma Aldrich). DRG growth cones were imaged using a commercial AFM (Nanowizard II, JPK, Berlin, Germany) combined with an inverted optical microscope (Axiovert 200, Zeiss, Milan, Italy). Soft tips with low force constant (OBL, 0.03N/m; Veeco, Santa Barbara, CA) were utilized, and forces were kept between 100 pN and 1 nN during scanning.

## RESULTS

DRG neurons isolated from P10–P12 rats were plated on poly-L-lysine-coated glass coverslips positioned on the stage

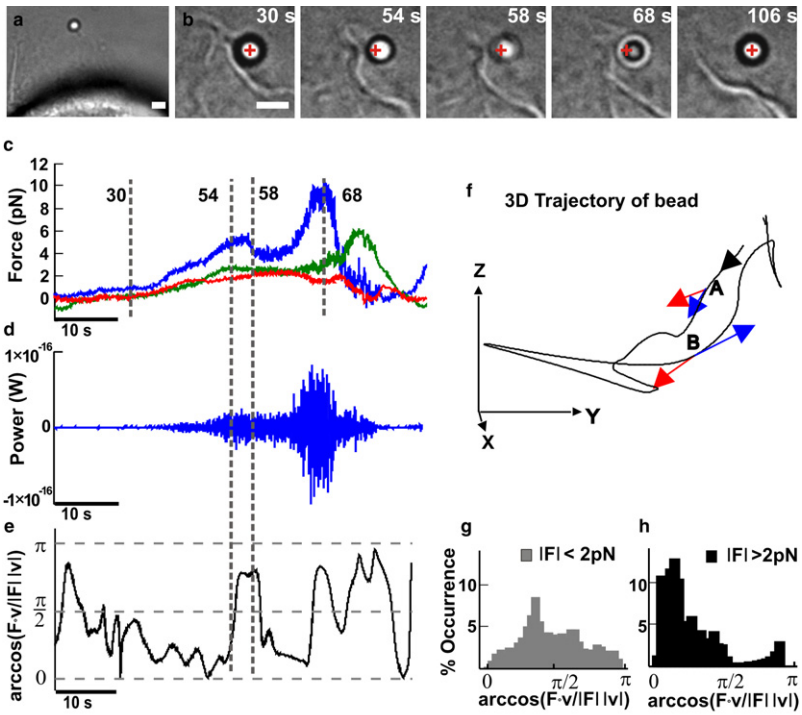


FIGURE 3 Mechanics of collisions between lamellipodia and beads. (*a*) Low-resolution image of a lamellipodium pushing a trapped bead. Scale bar, 2 $\mu$m. (*b*) Successive frames taken at different times during the push. The cross indicates the center of the optical trap. Scale bar, 2 $\mu$m. (*c*) The three components of the force, $F_x$ (*blue*), $F_y$ (*green*), and $F_z$ (*red*), exerted by a lamellipodium during the push smoothed at 10 Hz. (*d*) Instantaneous power $\mathbf{F}\cdot\mathbf{v}$ acting on the bead. (*e*) Time evolution of $\arccos(\mathbf{F}\cdot\mathbf{v}/|\mathbf{F}|\,|\mathbf{v}|)$ during the push. Data obtained after smoothing at 0.2 Hz. (*f*) The trajectory of the bead in a 3D space. The black arrow indicates the direction of the trajectory. Red and blue arrows on A and B indicate the instantaneous $\mathbf{F}$ and $\mathbf{v}$, respectively, at the two times corresponding to 54 and 58 s in *c*–*e*. When $\mathbf{F}$ and $\mathbf{v}$ are parallel, $\arccos(\mathbf{F}\cdot\mathbf{v}/|\mathbf{F}|\,|\mathbf{v}|)$ is close to 0, and when $\mathbf{F}$ and $\mathbf{v}$ are antiparallel, $\arccos(\mathbf{F}\cdot\mathbf{v}/|\mathbf{F}|\,|\mathbf{v}|)$ is close to $\pi$. (*g*) Histogram of the $\arccos(\mathbf{F}\cdot\mathbf{v}/|\mathbf{F}|\,|\mathbf{v}|)$ when $|\mathbf{F}|$ was <2 pN. (*h*) Histogram of the $\arccos(\mathbf{F}\cdot\mathbf{v}/|\mathbf{F}|\,|\mathbf{v}|)$ when $|\mathbf{F}|$ was >2 pN.

of an inverted microscope used for imaging and measuring forces (see Materials and Methods). After 1 or 2 days of incubation, neurites emerged from the DRG soma and their motion was analyzed. Filopodia and lamellipodia moved rapidly, exploring the 3D space in all directions. DRG lamellipodia were imaged with AFM (Fig. 2 *a*) and the height of their leading edges varied from 45 to 660 nm (Fig. 2 *b*). Silica beads of 1-$\mu$m diameter were trapped with a 1064 nm infrared (IR) laser tweezers and positioned in front of the leading edge of a lamellipodium (Fig. 2 *e*). When the center of the bead is located at ~800 nm above the coverslip, a thick lamellipodium can push the bead (Fig. 2 *c*). Visual inspection of lamellipodia indicates the existence of several stereotyped behaviors (29): the lamellipodium grows underneath the bead without displacing it (Fig. 2 *d* and Fig. S2); the bead adheres to the cell membrane, and when the lamellipodium retracts, the bead is removed from the trap (Fig. 2 *f*, *102 s*); the lamellipodium grows underneath the bead, displacing it upward (Fig. 2 *f*, *68.2 s*) (30); or the lamellipodium pushes the bead forward exerting a force in the direction of its growth (see Fig. 3, *a* and *b*). Often, two or more of these stereotyped behaviors were observed in the same experiment. In the example of Fig. 2 *f*, the lamellipodium initially pushed the bead upward (Fig. 2 *g*, *64–68.2 s*) and, after the lamellipodium retracted the bead, returned inside the trap (*94 s*). After a few seconds, the lamellipodium lifted up the bead again, and, because of the presence of adhesion forces, the bead remained attached to the lamellipodium membrane. Finally, the lamellipodium retracted, pulling the bead away from its trap (Fig. 2 *g*, *95–110 s*). Adhesion of the bead to the lamellipodium was often irreversible and could not be detached from the lamellipodium by increasing the power of the laser beam, but in other experiments, adhesion was reversible and the bead detached spontaneously. In all experiments, the growth cone behavior was followed with video imaging and the displacement of the bead, $\mathbf{x} = (x, y, z)$, was measured with a high temporal resolution using a QPD. The $z$ axis is perpendicular to the coverslip and parallel to the IR laser beam used for trapping. By determining the trap stiffness, $\mathbf{k} = (k_x, k_y, k_z)$, $\mathbf{F}$ was obtained as $(-xk_x, -yk_y, -zk_z)$ (24,27).

In what follows we will compute and analyze properties of the *Fv* relationships for the four most common stereotyped behaviors:

- Vertical pushes (42 experiments): when lamellipodia lifted the bead upward (Fig. 2 *f*, *55–68.2 s*) and $\mathbf{F}$ changed primarily along the $z$ component (Fig. 2 *g*, *64-68.2 s*);
- Lateral pushes (22 experiments): when lamellipodia pushed the bead laterally in the $xy$ plane (see Fig. 5 *b*), whereas $\mathbf{F}$ changed primarily along the $x$ and $y$ components (see Fig. 5, *c*–*e*);
- Vertical retractions (22 experiments): when the bead was displaced vertically toward the bottom of the coverslip after bead adhesion to the growth cone membrane and lamellipodia retraction. In these cases, either the lamellipodium grew under the bead or the bead was attracted toward the lamellipodium membrane by interactions with protruding structures such as ruffles (30);

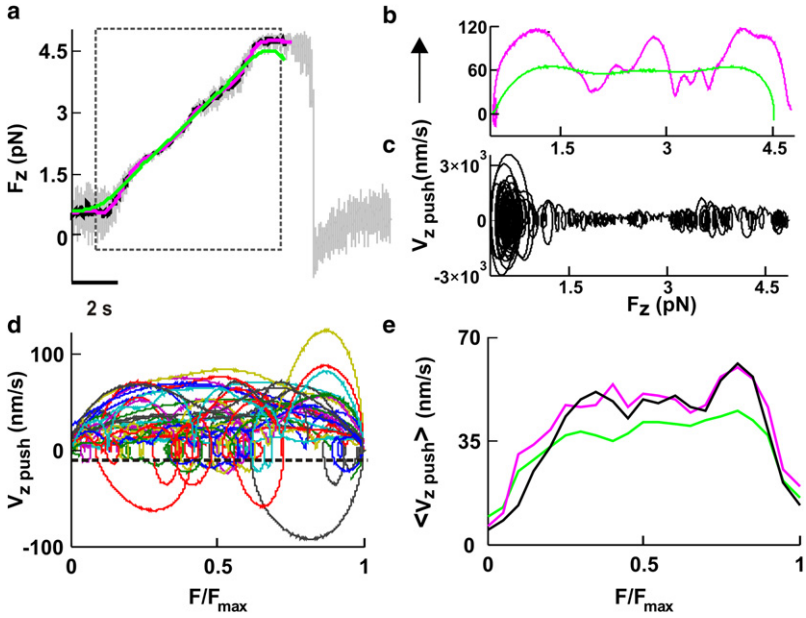


FIGURE 4 *Fv* relationships when lamellipodia lifted up the bead along the *z* direction. (*a*) The $F_z$ component of the force when the lamellipodium of Fig. 2 pushed the bead vertically. The dotted box indicates the section of force measurement used to compute the *Fv* relationship after Gaussian filtering at 0.2 (*green*), 1 (*pink*), and 10 Hz (*black*). (*b* and *c*) *Fv* relationships obtained after smoothing at 0.2 Hz (*b*, *green trace*) and 1 Hz (*b*, *pink trace*) and at 10 Hz (*c*). (*d*) Superimposed *Fv* relationships from 29 experiments normalized to $F_{max}$ from data filtered at 0.2 Hz. The black line represents $-3\sigma_v$ at the 0.2-Hz bandwidth (where $\sigma_v$ was calculated from bead fluctuations measured away from the lamellipodia). (*e*) $<Fv>_x$ relationships normalized to $F_{max}$. Data were filtered up to a bandwidth of *X* Hz. $<Fv>_{0.2}$ (*green*), $<Fv>_1$ (*pink*), and $<Fv>_{10}$ (*black*).

Lateral retractions (21 experiments): when the bead was displaced laterally after adhesion to lamellipodia (Fig. 2 *f*, *94–123 s* and Fig. 2 *g*, *95–110 s*).

The computation of *Fv* relationships from measured **x** and **F** requires careful data processing, as described in Materials and Methods (see Fig. 1). Before computing *Fv* relationships for the four stereotyped behaviors, it is necessary to analyze in detail the mechanics of collisions between beads and lamellipodia.

## Mechanics of collisions between beads and lamellipodia

When the lamellipodium leading edge (Fig. 3 *a*) pushed the bead (Fig. 3 *b*), $F_x$, $F_y$, and $F_z$ often change almost independently, reaching their maximum amplitude at different times (Fig. 3 *c*). In these cases, the bead moves along a trajectory that often changes its direction (Fig. 3 *f*, *black trace*). To investigate quantitatively the nature of these events, it is useful to monitor the vectors **F** and **v**, with their modulus and direction. The power dissipated by the lamellipodium is the scalar product $\mathbf{F} \cdot \mathbf{v}$. The amplitude of the instantaneous velocity depends on the bandwidth used for filtering the data, and $\mathbf{F} \cdot \mathbf{v}$ reaches values up to $2.5 \times 10^{-18}$ W when **v** is computed at a bandwidth of 0.2 Hz, but up to $10^{-16}$ W at a bandwidth up to 10 Hz (Fig. 3 *d*). The analysis of the angle $\phi$ between **F** and **v** provides information useful for understanding the mechanics of collision between beads and lamellipodia: when $\phi$ is close to 0 the lamellipodium pushes the bead and performs a positive work, and when $\phi$ is close to $\pi$, the lamellipodium retracts. When $\phi$ is close to $\pi/2$, lamellipodia do not carry out any work. A negligible work is performed primarily in two cases: first, when the lamellipodium exerts a force comparable to that caused by Brownian collisions with water molecules; and second, when the bead slides over the lamellipodium, **F** becomes orthogonal to **v**, and no work is done. The angle $\phi$ was determined by $\arccos(\mathbf{F} \cdot \mathbf{v}/|\mathbf{F}|\ |\mathbf{v}|)$ (Fig. 3 *e*). When the modulus of **F** was >2 pN, $\phi$ was usually close to either 0 or $\pi$ (Fig. 3 *h*), indicating that **F** and **v** have the same or opposite direction.

In contrast, when the modulus of **F** is <2 pN (Fig. 3 *g*), the value of $\phi$ is usually close to $\pi/2$. A sudden change of the bead motion (as shown in Fig. 3 *f*) could be caused either by a momentary sliding of the bead over the lamellipodium or by a transient retraction of the lamellipodium leading edge. The position of the lamellipodium was followed by video imaging with a CCD camera (see Fig. 3, *a* and *b*), and we could verify by visual inspection that the bead was always in contact with the lamellipodium leading edge. In addition, these two mechanisms can be easily distinguished by observing the work done: if the bead slides over the lamellipodium, no work is done and $\phi$ remains close to $\pi/2$. If, instead, the lamellipodium transiently retracts, the work done by the lamellipodium is negative, and $\phi$ remains close to $\pi$. Using this procedure, we verified that periods with negative velocity analyzed in Figs. 3–6, were indeed associated with values of $\phi$ close to $\pi$ and that therefore they were not caused by an occasional sliding of the bead but by transient retractions of the lamellipodium leading edge.

## During pushes, *Fv* relationships are flat only on average and growth alternates with transient retractions

When lamellipodia pushed the bead upward, they exerted forces up to 20 pN, and often only the $F_z$ component of the force changed (Fig. 2 *g*, *64–68.2 s*). In 5 of 42 vertical pushes, as in the experiment illustrated in Fig. 2 *g*, when

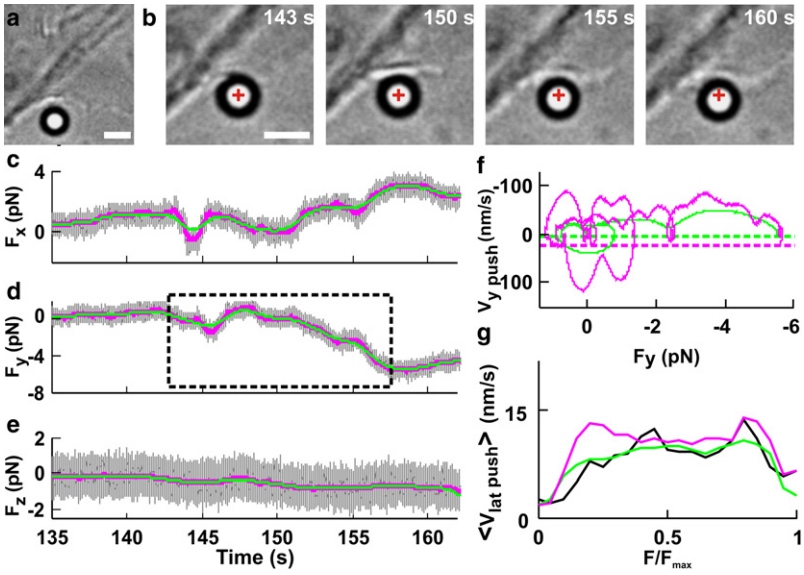


FIGURE 5 *Fv* relationships when a lamellipodium pushed the bead laterally along the *xy* direction. (*a*) Low-resolution image of a lamellipodium near the trapped bead. Scale bar, 2 $\mu$m. (*b*) Micrographs of the lamellipodium pushing the bead laterally during its protrusion. Images were taken at different times during force generation (see *c–e*). The cross indicates the center of the optical trap. Scale bar, 2 $\mu$m. (*c–e*) The three force components, $F_x$, $F_y$, and $F_z$ (*gray traces*), without filtering and after Gaussian filtering at 0.2 and 1 Hz (*green* and *pink traces*, respectively). The dotted box in *d* indicates the section of the recording used to compute the *Fv* relationships in *f*. (*f*) *Fv* relationships computed with Gaussian filtering at 0.2 and 1 Hz (*green* and *pink traces*, respectively) from a lateral component of the force $F_y$. Dotted green and pink lines represent $-3\sigma_v$ at the 0.2- and 1-Hz bandwidths, respectively (where $\sigma_v$ was calculated from bead fluctuations measured away from the lamellipodia). During the push, $F_y$ becomes negative, and transient retractions are therefore associated with positive velocities. (*g*) $<Fv>_x$ relationships normalized to $F_{max}$ from 22 experiments. Data were filtered up to a bandwidth of *X* Hz. $<Fv>_{0.2}$ (*green*), $<Fv>_1$ (*pink*), and $<Fv>_{10}$ (*black*).

the bead displacement was low-pass filtered at 0.2 Hz (Fig. 4 *a*, *green trace*), corresponding to a temporal averaging over a time window of 3–5 s, the computed velocity, $v_{z\ push}$, had little oscillations around an almost constant value. The obtained *Fv* relationship (Fig. 4 *b*, *green trace*), after an initial rise, was almost flat, indicating that the lamellipodium can increase the exerted force while lifting the bead away from the surface with an almost constant velocity. Nearly identical results were obtained when *Fv* relationships were computed from the modulus of **F** and not from a single component ($F_z$).

In 37 of 42 experiments, the *Fv* relationships exhibited transient periods where the velocity oscillated and could even reverse its direction, leading to the appearance of loops in *Fv* relationships (Fig. 4, *c* and *d*). We computed *Fv* relationships from the experiment of Fig. 4 *a* after smoothing at 0.2 (Fig. 4 *b*, *green trace*), 1 (Fig. 4 *b*, *pink trace*), and 10 Hz (Fig. 4 *c*). When data were smoothed at 1 and 10 Hz, the velocity oscillated around a constant value of ~60 nm/s, reaching occasional peak values from 0.12 (Fig. 4 *b*, *pink trace*) to 3 $\mu$m/s (Fig. 4 *c*), respectively.

The *Fv* relationships from individual experiments were normalized to $F_{max}$, defined as the maximal force beyond which the lamellipodium leading edge does not advance and the velocity is consistently negative for at least 10 s. Normalized *Fv* relationships, even those obtained from data filtered at 0.2 Hz, varied significantly in different experiments (Fig. 4 *d*), suggesting that force generation is not a deterministic but a probabilistic process. To characterize

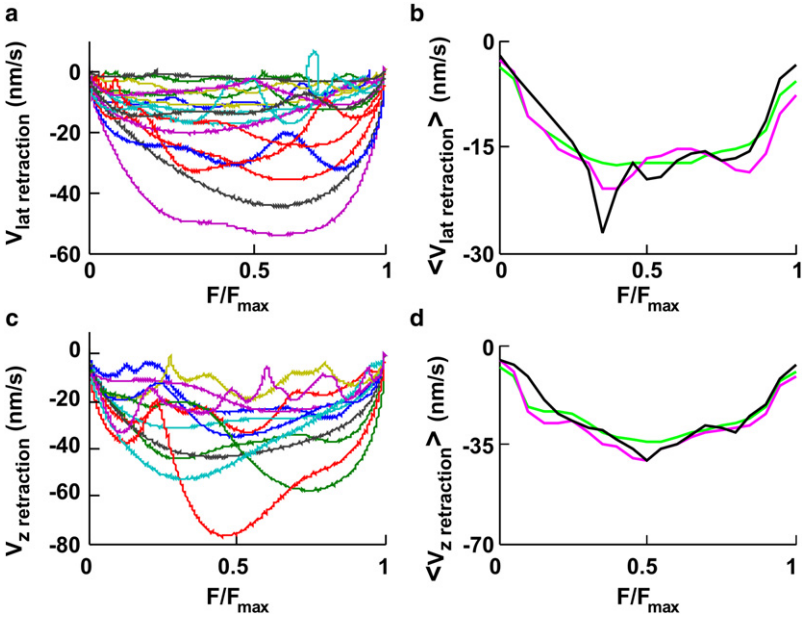


FIGURE 6 *Fv* relationships during retractions. (*a* and *c*) Superimposed *Fv* relationships from 18 lateral and 12 vertical retractions, respectively, from data filtered at 0.2 Hz. *F* is normalized to $F_{max}$. (*b* and *d*) $<Fv>_x$ relationships for lateral (21 experiments) and vertical (22 experiments) retractions, respectively. Data were filtered up to a bandwidth of *X* Hz. $<Fv>_{0.2}$ (*green trace*), $<Fv>_1$ (*pink trace*), and $<Fv>_{10}$ (*black trace*).

the underlying probabilistic dynamics, we determined average $Fv$ relationships, $<Fv>$, in vertical pushes for data filtered at 0.2, 1, and 10 Hz. The three average $Fv$ relationships exhibited the same overall behavior (Fig. 4 *e*), with the velocity increasing together with the force, up to ~65 nm/s, and remaining approximately constant up to $F_{max}$. Therefore, the $<Fv>$ for vertical pushes is flat.

In some experiments, the lamellipodium (Fig. 5 *a*) caused a pure lateral displacement (Fig. 5 *b*) so that only $F_x$ and $F_y$ changed appreciably (Fig. 5, *c* and *d*), whereas $F_z$ remained constant (Fig. 5 *e*). In $Fv$ relationships computed from these lateral pushes (Fig. 5 *f*), clear loops were detected, as observed in vertical pushes (Fig. 4, *c* and *d*).

The number of loops in the $Fv$ relationships computed for both the $F_x$ and $F_y$ components increased when the bandwidth of Gaussian filtering increased from 0.2 to 1 Hz (Fig. 5 *f*, *green* and *pink traces*, respectively). As in the case of the vertical push, normalized $Fv$ relationships for lateral pushes in individual experiments were different. $<Fv>$ relationships for lateral pushes filtered at 0.2, 1, and 10 Hz (Fig. 5 *g*) exhibited the same overall behavior, with a mean velocity of ~15 nm/s. As illustrated in the 3D representation of Fig. 2 *d*, a thin lamellipodium can grow under the bead without displacing it (see also Fig. S2); therefore, the measured mean velocity during lateral pushes could be lower than that for vertical pushes (65 nm/s) because fast lateral pushes of thin lamellipodia could not be measured.

### *Fv* relationships during retractions

Molecular mechanisms underlying both vertical and lateral pushes primarily involve actin filament polymerization, and it is not surprising that $<Fv>$ relationships for vertical and lateral pushes have a similar shape (compare Figs. 4 *e* and 5 *g*), but a different dynamics could be expected when the bead is pulled by a lamellipodium. Therefore, we computed $<Fv>$ relationships during vertical and lateral retractions.

Individual normalized $Fv$ relationships obtained during lateral and vertical retractions (Fig. 6, *a* and *c*) varied in different experiments. In 22 out of 22 vertical retractions, when data were filtered at 0.2 Hz, the velocity was consistently negative and did not change its direction. In contrast, during lateral retractions, the velocity transiently reversed its direction in 3 out of 21 experiments. $<Fv>$ relationships for retractions (Fig. 6, *b* and *d*) exhibited the same overall behavior, but with a mean velocity of about $-15$ and $-35$ nm/s for lateral and vertical retractions, respectively. Having observed that the lamellipodium leading edge could invert its velocity direction, we asked whether these transient inversions of the velocity had different properties during pushes and retractions, and whether they occurred more frequently near the maximal measured force, $F_{max}$. When data were filtered at 0.2 Hz, transient inversions of the velocity were evident for vertical and lateral pushes and for lateral retractions but completely absent for vertical retractions (Fig. 6 *c*). In contrast, at a bandwidth of 10 Hz, transient inversions were observed for vertical and lateral pushes and retractions (data not shown). The occurrence of a transient inversion of the velocity depends smoothly on $F/F_{max}$ (Fig. 4 *d*), indicating that transient retractions are not triggered by a strong load but originate from a random process.

## DISCUSSION

This study provides a precise characterization of force generation in DRG lamellipodia with millisecond time resolution and picoNewton sensitivity. Previous measurements made with the cantilever of an AFM were restricted to a temporal resolution in the second range and were obtained in migrating keratocytes producing forces in the nN range (22). Using optical tweezers, we measured force generation in DRG growth cones, and we could characterize several physical properties of the molecular network underlying force generation. As shown in Fig. 1 *a* (see Materials and Methods), relevant biological events occur on a timescale of <100 ms, and different dynamical properties are seen at a timescale of 3–5 s. Our results show that i), force generation is not a deterministic mechanism but follows a probabilistic process; ii), underlying dynamical events occur on different timescales varying from 100 ms to 5 s; iii), fast growths alternate with local retractions of the lamellipodium leading edge. These results give new insight on dynamical properties of force generation in neuronal growth cone lamellipodia and the biochemical network controlling them (10,31,32).

### Physical properties of force generation

The maximal force exerted by lamellipodia pushing on a bead with a diameter of 1 $\mu$m was ~20 pN (25). In some experiments, this force clearly stopped the lamellipodium growth and could be identified as the stall force, $F_{stall}$, i.e., the force capable of blocking protrusion. As lamellipodia very often retract spontaneously, in most experiments, $F_{stall}$ is expected to be larger than the measured maximum force, $F_{max}$. The contact area between pushing lamellipodia and beads was determined by the analysis of video images of the event under examination. For all frames $i$ corresponding to a detectable force measured with the QPD, we determined the arc $\Gamma_i$ of the bead in close contact with the leading edge of the lamellipodium and the corresponding angle $2\theta_i$ on the bead center (Fig. 7, *a–c*, *red*).

Then the contact surface at frame $i$, $S_c(i)$, is assumed to be equal to the corresponding spherical cap of the bead. Simple geometrical formulae indicate that $S_c(i) = 2\pi(1 - \cos\theta_i)r^2$, where $r$ is the bead radius. Fig. 7 *d* reproduces the time evolution of the estimated value of $S_c$ when a lamellipodium pushed a bead. The value of $S_c$ varied from 0.25 to 1.57 $\mu m^2$ (Fig. 7 *e*). Therefore, the maximal pressure exerted by DRG lamellipodia was 20–80 pN/$\mu m^2$. The maximum power/unit

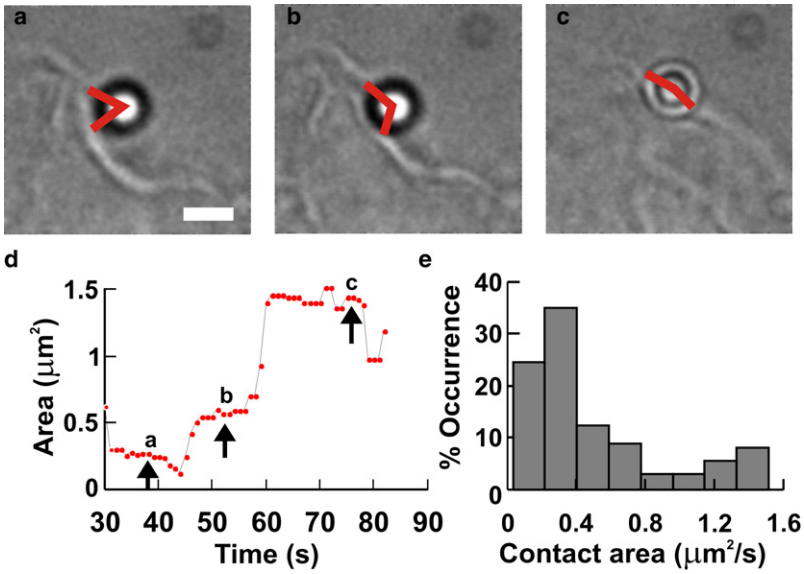


FIGURE 7 Contact area between a pushing lamellpodium and the bead. (*a–c*) Micrographs of a lamellipodium pushing the bead at different times (see timescale in *d*). Scale bar, 2 $\mu$m. Red angles drawn by eye. (*d*) Time evolution of estimated contact area, $S_c$, during the push. (*e*) Histograms of the value of $S_c$ obtained from four experiments during which a lamellipodium pushed the bead.

area exerted by lamellipodia was calculated to be 1-4 $\times$ $10^{-16}$ W/$\mu$m$^2$. Hydrolysis of one molecule of ATP provides energy of ~$10^{-19}$ J (33), and if this energy is converted into work with an efficiency of 60%, the hydrolysis of ~0.25–1 $\times$ $10^4$ s$^{-1}$ of ATP molecules/$\mu$m$^2$ is necessary to produce the measured power. The number of actin filaments in keratocyte and fibroblast lamellipodia has been estimated to be of the order of 100/$\mu$m$^2$ (22). Therefore, the number of elementary motors/$\mu$m$^2$ is likely to be of the order of 100, where each elementary motor consumes ~25–100 ATP molecules/s. These numbers should be compared with measurements obtained in the analysis undertaken in this study. One actin monomer is ~2 nm long, and if the consumption of one ATP is necessary for the addition of one actin monomer, actin filaments will grow at a velocity of 50–200 nm/s, very similar to the velocity of vertically pushing lamellipodia (Fig. 4). When these filaments elongate, the net protrusive force exerted across the membrane depends on a number of factors; in fact, when an actin monomer is added to an actin filament, an increase of the protrusive force depends on the angle between the filament and the membrane and on the rigidity of the membrane itself. Moreover, the observation that the load force necessary to stall the growth of a bundle of actin filaments is very similar to that for a single actin filament (34) indicates that the addition of actin monomers into nearby filaments does not necessarily lead to a linear summation of the protrusive force exerted by the polymerization of a single filament. As these factors could vary in different cells, it is not surprising that $F_{stall}$ in DRG lamellipodia, here reported, is smaller than the value of 2 nN observed in migrating keratocytes (22). In migrating keratocytes, the hydrodynamic load generated by a fluid flow producing an opposing force of just some pN/$\mu$m$^2$ arrests the forward movement of lamellipodia, suggesting that measurements of protrusive force at the leading edge are difficult to interpret because of the interplay between protrusion and adhesion (35).

The measure with optical tweezers here reported underestimates the velocity of protruding lamellipodia. The center of the bead is usually trapped at a distance varying from 600 to 900 nm from the underlying coverslip; as the radius of the bead is 500 nm, the height of the free space under the bead is between 100 and 400 nm. The height of protruding lamellipodia varies between 45 and 660 nm (Fig. 2 *b*), and thin lamellipodia therefore can grow below the bead without pushing it. This is the situation of many fast growing lamellipodia and is illustrated in Fig. S2 *a*, which shows a lamellipodium growing under the bead. In this experiment, and in several other cases, no significant bead displacement was measured (Fig. S2 *b*). We compared the maximal lateral velocity—obtained by the analysis of image sequences—in the same sample: the measured maximal lateral velocity of 15 thin protruding lamellipodia was 30 $\pm$ 22 nm/s and the same quantity for lamellipodia displacing a bead trapped in front of them was 15 $\pm$ 3 nm/s. The difference is ascribed to the larger protruding velocity of thin lamellipodia and the action of the bead-stalling protrusion. Therefore measured velocities in *Fv* relationships here reported are underestimated.

## *Fv* relationships

*Fv* relationships were computed for vertical (Fig. 4) and lateral pushes (Fig. 5) and for vertical and lateral retractions (Fig. 6). In all these cases, <*Fv*> relationships exhibited a flat shape, during which the mean velocity remained constant while the force increased. The mean velocity for vertical pushes and retractions was 65 and 35 nm/s respectively. Vertical pushes were usually faster than lateral pushes. However, the lower measured mean velocity for

lateral pushes could be caused by an experimental limitation of our measuring system: as illustrated in Fig. 2 *d* and Fig. S2, a fast-advancing lamellipodium with a height of <150 nm could grow under the bead without displacing it.

When position and force were filtered at 0.2 Hz, in some experiments, pushing lamellipodia exerted increasing force while maintaining a constant velocity (Fig. 4 *b*). In the great majority of the experiments performed, however, force generation was characterized by large fluctuations of the velocity. This observation shows that force generation in lamellipodia is probabilistic in nature and that only $<Fv>$ relationships (Fig. 4 *e*) exhibit a flat shape, during which the mean velocity remains constant while the force can increase. Therefore, autocatalytic models correctly describe force generation only in a mean approximation. In individual experiments, the velocity does not remain constant but oscillates and can change its direction. During these events, the actin filaments network retracts, possibly due to local catastrophe or organized depolymerization controlled by cofilin and other severing proteins (10). Therefore, force generation is not a smooth process but is characterized by a random alternation of fast growths and retractions of the lamellipodium leading edge.

### Possible mechanisms underlying transient inversions

What could be the mechanism underlying the unstable dynamics responsible for transient inversions of the velocity during growth and retraction? Several mechanisms could contribute to measured transient inversions of the velocity. In many experiments, we observed a combination of vertical and lateral pushes in which the bead could detach transiently from the lamellipodium leading edge. In our analysis, we carefully selected and analyzed pure lateral pushes during which we did not detect any vertical displacement. Indeed, in the experiment illustrated in Fig. 5, we did not measure any concomitant vertical shift at the time of the velocity reversal. In the reported $Fv$ relationships there was no significant correlation between lateral and vertical bead movement at the times of velocity reversal.

It is also possible that the bead slides locally on the lamellipodium surface because of an improper ''cupping'' around the bead and because of local inhomogeneity of the cell membrane. In several of the experiments where transient inversions of the velocity were measured, we observed a strong adhesion of the bead to the lamellipodium membrane. In these experiments, the bead remained sealed on the leading edge and when the lamellipodium retracted the bead was pulled away from the optical trap (Fig. 2 *f*, *102 s*). The possibility of local sliding is also addressed in Fig. 3. By analyzing the angle between the measured $F$ and $v$, we could rule out a possible local sliding of the bead at the time of the velocity reversal. In these conditions, movements of the bead are likely to be caused primarily by movements of the actin network operating behind the membrane.

As shown in Figs. 4 and 5, transient inversions of the velocity are more frequent during pushes than when the lamellipodia retract (Fig. 6). This observation suggests that different dynamics control push and retraction. During pushes, proteins controlling the network of actin filaments, such as cofilin, could randomly sever a large branch of actin filaments, leading to a local catastrophe and causing a transient retraction of the lamellipodium leading edge. When lamellipodia retract, a more global catastrophe of the network of actin filaments is likely to occur.

Although the occurrence of local catastrophes seems the most likely mechanism underlying local transient retractions, the complexity of biological events underlying force generation suggests a multiple origin of the observed events. Indeed, transient retractions could also be caused by the retrograde actin flow and contraction of myosin II (36,37). The driving force behind retrograde flow of actin originates from myosin II contractility and ''push'' of the plus-end of actin assembly at the lamellipodium leading edge (38). It is possible that a sudden increase of retrograde flow of actin and/or a burst of myosin II contractility, accompanied by lack of firm attachment to the coverslip, lead to a transient retraction of the lamellipodium leading edge.

Also, the mechanical interaction between the cellular membrane and the network of actin filaments could give rise to transient retractions. Growing and branching of the actin filaments can become unstable due to resistance from membrane tension. Indeed, the maximum measured force, $F_{max}$, is ~20–100 pN/$\mu$m$^2$, of the same order as the force exerted by a membrane with a surface tension, $\gamma$, equal to 0.005 $k_BT$/nm$^2$ axially deformed by 1 $\mu$m (39). The actin filament network is confronted with a membrane exerting a force similar to $F_{max}$, so that the actin filament network is only marginally stable and its propulsive force is almost counterbalanced by the membrane tension. Growing and retracting in conditions of marginal stability allows fast reactions and could provide lamellipodia with the flexibility necessary for their physiological functions.

The $Fv$ relationships reported here were obtained in intact neurons where protrusion and retraction are controlled by a sophisticated machinery, and it is somehow surprising that average $Fv$ relationships, $<Fv>$, are simple (Figs. 4–6).

## SUPPORTING MATERIAL

Two figures are available at http://www.biophysj.org/biophysj/supplemental/S0006-3495(09)05999-2.

This work was funded by the European Union Project N. 214566 NanoScale, within the FP7 Programme.

## REFERENCES

1. Solecki, D. J., E. E. Govek, and M. E. Hatten. 2006. mPar6 $\alpha$ controls neuronal migration. *J. Neurosci.* 26:10624–10625.

2. Ghashghaei, H. T., C. Lai, and E. S. Anton. 2007. Neuronal migration in the adult brain: are we there yet? *Nat. Rev. Neurosci.* 8:141–151.
3. Bray, D., C. Thomas, and G. Shaw. 1978. Growth cone formation in cultures of sensory neurons. *Proc. Natl. Acad. Sci. USA.* 75:5226–5229.
4. Goodman, C. S. 1996. Mechanisms and molecules that control growth cone guidance. *Annu. Rev. Neurosci.* 19:341–377.
5. Song, H. J., and M. M. Poo. 2001. The cell biology of neuronal navigation. *Nat. Cell Biol.* 3:E81–E88.
6. Mongiu, A. K., E. L. Weitzke, …, G. G. Borisy. 2007. Kinetic-structural analysis of neuronal growth cone veil motility. *J. Cell Sci.* 120:1113–1125.
7. Mogilner, A., and G. Oster. 1996. Cell motility driven by actin polymerization. *Biophys. J.* 71:3030–3045.
8. Suter, D. M., and P. Forscher. 2000. Substrate-cytoskeletal coupling as a mechanism for the regulation of growth cone motility and guidance. *J. Neurobiol.* 44:97–113.
9. Pollard, T. D., and G. G. Borisy. 2003. Cellular motility driven by assembly and disassembly of actin filaments. *Cell.* 112:453–465.
10. Pak, C. W., K. C. Flynn, and J. R. Bamburg. 2008. Actin-binding proteins take the reins in growth cones. *Nat. Rev. Neurosci.* 9:136–147.
11. Howard, J. 2001. Mechanics of Motor Proteins and the Cytoskeleton. Sinauer, Sunderland, MA.
12. Raucher, D., and M. P. Sheetz. 2000. Cell spreading and lamellipodial extension rate is regulated by membrane tension. *J. Cell Biol.* 148: 127–136.
13. Fletcher, D. A., and J. A. Theriot. 2004. An introduction to cell motility for the physical scientist. *Phys. Biol.* 1:T1–T10.
14. Carlsson, A. E. 2001. Growth of branched actin networks against obstacles. *Biophys. J.* 81:1907–1923.
15. Peskin, C. S., G. M. Odell, and G. F. Oster. 1993. Cellular motions and thermal fluctuations: the Brownian ratchet. *Biophys. J.* 65:316–324.
16. Mogilner, A., and G. Oster. 2003. Force generation by actin polymerization II: the elastic ratchet and tethered filaments. *Biophys. J.* 84: 1591–1605.
17. Carlsson, A. E. 2003. Growth velocities of branched actin networks. *Biophys. J.* 84:2907–2918.
18. Dickinson, R. B., L. Caro, and D. L. Purich. 2004. Force generation by cytoskeletal filament end-tracking proteins. *Biophys. J.* 87:2838–2854.
19. Mogilner, A. 2006. On the edge: modeling protrusion. *Curr. Opin. Cell Biol.* 18:32–39.
20. Marcy, Y., J. Prost, …, C. Sykes. 2004. Forces generated during actin-based propulsion: a direct measurement by micromanipulation. *Proc. Natl. Acad. Sci. USA.* 101:5992–5997.
21. Parekh, S. H., O. Chaudhuri, …, D. A. Fletcher. 2005. Loading history determines the velocity of actin-network growth. *Nat. Cell Biol.* 7:1219–1223.
22. Prass, M., K. Jacobson, …, M. Radmacher. 2006. Direct measurement of the lamellipodial protrusive force in a migrating cell. *J. Cell Biol.* 174:767–772.
23. Bustamante, C., J. C. Macosko, and G. J. L. Wuite. 2000. Grabbing the cat by the tail: manipulating molecules one by one. *Nat. Rev. Mol. Cell Biol.* 1:130–136.
24. Neuman, K. C., and S. M. Block. 2004. Optical trapping. *Rev. Sci. Instrum.* 75:2787–2809.
25. Cojoc, D., F. Difato, …, V. Torre. 2007. Properties of the force exerted by filopodia and lamellipodia and the involvement of cytoskeletal components. *PLoS One.* 2:e1072.
26. Gittes, F., and C. F. Schmidt. 1998. Interference model for back-focal-plane displacement detection in optical tweezers. *Opt. Lett.* 23:7–9.
27. Kress, H., E. H. K. Stelzer, G. Griffiths, and A. Rohrbach. 2005. Control of relative radiation pressure in optical traps: application to phagocytic membrane binding studies. *Phys. Rev. E.* 71:061927.
28. Bertero, M., T. A. Poggio, and V. Torre. 1988. Ill-posed problems in early vision. *Proc. IEEE.* 76:869–889.
29. Heidemann, S. R., P. Lamoureux, and R. E. Buxbaum. 1990. Growth cone behavior and production of traction force. *J. Cell Biol.* 111:1949–1957.
30. Kress, H., E. H. K. Stelzer, …, A. Rohrbach. 2007. Filopodia act as phagocytic tentacles and pull with discrete steps and a load-dependent velocity. *Proc. Natl. Acad. Sci. USA.* 104:11633–11638.
31. Weiner, O. D., W. A. Marganski, …, M. W. Kirschner. 2007. An actin-based wave generator organizes cell motility. *PLoS Biol.* 5:2053–2063.
32. Lacayo, C. I., Z. Pincus, …, J. A. Theriot. 2007. Emergence of large-scale cell morphology and movement from local actin filament growth dynamics. *PLoS Biol.* 5:2035–2052.
33. Bray, D. 1992. Cell Movements. Garland, New York.
34. Footer, M. J., J. W. J. Kerssemakers, …, M. Dogterom. 2007. Direct measurement of force generation by actin filament polymerization using an optical trap. *Proc. Natl. Acad. Sci. USA.* 104:2181–2186.
35. Bohnet, S., R. Ananthakrishnan, …, A. B. Verkhovsky. 2006. Weak force stalls protrusion at the leading edge of the lamellipodium. *Biophys. J.* 90:1810–1820.
36. Rochlin, M. W., K. Itoh, …, P. C. Bridgman. 1995. Localization of myosin II A and B isoforms in cultured neurons. *J. Cell Sci.* 108:3661–3670.
37. Brown, M. E., and P. C. Bridgman. 2003. Retrograde flow rate is increased in growth cones from myosin IIB knockout mice. *J. Cell Sci.* 116:1087–1094.
38. Medeiros, N. A., D. T. Burnette, and P. Forscher. 2006. Myosin II functions in actin-bundle turnover in neuronal growth cones. *Nat. Cell Biol.* 8:215–226.
39. Atilgan, E., D. Wirtz, and S. X. Sun. 2006. Mechanics and dynamics of actin-driven thin membrane protrusions. *Biophys. J.* 90:65–76.

## 2.2

# The elementary events underlying force generation in neuronal lamellipodia

L. Amin*****, E. Ercolini*****, R. Shahapure*****, G. Bisson, V. Torre,
Scientific Reports. 1, 153; DIO:10.1038/srep00153 (2011)
(***** Equally contributed)

SCIENTIFIC REPORTS

OPEN

SUBJECT AREAS:
CELL GROWTH
CELLULAR NEUROSCIENCE
BIOPHYSICS
DIFFERENTIATION

Received
13 May 2011

Accepted
14 October 2011

Published
11 November 2011

Correspondence and requests for materials should be addressed to V.T. (torre@sissa.it)

* These authors equally contributed and their names are in alphabetical order

† Present address: Leiden Institute of Chemistry, Molecular Genetics, Leiden, The Netherlands

# The elementary events underlying force generation in neuronal lamellipodia

Ladan Amin[1]*, Erika Ercolini[1,2]*, Rajesh Shahapure[1]*†, Giacomo Bisson[1] & Vincent Torre[1,3]

[1]Neurobiology Sector, International School for Advanced Studies (SISSA), IT-34136 Trieste, Italy, [2]Cluster in Biomedicine (CBM), Area Science Park Basovizza, IT-34012 Trieste, Italy, [3]Italian Institute of Technology (IIT), SISSA Unit, IT-34136 Trieste, Italy.

**We have used optical tweezers to identify the elementary events underlying force generation in neuronal lamellipodia. When an optically trapped bead seals on the lamellipodium membrane, Brownian fluctuations decrease revealing the underlying elementary events. The distribution of bead velocities has long tails with frequent large positive and negative values associated to forward and backward jumps occurring in 0.1–0.2 ms with varying amplitudes up to 20 nm. Jump frequency and amplitude are reduced when actin turnover is slowed down by the addition of 25 nM Jasplakinolide. When myosin II is inhibited by the addition of 20 μM Blebbistatin, jump frequency is reduced but to a lesser extent than by Jasplainolide. These jumps constitute the elementary events underlying force generation.**

Force generation is a fundamental process at the basis of cell motility[1] allowing neurons to explore the environment. Neuronal growth cones are the major motile structures located at the neurite tips[2] and are composed of lamellipodia and filopodia[3]. Lamellipodia are extended structures, from which filopodia emerge with a finger-like shape[4]. Their motion is essential during morphogenesis and for neuronal differentiation when their exploratory motion allows neurons to find the appropriate synaptic connections. Force generation is thought to be originating from the progressive addition of actin molecules to the existing network of actin filaments[5] and to be determined by the balance between actin polymerization and depolymerisation, modulated by controlling proteins[6] and by chemical and mechanical receptors coupled to the cytoskeleton[6–8]. However, very little is known about the elementary events underlying force generation.

Actin polymerization has been primarily investigated *in vitro* by analysing the rate of elongation of isolated actin filaments. These investigations were performed with a low time resolution, often of the order of some tens of seconds and with a sensitivity of some hundreds of nm, providing values for actin polymerization rate ranging between 11.6 and 38 (1/μM s)[9–12].

Previous investigations *in vivo* using Atomic Force Microscopy[13] and opposing liquid flow[14] were limited to a temporal resolution in the 100 ms range and sensitivity of 50–100 pN. These experimental limitations can be overcome by using optical tweezers[15,16], providing a ms resolution and pN sensitivity. In order to detect small displacements in the order of 2–5 nm it is necessary to reduce all perturbations by minimizing mechanical vibrations and performing the experiments under remote conditions (see Methods). By using these procedures, we have previously shown that force generation is not a deterministic mechanism but follows a probabilistic process and that underlying dynamical events occur on different time scales varying from 100 ms to 5 s[17].

For this study we have used optical tweezers to identify the elementary events underlying force generation. When an optically trapped bead seals on the lamellipodium membrane, Brownian fluctuations are drastically reduced revealing the fine structure of force generation: when a lamellipodium pushes a trapped bead, the autocorrelation function $\rho(t)$ of the bead position decays with multiple time constants up to 50 ms, while during Brownian fluctuations $\rho(t)$ decays with a single time constant less than 1 ms. The distribution of bead velocities has long tails with frequent large positive and negative values associated to forward and backward jumps occurring in 0.1–0.2 ms. These jumps have varying amplitudes up to 20 nm and their frequency and amplitude are reduced when actin turnover is slowed down by the addition of Jasplakinolide[18] and when the action of myosin II is inhibited by the addition of Blebbistatin[19,20]. These jumps constitute the elementary events underlying force generation.

## Results

Neurons from dorsal root ganglia (DRG) of P10–P12 rats were isolated and plated on poly-L-lysine-coated glass coverslips, positioned on the stage of an inverted microscope used for imaging and force measurement[17] (see

Methods). After 24 to 48 hours, lamellipodia emerged from DRG soma. Silica beads with a diameter of 1 μm were trapped with an infrared (IR) optical tweezer in front of the lamellipodia (Fig. 1a and f): when the lamellipodia protruded and displaced the bead, the exerted force $\boldsymbol{F} = (F_x,F_y,F_z)$ was measured with sub pN sensitivity at 10 kHz resolution. The bead position $\boldsymbol{x} = (x,y,z)$ was measured with a quadrant position detector (QPD) using back focal plane (BFP) interferometry[16,21]. Lamellipodia grew by 1 μm within 20–30 s and displaced the beads trapped with a low ($k_x$ and $k_y$ equal to 0.0155 pN/nm, and $k_z$ equal to 0.005 pN/nm) and a high stiffness ($k_x$, and $k_y$ equal to 0.1 pN/nm and, $k_z$ equal to 0.03 pN/nm; Fig. 1a–e). The QPD detects reliably lateral displacements less than 250 nm (see Methods) and bead displacements within this range were observed with the high trap stiffness. Often lamellipodia pushed the bead both laterally and axially (Fig. 1f–h) and recordings of the bead position became noisier (Fig. 1k). In contrast, when adhesion forces caused the bead to seal onto the cellular membrane of retracting lamellipodia (Fig. 1i–j) Brownian fluctuations decreased (Fig. 1k). If growth cones were fixed with paraformaldehyde, suppressing all cellular motility, no noise increase was observed (see Supplementary Methods and Supplementary Fig. S1 online).

During adhesion, the variance ($\sigma_x^2,\sigma_y^2,\sigma_z^2$) could decrease by 5–10 times reaching values below 10 nm$^2$ (Fig. 1m) so that the fine structure of force generation could be observed. The amplitude of the adhesion force $\boldsymbol{F_{ad}}$ was measured as the maximal force before the bead returned into the trap[22–24] (Fig. 1l). Large values of $\boldsymbol{F_{ad}}$ reduced more Brownian fluctuations (Fig. 1n). If $\boldsymbol{F_{ad}}$ is larger than 30 pN, i.e. the maximal restoring force of the optical trap, when the

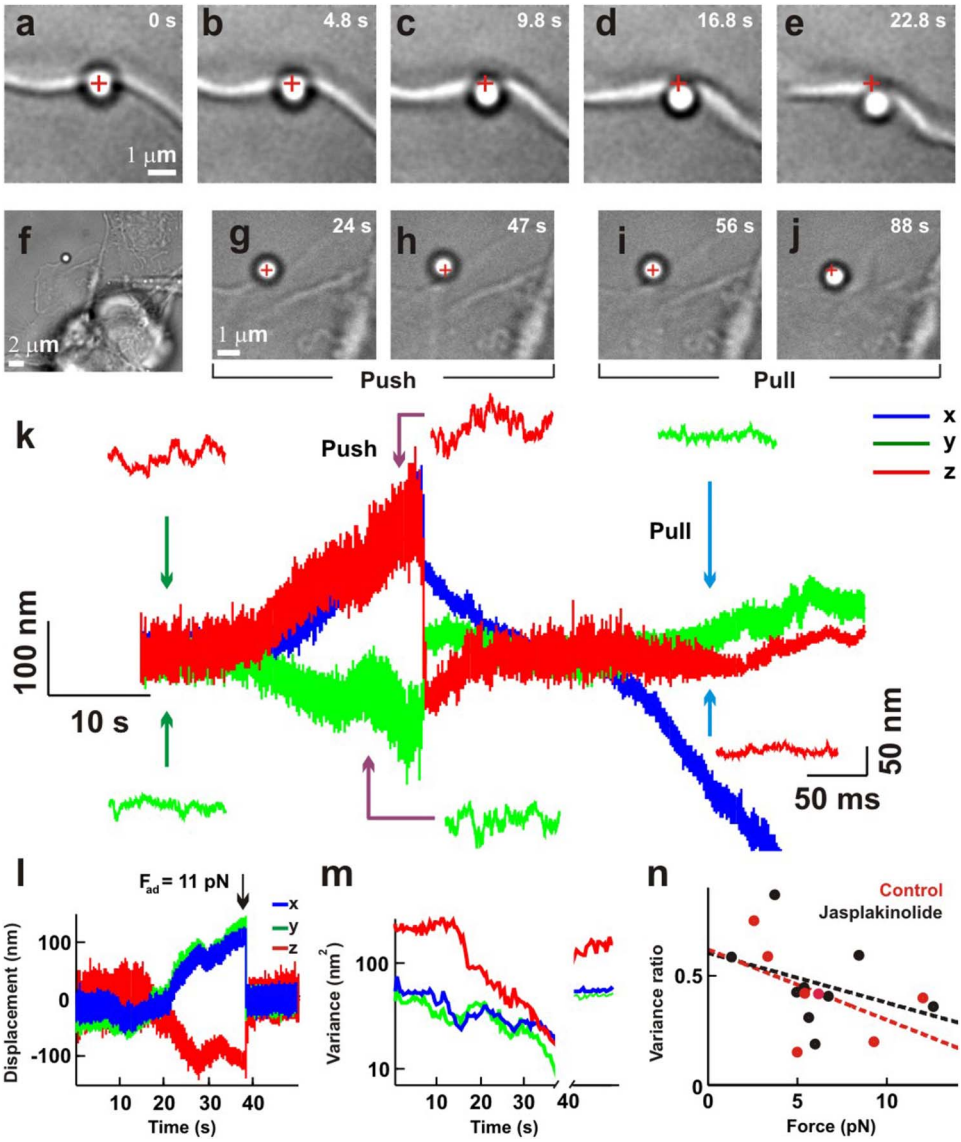


**Figure 1 | During a push, recordings of the bead position become noisier, but not during a pull.** (a)–(e) The protruding leading edge of a lamellipodium pushes an optically trapped bead by 1 μm within 25 s. (f) A bead trapped in front of a lamellipodium emerging from the soma of a DRG neuron. (g)–(h) High resolution images during a push. At 24 s the bead is in the optical trap (g) and when the lamellipodium grows, it pushes the bead (47 s) displacing it both laterally and axially (h). (i)–(j) As in (g–h) but during a pull. When the lamellipodium retracted, the bead returned inside the trap (56 s). Following bead adhesion, the bead was pulled away from the trap (88 s). Crosses indicate the centre of the optical trap. (k) The three components (x,y,z) of the bead displacement. Insets highlight the increase of noise during the push (violet arrows), the decrease of noise during the pull (cyan arrows), and green arrows refer to Brownian fluctuations. (l) The three components (x,y,z) of bead displacement during adhesion and retraction in another experiment. At 38 s the bead returned into the trap and the adhesion force was measured (11 pN). (m) Change of variance for the three components in (l). (n) Relation between fractional variance reduction and modulus of adhesion force in control conditions (red symbols) and in the presence of 25 nM Jasplakinolide (black symbols). The red and black lines represent the linear fit in control conditions and Jasplakinolide, respectively.

lamellipodium retracts or vigorously protrudes it could move the bead out of the trap. The bonding of a single integrin molecule to the lamellipodium leading edge is larger than 40 pN[25] and therefore, when integrin molecules cause adhesion, the bead is strongly attached and will follow the lamellipodium motion also out of the optical trap. During adhesion, the power spectrum density (PSD) of Brownian fluctuations was fitted by the sum of two or three Lorentzian distributions (see Supplementary Methods and Supplementary Fig. S1 online).

**When actin turnover is reduced no noise increase is observed.** During a push the variance of bead displacement increased by 2–4 times (Figs 1k and 2a) possibly because of modifications of the trap stiffness, fluctuations of adhesion forces or properties of force generation. The addition of 100 nM Jasplakinolide, known to reduce actin turnover[18] almost completely abolished force generation, but a lower concentration of 25 nM slowed down growth cone motion without blocking force generation. In the presence of 25 nM Jasplakinolide, lamellipodia were still able to displace beads laterally, but no increase of variance was observed (compare Fig. 2a and b). We computed the relation between the lateral component of the force ($F_x$ or $F_y$) and the associated changes of variance $\sigma_I^2$. In the presence of 25 nM Jasplakinolide, $\sigma_I^2$ never increased (grey black traces in Fig. 2d; n= 9), but often decreased. On the contrary, in control conditions, $\sigma_I^2$ increased by 2–4 times (red orange traces in Fig. 2d; n= 13). During protrusion the maximal average velocity $<v_{max}>$ was 50 nm/s (n = 24), whereas in the presence of Jasplakinolide it was 35 nm/s (n =15)[17]. The mean value of the modulus of $F_{ad}$ in control conditions was 6.2± 3.3 pN (n=7) and in the presence of 25 nM Jasplakinolide was 6.1± 3.1 pN (n=9) suggesting that adhesion between the bead and the lamellipodium is not affected by Jasplakinolide. Bead displacements and exerted forces were very similar in control conditions and in the presence of 25 nM Jasplakinolide suggesting that the observed variance increase is not caused by local changes of trap stiffness but it is a genuine property of force generation.

**When myosin II is inhibited force generation occurs with a reduced noise increase.** The molecular motor myosin II plays an important role in force generation by speeding up actin filament disassembly[26] and therefore we analysed the effect of Blebbistatin a well known inhibitor of myosin II[19,20]. The addition of 20 μM Blebbistatin slowed down lamellipodia motion, but did not abolish force generation (Fig. 2c). During lateral push, however, $\sigma_I^2$ did not increase by more than 100 % and in some cases (2 out of 6; blue traces in Fig. 2d) decreased, but not as observed with Jaslpakinolide (Fig. 2d).

**The increase of noise is related to the contact area between the bead and the lamellipodium leading edge.** The area in direct contact $A_c$ with a silica bead with a diameter of 1 μm could vary from less than 0.1 to up to 1.5 $\mu m^2$ [17]. This contact area mediates all mechanical interactions between the bead and force generation mechanisms inside lamellipodia. Therefore we have analysed the relation between $A_c$ and the amplitude of generated force F and associated changes of variance $\sigma_I^2$. In control conditions, during a lateral push it is possible to measure reliably changes of $A_c$ and when $A_c$ increases (Fig. 3a) we have often (7 out of 10 experiments) observed a concomitant increase of F (Fig. 3b) and of $\sigma_I^2$ (Fig. 3c). When the bead went out of the optical trap (broken vertical line) the $A_c$ - obtained from videomicrographs – remained constant or increased while measurements of F and of $\sigma_I^2$ are not reliable. Therefore, the increase of $\sigma_I^2$ observed during lateral pushes is caused by the combined effect of force generation and of the associated increase of $A_c$. $A_c$ is measured through the objective of the microscope, viewing axially the lamellipodium, therefore we were not able to determined changes of $A_c$ during a vertical push.

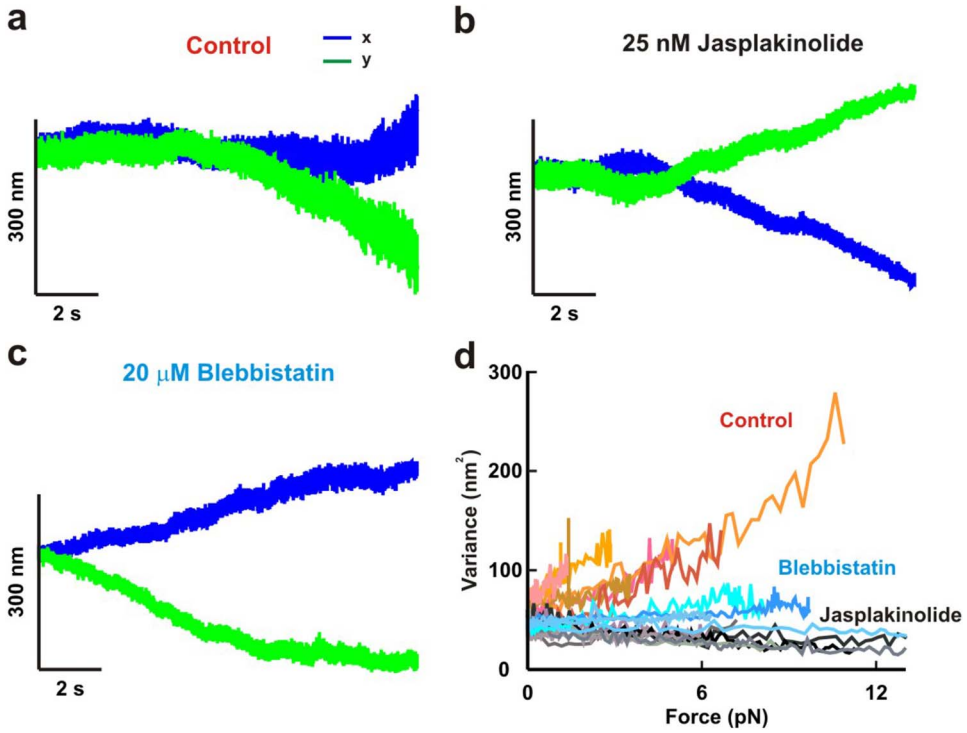


**Figure 2 | Change of noise in control conditions, in the presence of Blebbistatin and in the presence of Jasplakinolide.** (a) The longitudinal components of the bead displacement during a lateral push in control conditions showing a clear noise increase. (b) As in (a) but in the presence of 25 nM Jasplakinolide. No noise increase is observed. (c) As in (a) but in the presence of 20 μM Blebbistatin. In this case $\sigma_I^2$ slightly increased in 4 out of 6 cases. In 2 out of 6 cases $\sigma_I^2$ decreased but to a lesser extent in comparison to Jasplakinolide. (d) Relation between force and variance for lateral push in control conditions (red shades), in the presence of 20 μM Blebbistatin (blue shades) and 25 nM Jasplakinolide (black shades).

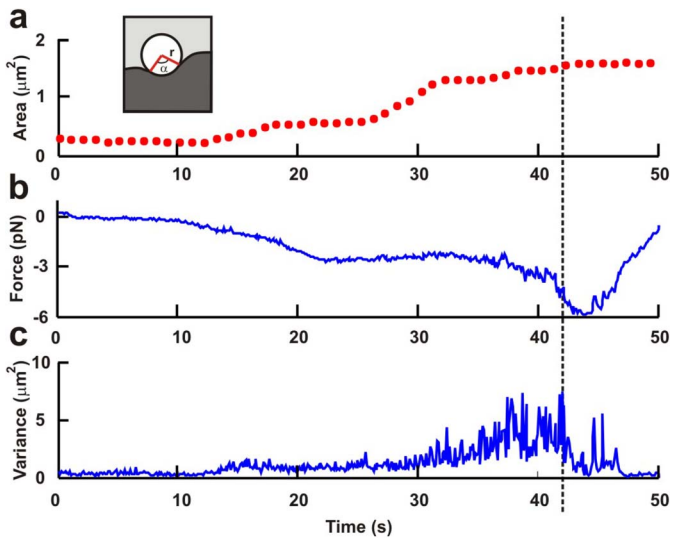


**Figure 3 | Concomitant change of variance and contact area during force generation.** (a) Time evolution of estimated contact area $A_c$ (see Ref. 17) between the bead and the lamellipodium leading edge, $A_c$, during a push. $A_c$ at frame i, $A_c(i)$, is calculated as $A_c(i) = 2\pi\,[1-\cos(\alpha_i/2)]\,r^2$, where $\alpha_i$ is the angle corresponding to the arc of the bead in close contact with the leading edge of the lamellipodium and r is the bead radius, as shown in the inset, representing a lamellipodium pushing the trapped bead. (b) Concomitant time evolution of the force exerted by the lamellipodium during the push analyzed in (a). (c) Concomitant time evolution of the variance during the push analyzed in (a). The broken vertical line indicates the time when the bead is pushed out of the trap.

**Properties of noise during pushes.** Following adhesion, in several experiments (n=4 in control conditions; n=6 with Jasplakinolide; n=5 with Blebbistatin) the variance of the axial component, $\sigma_a^2$, decreased to less than 6 nm$^2$ (Fig. 4a) and subsequently, when the lamellipodium pushed the bead, $\sigma_a^2$ increased and fluctuations with novel properties appeared.

Visual inspection indicated the existence of rapid discontinuities, i.e. of jumps. Therefore, we computed the bead velocity v (Fig. 4b), by convolution of bead position with the derivative of a Gaussian function, $(-t/((2*\pi)^{1/2}*a^3)\exp(-t^2/2*a^2)$ with a value of *a* varying from 0.2 to 0.4 ms. During Brownian fluctuations, velocities had a Gaussian distribution (Fig. 4c) but not during a push (Fig. 4d): indeed their distribution had a central lobe fitted by a Gaussian distribution, but had also long tails with large positive and negative values. These sudden changes of velocity correspond to forward ($j^+$) and backward ($j^-$) jumps. Similar tails, but less pronounced, could be detected also when force generation was not preceded by adhesion. During Brownian fluctuations the autocorrelation function $\rho_{zz}(t)$ of bead displacement decayed with a single time constant θ of 0.64 ± 0.12 ms (n=20), but during pushes $\rho_{zz}(t)$ decayed with multiple time constants varying from less than 1 ms up to 50 ms (Fig. 4e). During force generation, fluctuations in three coordinates (x,y,z) were more correlated: during Brownian fluctuations the cross-correlation $\rho_{zl}(t)$ between z and one lateral component (x or y) decayed with a time constant θ of 0.62 ± 0.15 ms (black traces in Fig. 4g), but during a push the value of θ increased to 6.0 ± 1.4 ms (red traces in Fig. 4g). The increase of the time constant θ of $\rho_{zz}(t)$ and $\rho_{zl}(t)$ observed during a push was attenuated by 25 nM Jasplakinolide (black trace in Fig. 4f and red traces in Fig. 4h).

All these observations indicate that: i- fluctuations observed during pushes do not originate from thermal motion but are caused by the randomness of the elementary events underlying force generation; ii - molecular mechanisms underlying force generation are

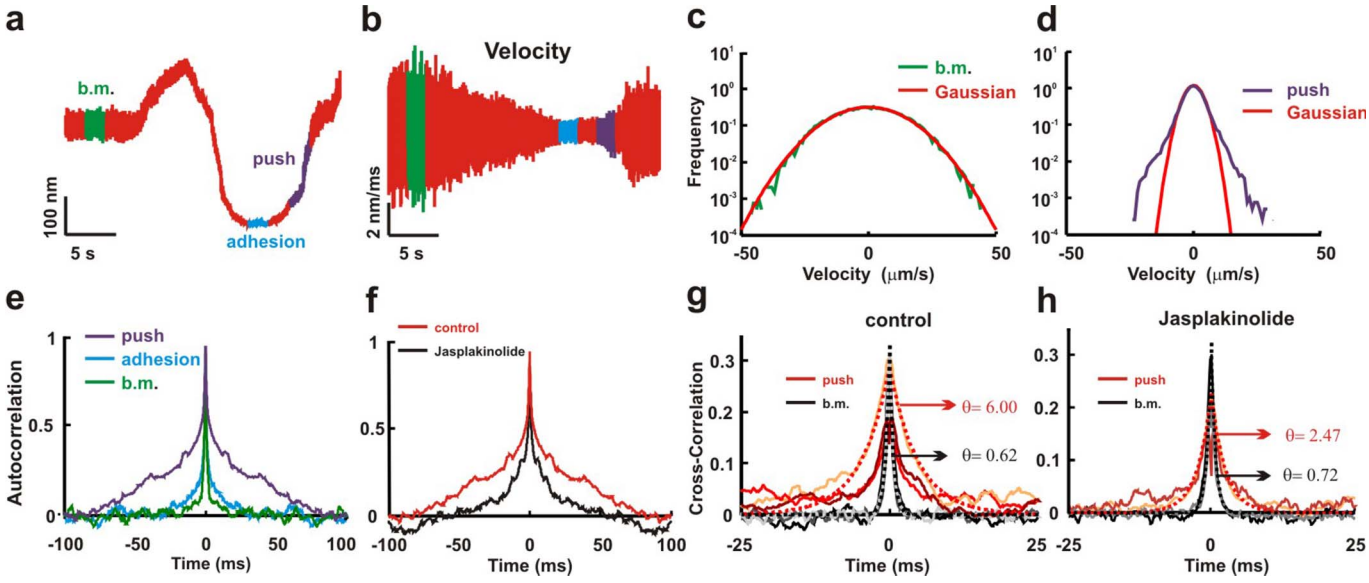


**Figure 4 | During pushes the autocorrelation function ρ(t) of bead position decays with multiple time constants and the distribution of bead velocities has long tails.** (a) The z component of the bead displacement during Brownian fluctuations (b.m), adhesion and push. (b) Velocity of bead displacement in (a). (c) Distribution of velocities during Brownian fluctuations shown in (b). A Gaussian function (red line) fits perfectly the experimental distribution. (d) As in (c) during the push shown in (b). (e) Autocorrelation function of vertical bead displacement $\rho_{zz}(t)$, during Brownian fluctuations, adhesion, and push after high pass filtering with a cut-off frequency at 1 Hz (see Supplementary Methods and Supplementary Fig. S2 online). $\rho_{zz}(t)$ decays with a time constant θ equal to 0.64 ms during b.m. but, during pushing, it has multiple time constants up to 50 ms. (f) The effect of 25 nM Jasplakinolide on $\rho_{zz}(t)$, during pushing (black). The longest time constant of the auto-correlation decreases to 20 ms (red trace). (g) Cross-correlation $\rho_{zx}(t)$ during b.m. (black shades) and during a push (red shades). $\rho_{zx}(t)$ decays with a time constant θ equal to 0.62 ms during b.m. and increases to 6.0 ms during a push. (h) The effect of 25 nM Jasplakinolide on $\rho_{zx}(t)$ during pushing. $\rho_{zx}(t)$ decays with a time constant θ equal to 0.72 ms during b.m. and increases to 2.47 ms during a push.

spatially coherent and structured; iii- force generation is characterized by jumps.

**Jumps underlie force generation.** Among the vast repertoire of algorithms used to detect jumps, we adopted a nonlinear diffusion filtering[27,28], approximating the original data (grey traces in Fig. 5a, b and c) with a smooth piece-wise function (red lines) interrupted by $j^+$ or $j^-$ jumps (black vertical segments). This algorithm depends on two parameters (see Methods): the contrast λ, related to the smallest detectable jump, and the scale τ determining the temporal window. In order to establish our sensitivity and to determine the values of λ and τ we attached a silica bead to the bottom of a coverslip which was moved by a piezo manipulator. When the variance of displacement fluctuations of the stuck bead was 3.8 $nm^2$, as during adhesion (Fig. 4a), with the values of 0.5 nm and 0.1 ms for λ and τ respectively, we could detect jumps of 2 nm. With these values of λ and τ, the algorithm detected jumps primarily during pushes (Fig. 5a, b and c).

Immediately after adhesion during the push, (Figs 4a and 5a), we detected forward $j^+$ and backward $j^-$ jumps ranging from 2 to 20 nm (Fig. 5d). Jumps were observed only when lamellipodia pushed the bead, but very rarely when beads sealed on the lamellipodia membrane and retracted, suggesting that jumps do not reflect unspecific attachment/detachment events between the lamellipodium and the substratum and/or between the actin network and the membrane. Jumps lower than 2 nm could not be detected because of noise limitations. These jumps appear to be the elementary events underlying force generation in neuronal lamellipodia.

Distributions of jumps amplitude in control conditions (Fig. 5d) were fitted by the exponential distributions $A_+ \, e^{-(j+/j+*)}$ and $A_- \, e^{-(j-/j-*)}$ with values of 5.2±1.3 and 4.9±1.2 nm for the mean size of positive $j^+*$ and negative jumps $j^-*$ (n=4). In the presence of 25 nM Jasplakinolide (Fig. 5c) smaller jumps (Fig. 5f) ranging from 2 to 8 nm were detected (n=6) and jump distributions were fitted by the same exponential distributions but with lower values of $j^+$ and $j^-$ equal to 2.4±0.3 and 2.2±0.4 nm, similar in size to the polymerization step size (2.7 nm). If Jasplakinolide is reducing jump frequency by stiffening the connection between the lamellipodium and the bead, it is expected also to modify the adhesion force between the bead and the lamellipodium, but this was not observed

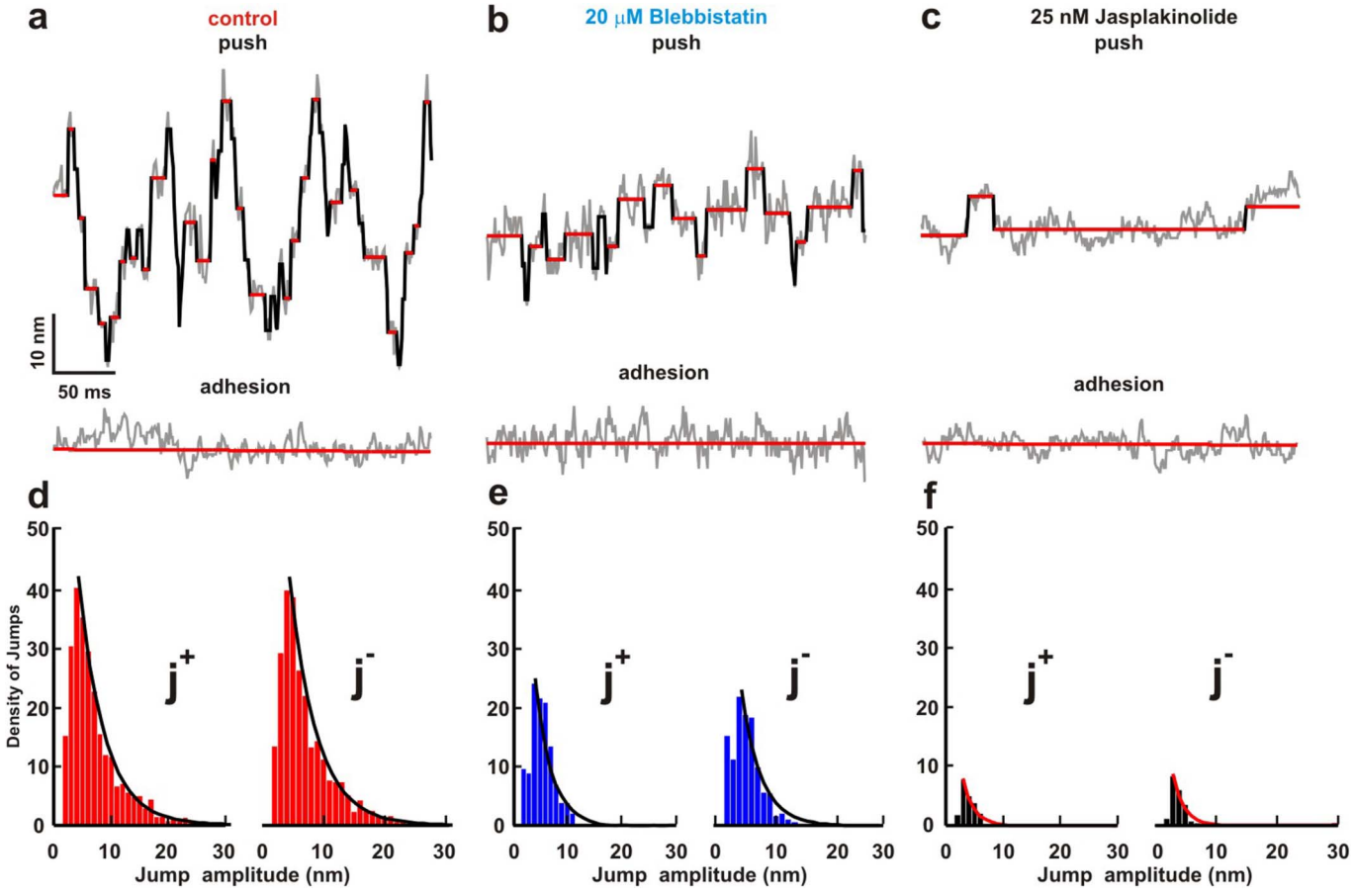


**Figure 5 | Forward and backward jumps are the elementary events underlying force generation.** (a) Magnification of the z component of Fig. 4a during adhesion and push. Original traces in grey were filtered by the non linear diffusion algorithm (see Methods) providing a smooth component (red curves) and jumps (in black). Very few jumps were detected during adhesion but they could be observed very often during a push. (b) Magnification of the z component during adhesion and push in the presence of 20 μM Blebbistatin. The original traces (in gray) were filtered as in (a). Jumps with smaller amplitude than in control conditions were detected. (c) As in (a) and (b) in the presence of 25 nM Jasplakinolide. In this case jumps with an amplitude smaller than the amplitude obtained both in control conditions and in the presence of Blebbistatin were detected. (d)–(f) Density of upward $j^+$ and downward $j^-$ jumps during push in control conditions (d), in the presence of Blebbistatin (e), and Jasplakinolide (f). These distributions of jump amplitude were fitted (black lines in (d) and (e), red lines in (f)) - for values of $j^+$ and $j^-$ larger than 2 nm-by the exponential distributions $A_+ \, e^{-(j+/j+*)}$ and $A_- \, e^{-(j-/j-*)}$. The fitting was performed with the values of of 129 and 128 events/s for the jump frequency of positive and negative jumps, $A_+$ and $A_-$, respectively, and 5 and 4.8 nm for the mean size of positive and negative jumps, $j^+*$ and $j^-*$, respectively (d). In the presence of Blebbistatin the values of $A_+$, $A_-$, $j^+*$ and $j^-*$ were 87 and 80 events/s and 3.5 and 3.3 nm, respectively (e). In the presence of Jasplakinolide the values of $A_+$, $A_-$, $j^+*$ and $j^-*$ were 44 and 50 events/s and 2.5 and 2.3 nm, respectively (f).

experimentally (Fig. 1n). Therefore, the effect of Jasplakinolide on jump frequency is likely to be caused by a reduced actin turnover. In the presence of 20 μM Blebbstatin (Fig. 5b) detected jumps have an amplitude ranging from 2 to 15 nm (n=5). Distributions of jumps amplitude in the presence of Blebbistatin were fitted by exponential distributions with values of $j^{+*}$ and $j^{-*}$ equal to 3.4±0.9 and 3.2±0.8 nm. Jumps in the presence of Blebbistatin occurred with a frequency 50% lower than in control conditions. Therefore Jasplakinolide decreased the jumps frequency and their amplitude more than Blebbistatin.

The detection and measurements of jumps in the presence of noise is a difficult (ill-posed) problem[29] that should not be underestimated. Therefore, in order to show that jumps are real and not artifacts of used algorithms, it is needed to verify that large values of bead velocity v (Fig. 6a) were coincident with jumps (Fig. 6b) detected by the non linear diffusion algorithm (see vertical lines in panels 6a and 6b). Given the time series of bead position ($x_n$ n=1,..N) the computation of the instantaneous velocity does not require any parameter, because the velocity is equal to $(x_{n+1} - x_n)/\Delta t$, but two parameters are involved in the nonlinear diffusion algorithm (λ and τ). In order to establish co-localization in a quantitative way, large values of v were assumed to be those belonging to the tails of the velocity distribution outside the Gaussian function fitting its central lobe (see Fig. 4d) and these values of v co-localized in a time window Δt of less than 0.3 ms with detected jumps. The analysis of the Rate of True Positive (RTP) and of False Positive co-localization[30] (Fig. 6c) indicates that for Δt equal to 100 μs, i.e. the used sampling interval, RTP is larger than 80% and becomes close to 100% for Δt equal to 300 μs. This analysis indicates that jumps detected by the non linear diffusion algorithm co-localize very precisely with large values of bead velocity.

Jumps were clearly detected when force generation developed following adhesion. i.e. when Brownian fluctuations were reduced (Fig. 5). However, more often force generation developed without being preceded by bead adhesion (Fig. 7a). Therefore we asked whether it was possible to determine the existence of jumps also when force generation did not follow bead adhesion. As force generation is characterized by a large value of the autocorrelation function (Fig. 4) we computed for all three components x,y and z, $\rho_{xx}(t)$, $\rho_{yy}(t)$, $\rho_{zz}(t)$. During Brownian fluctuations $\rho_{ii}(t)$ are exponentially distributed with a value of τ less than 1 ms, but during push $\rho_{ii}(t)$ become broader decaying with several time constants (Fig. 4). Therefore we computed the integral $C_i(t)$ of $\rho_{ii}(t)$ at each time and force generation was identified to occur when $C_i(t)$ increased by at least 10 times (Fig. 7b). Under these circumstances the variance of bead fluctuations at the peak of force generation was significantly higher than during Brownian fluctuations (Fig. 7c). During this phase the central lobe of the distributions of dx/dt, dy/dt and dz/dt was fitted by a Gaussian function, but tails corresponding to large positive and negative velocities were detected (see arrows in Fig. 7d–f) indicating the existence of forward and backward jumps. Jumps detected by the non linear diffusion algorithm during these events (Fig. 7g–i) have amplitudes ranging up to 20 nm, as those detected after adhesion (Fig. 5).

If jumps are the elementary events underlying force generation their sum must be close to the observed net protrusion. Therefore we compared the net protrusion Prot(Δt) in the time window Δt with the sum of all forward jumps ($\Sigma_{\Delta t}\, j^{+}$) minus the sum of all backward jumps ($\Sigma_{\Delta t}\, j^{-}$) occurring in Δt: P(Δt) (red line) was very similar to $\Sigma_{\Delta t}\, j^{+} - \Sigma_{\Delta t}\, j^{-}$ (black line in Fig. 8a and b) in control conditions as well as in the presence of Jasplakinolide. We next asked whether force generation developed by an increase of the frequency of jumps, i.e. $A_+$ and $A_-$ or by their mean amplitude, i.e. $j^{+*}$ and $j^{-*}$. Therefore we estimated $A_+$, $A_-$, $j^{+*}$ and $j^{-*}$ in 0.5 s intervals during force generation: force generation developed by a combination of an increase of jumps frequency and of their mean values. The observation that forward and backward jumps sum to net protrusion is an additional test for internal consistency of the used procedure for jump detection, providing further support that jumps are the elementary events underlying force generation.

## Discussion

The results of the present manuscript show that force generation in neuronal lamellipodia of rat DRG neurons, is composed by

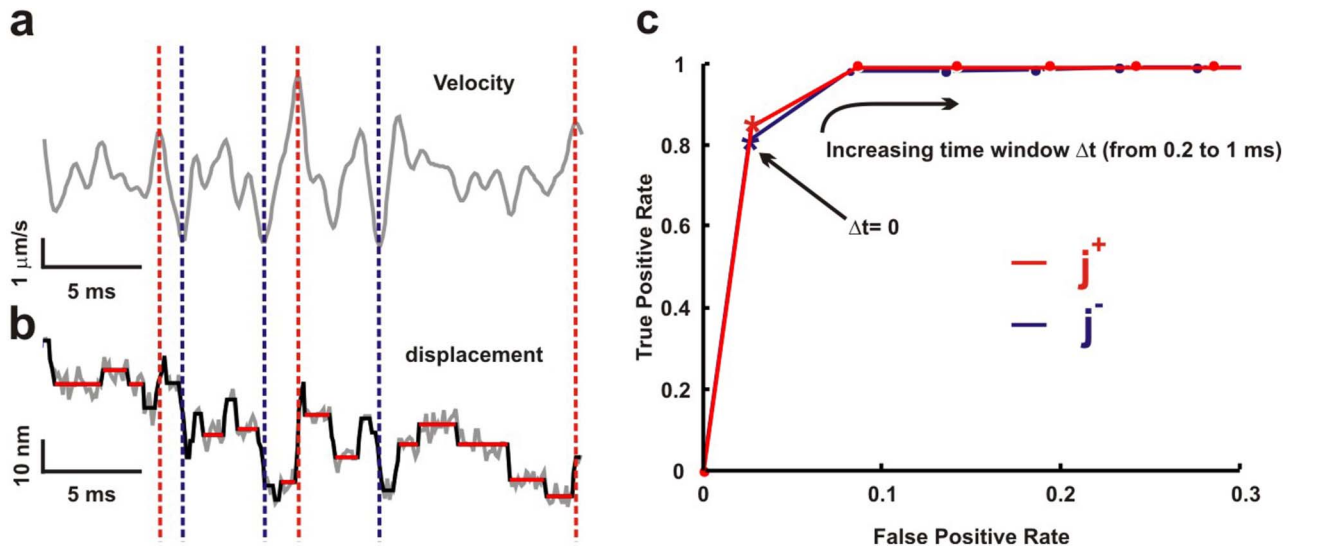


**Figure 6 | Colocalization of jumps and large values of bead velocity.** (a) Bead velocity during a push obtained by the convolution of the bead displacement with the derivative of a Gaussian function $(-t/(2*\pi)^{1/2} * a^2) \exp(-t^2/2*a^2)$ with $a = 0.1$ ms. A jump and a large value of v colocalize if they occur in a time window Δt of less than 0.3 ms. Large values of v were those belonging to the long tails of velocity distribution. These velocities had an absolute value larger than 3 times the standard deviation of the Gaussian fitting the central lobe of the velocity distribution (see Fig. 4d). (b) Jumps detected by nonlinear diffusion in the same portion of the push shown in (a), where velocity was computed. Original trace, gray; smoothed component, red; detected jumps, black. Red and black dotted lines highlight colocalization of positive $j^+$ and negative $j^-$ jumps, respectively with large values of v. (c) Rate of True Positive colocalization and of False Positive colocalization for increasing values of Δt from 0 to 1 ms, Asterisks represent the classifiers in which positive (red) and negative (black) jumps colocalize exactly with large values of v[30].

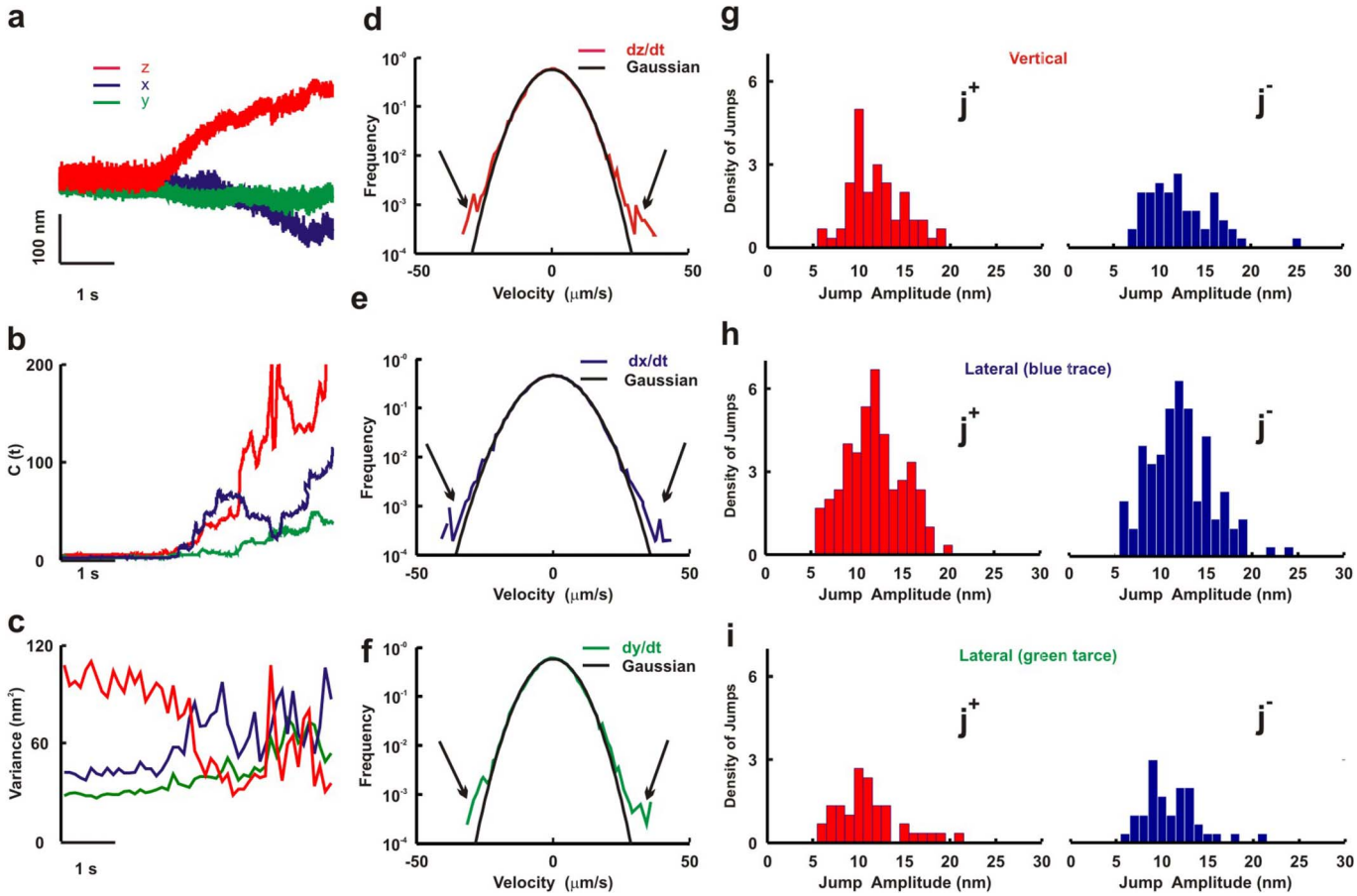


**Figure 7 | Characterization of force generation during a push in the absence of adhesion.** Episodes of force generation were identified as increases of at least 10 times of the integral $C_i(t)$ of $\rho_{ii}(t)$, i=x,y,z. (a) The three components (x,y,z) of the bead displacement during a push. (b) Integral $C_x(t)$ (blue), $C_y(t)$(green), and $C_z(t)$(red) of the autocorrelation function $\rho_{xx}(t)$, $\rho_{yy}(t)$, and $\rho_{zz}(t)$ of each of the three components of the bead displacements shown in (a). (c) Change in time of the bead displacement variance for the three components in (a). Variance computed in time windows of 0.1 s after high pass filtering at 1 Hz. (d)–(f) Distribution of values of velocity dz/dt (d), dx/dt (e), and dy/dt (f), during force generation shown in (a). The black line represents the Gaussian fit to the distribution. The arrows highlight the tails associated to forward and backward jumps. (g)–(i) Density of upward $j^+$ (red histograms) and downward $j^-$ (blue histograms) jumps during the push shown in (a) for the z (g), x (h), and y (i) component, respectively.

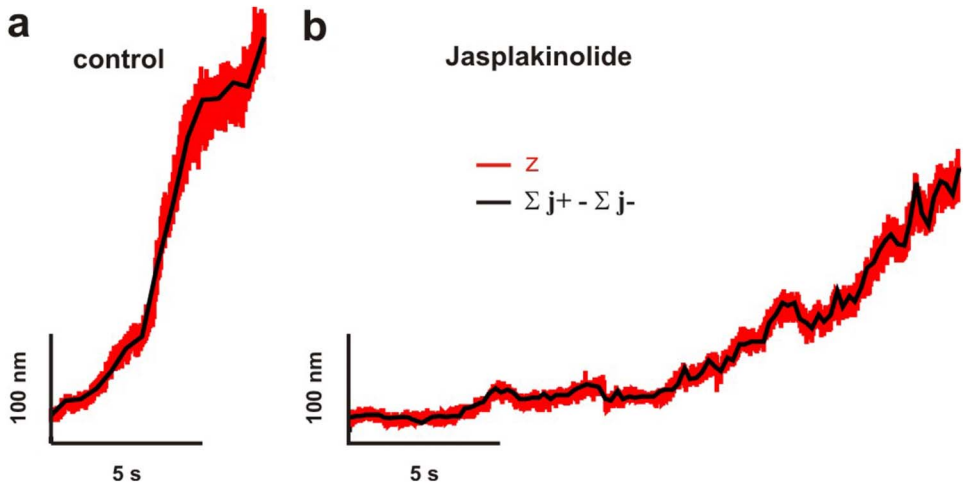


**Figure 8 | The sum of forward and backward jumps is equal to the net protrusion.** (a) Bead vertical displacement during a push (red line) in control conditions. The black line represents the sum of all forward jumps ($\Sigma_{\Delta t} j^+$) minus the sum of all backward jumps ($\Sigma_{\Delta t} j^-$) occurring in the time window $\Delta t$=0.5 s, calculated over the whole push. (b) As in (a) in the presence of 25 nM Jasplakinolide.

elementary events corresponding to forward and backward jumps. These jumps have an amplitude ranging from 2 to 20 nm and have varying orientation in the 3D space. These jumps are not observed when growth cones were fixed with paraformaldehyde, suppressing all cellular motility (Supplementary Methods and Supplementary Fig. S1 online) and their amplitude and frequency were reduced by treating growth cones with 25 nM Jasplakinolide (Fig. 5). Jumps detected by the nonlinear diffusion algorithm colocalize with high values of the instantaneous bead velocity (Fig. 6) and the net protrusion of lamellipodia is the net sum of forward and backward jumps (Fig. 8). For all these reasons, jumps - here described-are neither artifacts of the detection procedure nor are caused by changes of properties of the optical trap. Detected jumps represent the elementary events underlying force generation in DRG lamellipodia.

Force generation occurs at different rates. At the slowest rate the lamellipodium leading edge advances smoothly with forward and backward jumps (Fig. 5f) with an amplitude similar in size to the mean polymerization step size (2.7 nm) observed during actin filament polymerization[31,32] suggesting that actin monomers are added one by one to the existing network of filaments. At the fastest rate (Fig. 5d) larger jumps are observed and they could result from the insertion of small actin oligomers[33] and by the occurrence of a burst of actin polymerization in a single or neighboring actin filaments. Oligomers of 5–10 actin molecules are present in lamellipodia, primarily as a result of actin filaments depolymerization and could be used for actin filament assembly, as in yeast *Saccharomyes cervisiae*[33]. Experimental determinations of free G-actin in lamellipodia varied from 1–3 μM[9–12] to values 100 higher[34]. *In vitro* determination of actin polymerization rates provides values ranging from 11.6 to 38 (1/μM s)[9–12], but the bulk turnover of actin subunits is 100–200 times faster in cells than *in vitro*[1,35,36]. Therefore, the occurrence of a fast and vigorous polymerization rate of a single actin filament is possible. As the estimated density of actin filaments impinging upon the leading edge of a lamellipodium is between 100 and 200 per $\mu m^2$ [13,32] a burst of polymerization of several actin filaments and an appropriate spatial environment could also produce a discrete forward step of 10–20 nm of the lamellipodium leading edge. When actin turnover is reduced by Jasplakinolide[18] and when myosin II is inhibited by Blebbistatin[19,20], force generation still occurs but at a slower rate (Fig. 5e and f). Jumps produced by DRG lamellipodia do not have a discrete amplitude as observed in the actin-based movement of the bacterium *Listeria monocytogenes*, with a predominant jump size of 5.4 nm[37].

Force generation in lamellipodia depends on several factors such as the availability of actin monomers/oligomers, the presence of molecular motors such as myosin II and a large variety of controlling proteins[6]. This complexity is at the basis of the observed dynamics, reminiscent of self organized criticality[38].

## Methods

**Neuron preparation.** Wistar rats (P10–P12) were anaesthetized with CO2 and sacrificed by decapitation in accordance with the Italian Animal Welfare Act. The Ethics Committee of the International School for Advanced Studies (SISSA-ISAS) has approved the protocol (Prot.n. 2189-II/7). Dorsal Root Ganglia (DRG) were incubated with trypsin (0.5 mg/ml, Sigma-Aldrich, Milan, Italy), collagenase (1 mg/ml, Sigma-Aldrich), and DNase (0.1 mg/ml, Sigma-Aldrich) in 5 ml Neurobasal medium (Gibco, Invitrogen, Milan, Italy) in a shaking bath (37°C, 35–40 minutes). DRGs were mechanically dissociated, centrifuged at 300 rpm, resuspended in culture medium and plated on poly-L-lysine-coated (0.5 μg/ml, Sigma-Aldrich) coverslips. Cells were incubated for 24 to 48 hours followed by the addition of nerve growth factor (50 ng/ml; Alomone, Israel) before the measurements.

**Optical tweezer set-up.** The optical tweezers set-up was built as previously described[17,39]. The dish containing the differentiating neurons and the beads (PSI-1.0NH2, G.Kisker GbR, Steinfurt Germany) was placed on the microscope stage which could be moved by a 3 axis piezoelectric nanocube (17 MAX 301, Melles Griot Inc., USA). The temperature of the dish was kept at 37°C by a Peltier device. The bead position was determined in the x,y and z plane with a lateral and axial accuracy of 2 and 5 nm respectively, which was obtained from the analysis of the interference between forward scattered light from the bead and unscattered light[16,21]. The back focal plane of the condenser was imaged onto a QPD (C5460SPL 6041, Hamamatsu, Milan, Italy) and the light was converted to differential outputs digitized at 10 kHz and low pass filtered at 5 kHz. Both the lateral and axial trap stiffness, $\mathbf{k}\,xy = (kx, ky)$ and $kz$, respectively, as well as the detector sensitivity were calibrated using the power spectrum method[16] with voltage signals filtered and digitized at 5 kHz. In order to reduce and possibly avoid all mechanical perturbations affecting the measurement of $\mathbf{x}=(x, y, z)$, the optical tweezers set-up was kept in an isolated and sound-proof room and the scientists performing the experiments, controlled all operations remotely from a separate room. In order to have good mechanical stability it was necessary to position all power supplies of used equipment in a separate room and to avoid flying cables by properly securing them. In this way we reduced perturbations, which could have affected previous investigations.

**Jumps determination by non linear diffusion filtering.** In order to detect jumps, we used an algorithm based on non linear diffusion[27,28]. After selecting the part of the trace of interest, the original signal was approximated with a smooth piece-wise function where the discontinuities, i.e. rapid and large changes, were identified as jumps. The non-linear diffusion is an iterative process based on the choice of two parameters: the contrast λ, related to the minimal jump amplitude detected, and the scale τ, determining the temporal window of jumps. The values of λ and τ were set equal to 0.5 nm and 0.1 ms, respectively, so to detect 2 ground truth jumps (see Supplementary Methods and Supplementary Fig. S3 online). The algorithm is based on the Toolbox of Frederico D'Almeida (see http://www.mathworks.com/matlabcentral/fileexchange/3710-nonlinear-diffusiontoolbox).

We compared the detection of jumps using the same values of λ and τ from traces obtained in different conditions (Brownian fluctuation recording, adhesion, and push; see Supplementary Methods and Supplementary Fig. S3 online), but scaled so to have the same width of the central lobe of the velocity distribution. During pushes, jumps were detected with a rate about 4 times higher than in the other conditions. Therefore, if the variance of Brownian fluctuations of the trapped bead decreases to or below 4 $nm^2$, the overall system can detect reliably 2 nm jumps.


1. Pollard, T. D. & Borisy, G. G. Cellular motility driven by assembly and disassembly of actin filaments. *Cell* **112**, 453–465 (2003).
2. Bray, D., Thomas, C. & Shaw, G. Growth cone formation in cultures of sensory neurons. *Proc. Natl. Acad. Sci. U. S. A* **75**, 5226–5229 (1978).
3. Huber, A. B., Kolodkin, A. L., Ginty, D. D. & Cloutier, J. F. Signaling at the growth cone: ligand-receptor complexes and the control of axon growth and guidance. *Annu. Rev. Neurosci.* **26**, 509–563 (2003).
4. Landis, S. C. Neuronal growth cones. *Annu. Rev. Physiol.* **45**, 567–580 (1983).
5. Pollard, T. D., Blanchoin, L. & Mullins, R. D. Molecular mechanisms controlling actin filament dynamics in nonmuscle cells. *Annu. Rev. Biophys. Biomol. Struct.* **29**, 545–576 (2000).
6. Song, H. J. & Poo, M. M. The cell biology of neuronal navigation. *Nat. Cell Biol.* **3**, E81–E88 (2001).
7. Gallo, G. & Letourneau, P. C. Neurotrophins and the dynamic regulation of the neuronal cytoskeleton. *J. Neurobiol.* **44**, 159–173 (2000).
8. Gordon-Weeks, P. R. Microtubules and growth cone function. *J. Neurobiol.* **58**, 70–83 (2004).
9. Pollard, T. D. & Mooseker, M. S. Direct measurement of actin polymerization rate constants by electron microscopy of actin filaments nucleated by isolated microvillus cores. *J. Cell Biol.* **88**, 654–659 (1981).
10. Pollard, T. D. Rate constants for the reactions of ATP- and ADP-actin with the ends of actin filaments. *J. Cell Biol.* **103**, 2747–2754 (1986).
11. Quinlan, M. E., Heuser, J. E., Kerkhoff, E. & Mullins, R. D. Drosophila Spire is an actin nucleation factor. *Nature* **433**, 382–388 (2005).
12. Michelot, A. *et al.* Actin-filament stochastic dynamics mediated by ADF/cofilin. *Curr. Biol.* **17**, 825–833 (2007).
13. Prass, M., Jacobson, K., Mogilner, A. & Radmacher, M. Direct measurement of the lamellipodial protrusive force in a migrating cell. *J. Cell Biol.* **174**, 767–772 (2006).
14. Bohnet, S., Ananthakrishnan, R., Mogilner, A., Meister, J. J. & Verkhovsky, A. B. Weak force stalls protrusion at the leading edge of the lamellipodium. *Biophys. J.* **90**, 1810–1820 (2006).
15. Bustamante, C., Macosko, J. C. & Wuite, G. J. L. Grabbing the cat by the tail: Manipulating molecules one by one. *Nat Rev Mol Cell Biol* **1**, 130–136 (2000).
16. Neuman, K. C. & Block, S. M. Optical trapping. *Rev. Sci. Instrum.* **75**, 2787–2809 (2004).
17. Shahapure, R. *et al.* Force generation in lamellipodia is a probabilistic process with fast growth and retraction events. *Biophys. J.* **98**, 979–988 (2010).
18. Bubb, M. R., Spector, I., Beyer, B. B. & Fosen, K. M. Effects of jasplakinolide on the kinetics of actin polymerization. An explanation for certain in vivo observations. *J. Biol. Chem.* **275**, 5163–5170 (2000).
19. Straight, A. F. *et al.* Dissecting temporal and spatial control of cytokinesis with a myosin II inhibitor. *Science* **299**, 1743–1747 (2003).
20. Kovacs, M., Toth, J., Hetenyi, C., Malnasi-Csizmadia, A. & Sellers, J. R. Mechanism of blebbistatin inhibition of myosin II. *Journal of Biological Chemistry* **279**, 35557–35563 (2004).
21. Gittes, F. & Schmidt, C. F. Interference model for back-focal-plane displacement detection in optical tweezers. *Opt. Lett.* **23**, 7–9 (1998).

22. Simpson, K. H., Bowden, G., Hook, M. & Anvari, B. Measurement of adhesive forces between individual Staphylococcus aureus MSCRAMMs and protein-coated surfaces by use of optical tweezers. *J. Bacteriol.* **185**, 2031–2035 (2003).
23. Jass, J. *et al.* Physical properties of Escherichia coli P pili measured by optical tweezers. *Biophys. J.* **87**, 4271–4283 (2004).
24. Knoner, G. *et al.* Mechanics of cellular adhesion to artificial artery templates. *Biophys. J.* **91**, 3085–3096 (2006).
25. Helenius, J., Heisenberg, C. P., Gaub, H. E. & Muller, D. J. Single-cell force spectroscopy. *Journal of Cell Science* **121**, 1785–1791 (2008).
26. Medeiros, N. A., Burnette, D. T. & Forscher, P. Myosin II functions in actin-bundle turnover in neuronal growth cones. *Nat Cell Biol* **8**, 215–226 (2006).
27. Perona, P. & Malik, J. Scale-Space and Edge-Detection Using Anisotropic Diffusion. *Ieee Transactions on Pattern Analysis and Machine Intelligence* **12**, 629–639 (1990).
28. Weickert, J. Applications of nonlinear diffusion in image processing and computer vision. *ACTA MATHEMATICA UNIVERSITATIS COMENIANAE* **70**, 33–50 (2001).
29. Bertero, M., Poggio, T. A. & Torre, V. Ill-Posed Problems in Early Vision. *Proc IEEE* **76**, 869–889 (1988).
30. Fawcett, T. An introduction to ROC analysis. *Pattern Recognition Letters* **27**, 861–874 (2006).
31. Egelman, E. H. The Structure of F-Actin. *Journal of Muscle Research and Cell Motility* **6**, 129–151 (1985).
32. Abraham, V. C., Krishnamurthi, V., Taylor, D. L. & Lanni, F. The actin-based nanomachine at the leading edge of migrating cells. *Biophys. J.* **77**, 1721–1732 (1999).
33. Okreglak, V. & Drubin, D. G. Loss of Aip1 reveals a role in maintaining the actin monomer pool and an in vivo oligomer assembly pathway. *J. Cell Biol.* **188**, 769–777 (2010).
34. Koestler, S. A. *et al.* F- and G-actin concentrations in lamellipodia of moving cells. *PLoS. One.* **4**, e4810 (2009).
35. Pantaloni, D., Le Clainche, C. & Carlier, M. F. Mechanism of actin-based motility. *Science* **292**, 1502–1506 (2001).
36. Small, J. V., Stradal, T., Vignal, E. & Rottner, K. The lamellipodium: where motility begins. *Trends Cell Biol.* **12**, 112–120 (2002).
37. Kuo, S. C. & McGrath, J. L. Steps and fluctuations of Listeria monocytogenes during actin-based motility. *Nature* **407**, 1026–1029 (2000).
38. Cardamone, L., Laio, A., Torre, V., Shahapure, R. & DeSimone, A. Cytoskeletal actin networks in motile cells are critically self-organized systems synchronized by mechanical interactions. *Proceedings of the National Academy of Sciences of the United States of America* **108**, 13978–13983 (2011).
39. Cojoc, D. *et al.* Properties of the force exerted by filopodia and lamellipodia and the involvement of cytoskeletal components. *PLoS ONE* **2**, e1072 (2007).

## Acknowledgments

We thank Walter Vanzella (Glance Vision Technologies s.r.l.) for computational support. This work was funded by the European Commission under the Seventh Framework Programme: Project CP – FP 214566-2 NanoScale and Project n.229375 SMD.

## Author contributions

L.A., E.E., and R.S. equally contributed and their names are in alphabetical order. V.T. conceived the project and designed the experiments. L.A., E.E., and R.S. performed the experiments and analyzed the data. L.A., E.E., R.S., and G.B. contributed to reagents/materials/analysis tools. V.T., L.A., E.E., and R.S. wrote the paper.

## Additional information

**Supplementary information** accompanies this paper at http://www.nature.com/scientificreports

**Competing financial interests:** The authors declare no competing financial interests.



**How to cite this article:** Amin, L., Ercolini, E., Shahapure, R., Bisson, G. & Torre, V. The elementary events underlying force generation in neuronal lamellipodia. *Sci. Rep.* **1**, 153; DOI:10.1038/srep00153 (2011).

## 2.3

# The Role of Membrane Stiffness and Actin Turnover on the Force Exerted by DRG Lamellipodia

L. Amin, E. Ercolini, R. Shahapure, E. Migliorini, V. Torre, Biophysical journal, (2012) DIO: 10.1016/j.bpj.2012.04.036

# The Role of Membrane Stiffness and Actin Turnover on the Force Exerted by DRG Lamellipodia

Ladan Amin,[†] Erika Ercolini,[†‡] Rajesh Shahapure,[†] Elisa Migliorini,[‡§] and Vincent Torre[†¶*]
[†]Neuroscience Department, International School for Advanced Studies (SISSA), Trieste, Italy; [‡]Cluster in Biomedicine and [§]IOM-CNR, Area Science Park, Basovizza-Trieste, Italy; and [¶]Italian Institute of Technology, SISSA Unit, Trieste, Italy

ABSTRACT We used optical tweezers to analyze the effect of jasplakinolide and cyclodextrin on the force exerted by lamellipodia from developing growth cones (GCs) of isolated dorsal root ganglia (DRG) neurons. We found that 25 nM of jasplakinolide, which is known to inhibit actin filament turnover, reduced both the maximal exerted force and maximal velocity during lamellipodia leading-edge protrusion. By using atomic force microscopy, we verified that cyclodextrin, which is known to remove cholesterol from membranes, decreased the membrane stiffness of DRG neurons. Lamellipodia treated with 2.5 mM of cyclodextrin exerted a larger force, and their leading edge could advance with a higher velocity. Neither jasplakinolide nor cyclodextrin affected force or velocity during lamellipodia retraction. The amplitude and frequency of elementary jumps underlying force generation were reduced by jasplakinolide but not by cyclodextrin. The action of both drugs at the used concentration was fully reversible. These results support the notion that membrane stiffness provides a selective pressure that shapes force generation, and confirm the pivotal role of actin turnover during protrusion.

## INTRODUCTION

Neurons are able to self-organize in complex networks with a precise wiring of synaptic connections. They find the appropriate path by means of protruding neurites, highly motile structures that explore the environment in search of chemical cues to guide the formation of correct synaptic connections (1,2). Neuronal exploration is guided by growth cones (GCs) located at the neurite tips (3,4). GCs are composed of a 2- to 10-$\mu$m-diameter lamellipodium from which thin filopodia with a submicron diameter emerge (5). Filopodia tips can move at a velocity reaching 0.8–1 $\mu$m/s and their motility is at the basis of neuronal network formation. The primary source of motility in GCs is polymerization of actin filaments (6,7), which is controlled by a large set of regulatory proteins (e.g., Arp2/3 and WASP (8)). The addition of actin polymers to actin filaments in close contact with the membrane pushes the cellular membrane forward, exerting a protrusive force (9,10). A different dynamics characterizes GC retraction. In this case, the actin network retracts, possibly because of local catastrophe or depolymerization controlled by severing proteins, such as cofilin (8).

The overall dynamics that regulates these processes is not clear, and mathematical models linking molecular events to force generation have been proposed (11). These models predict *Fv* relationships, i.e., the relation between the force *F* exerted by the actin filament network and the velocity *v* of the lamellipodium leading edge (6,12–15). Fluctuation of contacts between the tip of actin filaments and the surrounding membrane is an essential feature of Brownian ratchet models (6,12,13) that predict *Fv* relationships in which *v* decreases with increasing values of *F*. In contrast, in autocatalytic models (13,14), when an obstacle is encountered, the actin network gives rise to new branches. As a result of these new branches, the *Fv* relationships are almost flat, so the velocity *v* is constant even when *F* increases. In all proposed models, force generation occurs because of this growth of the actin filament network pushing the lamellipodia membrane. This process must be affected by the membrane stiffness, and in this study we investigate its role in force generation.

Cyclodextrin is known to reduce the cholesterol concentration in biological membranes (16), and exposure of GCs to a millimolar amount of cyclodextrin is expected to reduce the stiffness of the cellular membrane enveloping the actin filament network. Cyclodextrins are often used to sequester cholesterol molecules, which are essential components of membranes and determine several mechanical properties of the cellular membrane, such as its elasticity and permeability (17–20). Cholesterol is an important constituent of lipid rafts (specialized membrane microdomains that are rich in cholesterol, sphingolipids, and saturated phospholipids) (18,19). Lipid rafts often harbor membrane receptors, such as epidermal growth factors and integrins (20).

Another important determinant of force generation is the turnover of actin filaments. During this process, actin monomers or small oligomers are added to the barbed end of actin filaments (polymerization) and removed from the other end (depolymerization) (21). Jasplakinolide (22) stabilizes actin filaments by reducing their depolymerization rate and hence slowing down actin turnover. Jasplakinolide and phalloidin decrease the rate constant for the dissociation of actin subunits from filament ends, stabilizing

*Submitted December 2, 2011, and accepted for publication April 17, 2012.*

*Correspondence: torre@sissa.it

Rajesh Shahapure's present address is Leiden Institute of Chemistry, Molecular Genetics, Leiden, The Netherlands.

Editor: Jason Haugh.



0006-3495/12/06/2451/10 $2.00

doi: 10.1016/j.bpj.2012.04.036

actin filaments by preventing filament depolymerization. Jasplakinolide moderately decreases the speed of migrating keratocytes (23) as a result of actin monomer depletion caused by inhibition of actin filament disassembly.

In this work, we analyzed the role of membrane stiffness and actin turnover on force generation by using optical tweezers (24–26) and studying the effects of jasplakinolide and cyclodextrin. Using atomic force microscopy (AFM), we then verified that cyclodextrin decreased the membrane stiffness of dorsal root ganglia (DRG) neurons.

## MATERIALS AND METHODS

Details of the neuron preparation, optical tweezers setup, and computation of the $Fv$ relationship can be found elsewhere (24–26) and in the Supporting Material.

### Measurement of elasticity modulus

The elasticity modulus $E$ of the cellular membrane of DRG neurons was measured by AFM. Tipless cantilevers with a 5-$\mu$m-diameter bead attached to the edge were used as soft nanoindenters, which allowed local testing of cells and tissue. $E$ was derived from force-displacement curves obtained with the AFM when the deflection of the AFM cantilever was monitored as it approached the sample. We used the standard Hertz model (27), which describes the indentation $\delta$ of a silica bead with a specified radius ($R$) in a soft sample and predicts that the force $F$ produced is

$$F = \frac{4ER^{1/2}\delta^{3/2}}{(3(1-\nu^2))} \quad (1)$$

where $\nu$ is the Poisson's ratio (assumed to be 0.5 for cells) (28). We operated the AFM so to have a maximal indentation value no larger than 500 nm. In this range, the forces applied by the cantilever to the sample were always $<$ 0.5 nN. We obtained AFM force spectroscopy measurements by choosing similar positions on different cells, close to the cellular soma and in the central domain of DGR GCs. $E$ was obtained by a best linear fit of the force-distance curve (method 1). The contact point between the tip and the membrane was detected by the cantilever deflection according to the noise defined in the off-contact part of the force-displacement curve.

When $E$ has to be measured and the height of the specimen $h$ is small, the Hertz model is not adequate, because the Hertz model is appropriate only when $h$ is larger than $\delta$, which is not the case for thin GCs with a height varying between 200 and 600 nm (25). Therefore, we measured $E$ in GCs either by considering only indentations of $<$50 nm (method 2) or by using the corrected Hertz model for thin samples (29) (method 3):

$$F = \left(\frac{16E}{9}\right)R^{1/2}\delta^{3/2}\left[1 + 1.33\chi + 1.283\chi^2 + 0.769\chi^3 + 0.0975\chi^4\right], \quad (2)$$

where $\chi = \sqrt{R\delta}/h$ and $R$ is the bead radius. The first term outside the brackets represents the standard Hertz model, and the terms inside the bracket are the corrections needed to account for thin GCs.

## RESULTS

Neurons from DRG of P10-P12 Wistar rats were isolated, and after 24–48 h of culture, coverslips containing DRG neurons were positioned on the stage of an inverted microscope (25) (see also Supporting Material). Silica beads with a diameter of 1 $\mu$m were trapped with an infrared optical tweezer (30) in front of GCs and we were able to measure the force exerted by lamellipodia on these beads with subpiconewton sensitivity at 10 kHz resolution. After verifying by visual inspection that GCs moved as previously described (24,25), we added 25 $\mu$l of a stock solution of 1 $\mu$M of jasplakinolide to obtain a final concentration of the drug of 25 nM. In other experiments, we added 100 $\mu$l of a stock solution of 25 mM of cyclodextrin to obtain a final concentration of the drug of 2.5 mM.

Untreated lamellipodia pushed the trapped beads (Fig. 1, *a–c*) and exerted forces up to 10–20 pN (Fig. 1 *d*) as previously described. Lamellipodia of DRG treated with 25 nM jasplakinolide (Fig. 1, *i–k*) were able to pull and push a trapped bead, but with a lower force and velocity (see Fig. 2). During their retraction, these lamellipodia could pull a trapped bead with a force up to 15 pN (Fig. 1 *l*). Lamellipodia of DRG neurons treated with 2.5 mM cyclodextrin (Fig. 1, *e–h*) protruded with a higher velocity (Fig. 2 *a*) and exerted larger forces (Fig. 2 *b*). At the mentioned concentrations, neither jasplakinolide nor cyclodextrin affected the morphological properties of the treated DRG neurons in a visible way.

For each DRG preparation, we typically obtained six coverslips (two untreated controls, two treated with jasplakinolide, and two treated with cyclodextrin). The addition of $\geq$50 nM of jasplakinolide to the extracellular medium bathing DRG neurons almost completely blocked the motion of DRG GCs and the associated force generation. However, a concentration of 25 nM jasplakinolide modified both motion and force generation without blocking them completely, and therefore we investigated in detail the effect of 25 nM jasplakinolide. Prolonged exposure (i.e., for $>$30 min) of cyclodextrin in a concentration varying from 1 to 5 mM increased the motility of DRG GCs similarly, with higher concentrations evoking faster but not larger effects. Therefore, we analyzed the effect of 2.5 mM cyclodextrin after exposure for at least 30 min. Using the above-described protocol, we collected data from $>$20 DRG preparations. We then measured and compared the maximal exerted force $F_{max}$ and maximal protruding velocity $v_{max}$ under control conditions (53 vertical and 28 lateral pushing events) in the presence of the two drugs (48 and 61 pushing events for jasplakinolide and cyclodextrin, respectively). Vertical refers to the $z$ axis (perpendicular to the coverslip) and lateral refers to the $(x,y)$ plane of the coverslip. Under control conditions, for vertical push $F_{max}$ varied from 5 to 9 pN with an average value $<F_{max}>$ equal to 6.3 $\pm$ 0.4 pN, and $v_{max}$ varied from 25 to 80 nm/s with an average value $<v_{max}>$ equal to 44.3 $\pm$ 5.0 nm/s (Fig. 2, *a* and *b, red histograms*). In the presence of 25 nM jasplakinolide, $F_{max}$ varied from 1 to 5.5 pN with an average value $<F_{max}>$ equal to 2.9 $\pm$ 0.4 pN, and $v_{max}$ varied from 15 to 55 nm/s with an average value $<v_{max}>$ equal to 31.1 $\pm$ 4.3 nm/s

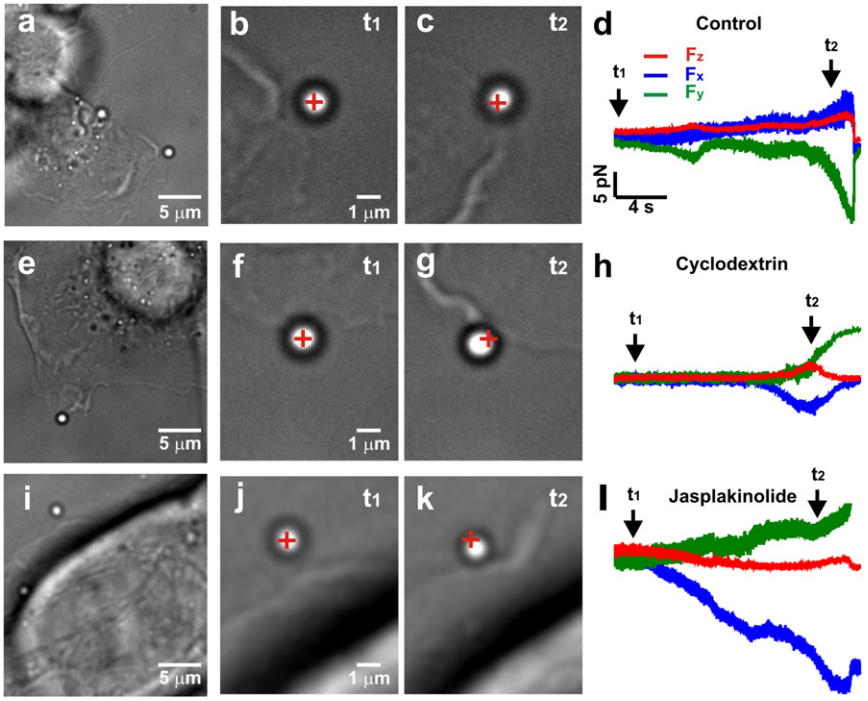


FIGURE 1 Push and retraction by a lamellipodium. (*a*) Low-resolution image of a bead trapped in front of a lamellipodium emerging from the soma of a DRG neuron in control conditions. (*b* and *c*) High-resolution images during a push. At $t_1$ the bead is in the optical trap (*b*), and when the lamellipodium grows, at $t_2$, it pushes the bead (*c*). The cross indicates the center of the optical trap. (*d*) The three components $F_x$, $F_y$, and $F_z$ of the force exerted when the lamellipodium pushes the bead. (*e–h*) As in *a–d* but in the presence of cyclodextrin. (*i–l*) As in *a–c* but during retraction and in the presence of jasplakinolide. (*j*) At $t_1$ the bead is in the optical trap. (*k*) At $t_2$, when the lamellipodium retracts, the bead is pulled away from trap. (*l*) The lamellipodium retracts and displaces the bead both laterally and vertically. In panels *a–h* the trap stiffness is $k_{x,y} = 0.015$, $k_z = 0.005$, and in panels *i–l* it is $k_{x,y} = 0.07$, $k_z = 0.03$.

(Fig. 2, *a* and *b*, *black histograms*). In the presence of 2.5 mM cyclodextrin, both $F_{max}$ and $v_{max}$ were larger. $F_{max}$ varied from 3.5 to 13.5 pN with an average value $<F_{max}>$ equal to 6.8 ± 0.5 pN, and $v_{max}$ varied from 8 to 120 nm/s with an average value $<v_{max}>$ equal 55.9 ± 7.3 nm/s (Fig. 2, *a* and *b*, *green histograms*). The relation between $v_{max}$ and $F_{max}$ during vertical pushes in the three cases are shown in Fig. 2 *c*.

When GCs were treated with cyclodextrin, lamellipodia pushed the bead out of the optical trap in ~32% of the experiments. i.e., ~3 times more often than in control conditions (~9% of experiments). This observation shows that GCs treated with cyclodextrin could exert a force exceeding the maximal trapping force of 16.5 pN, corresponding to the strongest used stiffness of the optical trap ($k_{x,y} = 0.07$ and $k_z = 0.03$). The histograms reported in Fig. 2, *a* and *b*, were obtained from experiments in which the bead was always in the optical trap, and they do not include data from experiments in which the lamellipodia pushed the bead out of the trap. Therefore, we can conclude that GCs treated with cyclodextrin develop a force larger than occurs under control conditions.

## Reversibility of the effect of jasplakinolide and cyclodextrin

Lamellipodia that emerged from DRG GCs after 1 day of culture moved vigorously, undergoing repetitive cycles of protrusions and retractions. We followed their motion by video imaging at 5 Hz and measured the velocity of the lamellipodia leading edge. In control conditions, lamellipodia exhibited waves of protrusion and retraction (Fig. 3, *a–c*) with a period $T$ of 165.0 ± 16.7 s that could be observed for several hours. During protrusions, the leading-edge maximal velocity $v_{max}$ was 48.4 ± 5.6 nm/s (Fig. 3, *e* and *f*, *red histograms*).

During these cycles, protrusion ended with an upward bending of the lamellipodium, reminiscent of the upward bending of ruffles previously described in fibroblasts (31). Some seconds after the transient upward bending, the lamellipodia collapsed and retracted. We analyzed the effect of jasplakinolide and cyclodextrin on these cycles of protrusions and retractions (Fig. 3, *d–g*). After addition of cyclodextrin, the lamellipodia increased the frequency of these waves, $T$ decreased to 96.1 ± 7.9 s, and $v_{max}$ increased to 66.4 ± 1.8 nm/s (Fig. 3, *e* and *f*, *green histograms*). These effects were completely reversible after removal of cyclodextrin from the extracellular medium, and $T$ increased to 168.8 ± 16.6 s and $v_{max}$ decreased to 44.6 ± 1.2 nm/s (Fig. 3, *e* and *f*, *blue histograms*).

A different picture, however, was observed with jasplakinolide. Indeed, after addition of jasplakinolide, the maximal protrusion decreased and GCs retracted gradually and often stopped moving (43/65 experiments). In the presence of jasplakinolide, $T$ and $v_{max}$ decreased to 136.1 ± 11.6 s and 34.3 ± 3.3, respectively (Fig. 3, *h* and *i*, *black histograms*). When jasplakinolide was removed from the bath, both $T$ and $v_{max}$ returned to approximately their original values (Fig. 3, *e* and *f*, *blue histograms*).

## *Fv* relationships

The *Fv* relationships from individual experiments were normalized to $F_{max}$, defined as the maximal force beyond

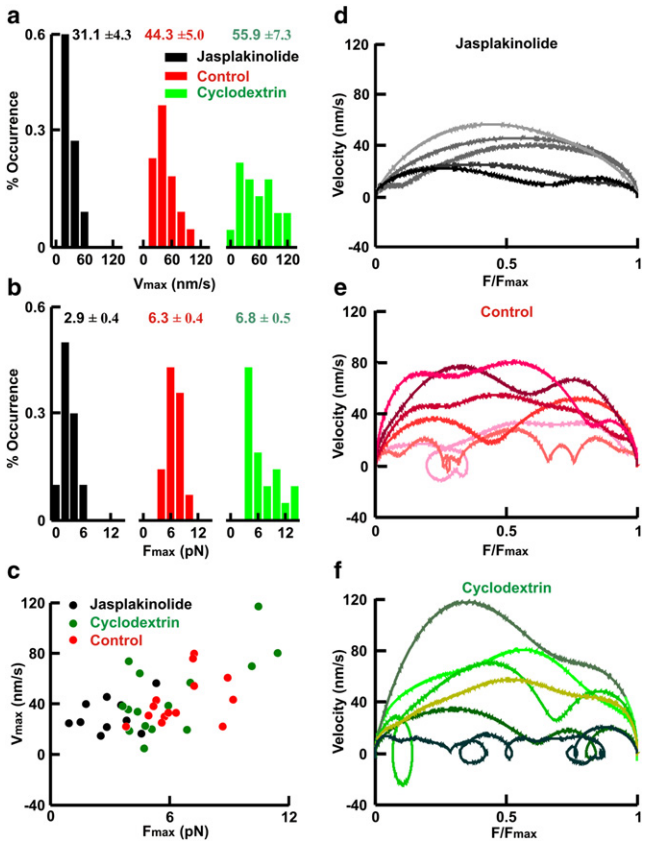


FIGURE 2 Maximal force and velocity. (*a*) Histograms of the maximal protruding velocity during vertical pushes $v_{max}$, in control conditions and in the presence of jasplakinolide or cyclodextrin. (*b*) As in panel *a* but for maximal force exerted in vertical pushes $F_{max}$. (*c*) The relation between $v_{max}$ and $F_{max}$ during vertical pushes. (*d–f*) Superimposed *Fv* relationships from five individual vertical pushes in the presence of jasplakinolide (*d*), in control conditions (*e*), and in the presence of cyclodextrin (*f*).

which the lamellipodium leading edge does not advance and the velocity is consistently negative for at least 10 s. Normalized *Fv* relationships, even those obtained from data filtered at 0.2 Hz, varied significantly among different experiments (25). In some experiments, in control conditions (Fig. 2 *e*) *Fv* relationships had knots corresponding to instances with a negative velocity or transient retractions of the lamellipodium leading edge. These knots were less frequent in the presence of jasplakinolide, presumably because of a reduced rate of actin depolymerization caused by the drug (Fig. 2 *d*). In cyclodextrin, in contrast, knots were more frequent and the lamellipodium leading edges protruded with a larger velocity (Fig. 2 *f*). These knots could be caused by transient microscopic curling and ruffling similar to those previously described in fibroblasts (31).

We computed the *Fv* relationships for the four most common stereotyped behaviors (i.e., vertical pushes, lateral pushes, vertical retractions, and lateral retractions) in control conditions and when cells were exposed to 25 nM jasplakinolide or 2.5 mM cyclodextrin for at least 30 min. To characterize the effect of jasplakinolide and cyclodextrin on the probabilistic dynamics underlying force generation, we determined the average *Fv* relationships $<Fv>$ for data filtered at 0.2 Hz for vertical/lateral push and retraction (Fig. 4). For vertical push in control conditions, $<Fv>$ after an initial rise $<v>$ reached a value of ~35 nm/s, which was maintained for most of the push duration (Fig. 4 *a*, *red line*). In the presence of jasplakinolide, $<Fv>$ had a broadly similar shape but the average maximal velocity was lower (~25 nm/s). In the presence of cyclodextrin, in contrast, the average maximal velocity was consistently higher and equal to 55.9 ± 7.3 nm/s. Very similar effects were observed for lateral pushes: jasplakinolide similarly decreased the average maximal velocity and cyclodextrin increased it (Fig. 4 *b*).

If 25 nM jasplakinolide and 2.5 mM cyclodextrin clearly modified force generation during push, they had a very limited effect, if any, on the force exerted during retraction (Fig. 4, *c* and *d*). Indeed, during vertical and lateral retraction, the $<Fv>$ were very similar in shape and size in control conditions and in the presence of jasplakinolide and cyclodextrin.

As shown in Fig. 2, we saw that knots appeared to be less frequent in the presence of jasplakinolide. Therefore, we analyzed in more detail transient retractions during sustained pushes and transient pushes during sustained retractions (see Supporting Material).

We also measured the fraction of time $\Delta t_{ret}/\Delta t_{push}$ of transient retractions (Fig. S1) over the total duration of the push $\Delta t_{push}$. In control conditions, $\Delta t_{ret}/\Delta t_{push}$ was 0.07 ± 0.02, and this value was significantly decreased by jasplakinolide but not by cyclodextrin, for both vertical and lateral pushes. Very similar results were observed when the maximal (or positive) velocity $v_{max}$ during retractions was analyzed (Fig. S1).

## Effect of jasplakinolide and cyclodextrin on elementary events

A remarkable feature of force generation during vertical and lateral push is a concomitant increase of noise observed when the lamellipodia push the bead (26). This increase of noise is not present when the lamellipodium retracts and pulls the bead away from the optical trap. We previously showed that this increase of noise is blocked by 25 nM jasplakinolide (26). In contrast, in the presence of 2.5 mM cyclodextrin, when lamellipodia pushed a bead laterally, we observed a significant increase in noise (Fig. 5 *a*) similar to what we observed in control conditions.

As shown in Fig. 5 *b*, the relation between variance and exerted force in GCs treated with 2.5 mM cyclodextrin (*blue shades*) was similar to and almost indistinguishable from that measured in control conditions (*red shades*). In contrast, in the presence of 25 nM jasplakinolide, GCs could exert forces up to 10–15 pN without the concomitant

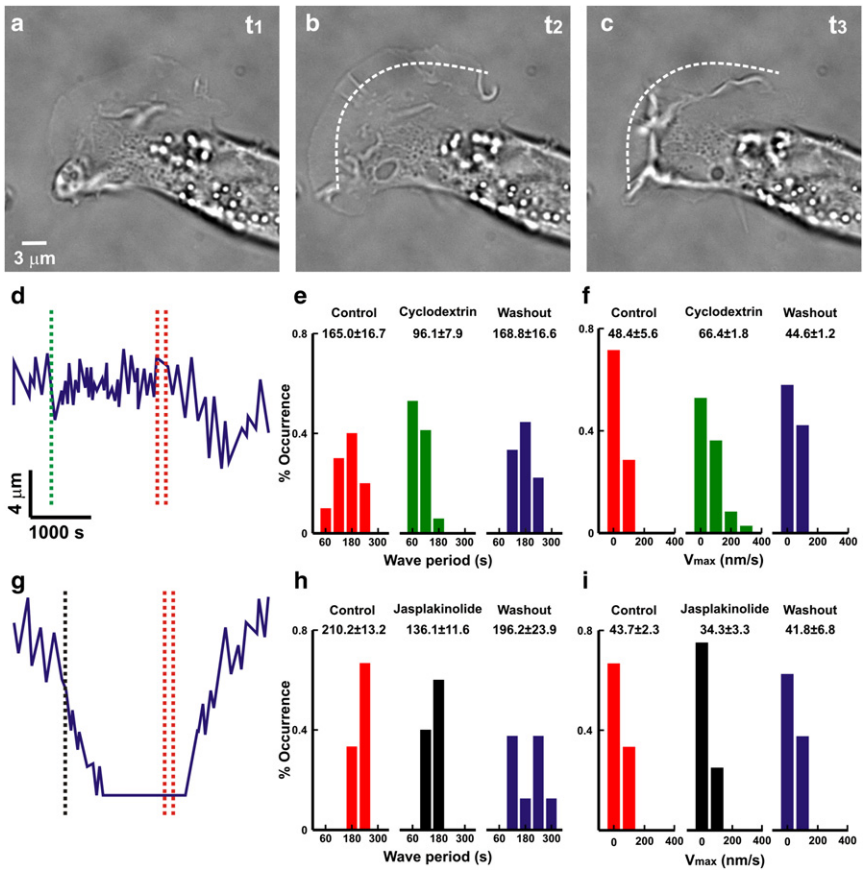


FIGURE 3 Reversibility of the effect of jasplakinolide and cyclodextrin after washout. (*a–c*) Lamellipodia emerging from DRG GCs moving in cyclic waves of protrusions (*b*) and retractions (*c*); the dotted line represents the leading edge of lamellipodia in panel *a*. (*d*) Maximal protrusion/maximal retraction of lamellipodium versus time. The single dotted line represents the time of cyclodextrin addition, and the double dotted lines indicate the time of washout. (*e*) Histograms of the wave period in control conditions and in the presence of cyclodextrin and after washout. (*f*) Histograms of maximal protruding velocity in control conditions and in the presence of cyclodextrin and after washout. (*g–i*) As in *d–f* but in the presence of jasplakinolide.

increase of noise (*black shades*) observed both in control conditions and in the presence of cyclodextrin. Data for the control and jasplakinolide are taken from our previous work (26). In that work, we showed that upon bead adhesion to the lamellipodium membrane, in several experiments the variance of the bead displacement could decrease to $<6$ nm$^2$ and subsequently, when the lamellipodium pushed the bead, the variance increased, and forward and backward jumps constituting the elementary events underlying force generation appeared. In the presence of 25 nM jasplakinolide or 2.5 mM cyclodextrin, the beads were able to seal onto the lamellipodium membrane, and the variance of bead displacement could decrease to $<10$ nm$^2$ (Fig. 6). Therefore, we compared forward and backward jumps in control conditions and in the presence of jasplakinolide and cyclodextrin.

After the decrease of variance caused by bead adhesion on the lamellipodium leading edge during push, forward and backward jumps were clearly visible in control conditions (Fig. 6 *a*) and had properties similar to those described previously (26). The amplitudes of forward and backward jumps $j^-$ were exponentially distributed (Fig. 6 *d*) and were fitted by the equations $A_+\, e^{-j+/j+*}$ and $A_-\, e^{-j-/j-*}$, where $A_+$ and $A_-$ are the rates of forward and backward jumps, respectively, and $j^{+*}$ and $j^{-*}$ are the mean amplitudes of forward and backward jumps, respectively. Because of a residue noise, jumps with an amplitude lower than 2–3 nm could not be detected. The mean values of these parameters obtained in control conditions and in the presence of jasplakinolide and cyclodextrin are shown in Table 1. In control conditions, the mean values of $j^{+*}$ and $j^{-*}$ were 5.1 ± 1.3 and 4.9 ± 1.2 nm, respectively, with corresponding rates $A_+$ and $A_-$ of 157.3 ± 12.0 and 155.5 ± 11.0 events/s. In the presence of jasplakinolide (Fig. 6 *c*), the mean amplitudes of detected forward and backward jumps decreased to 2.5 ± 0.3 and 2.2 ± 0.4 and their rates decreased to 50.0 ± 4.5 and 44.0 ± 5.3 events/s, respectively (Fig. 6 *f*). In contrast, in the presence of cyclodextrin (Fig. 6 *b*), the mean amplitudes of detected forward and backward jumps were equal to 4.6 ± 1.9 and 4.4 ± 1.7 and their rates were 226.2 ± 13.5 and 224.8 ± 14.7 events/s, respectively (Fig. 6 *e*). The collected data show that jumps amplitude and frequency were reduced by 25 nM jasplakinolide, whereas 2.5 mM cyclodextrin increased their frequency without affecting their size.

## Effect of jasplakinolide and cyclodextrin on membrane elasticity modulus

Exposure to cyclodextrin reduces the content of cholesterol in cellular membranes, but its overall effect on the membrane elasticity modulus $E$ (i.e., stiffness) is controversial

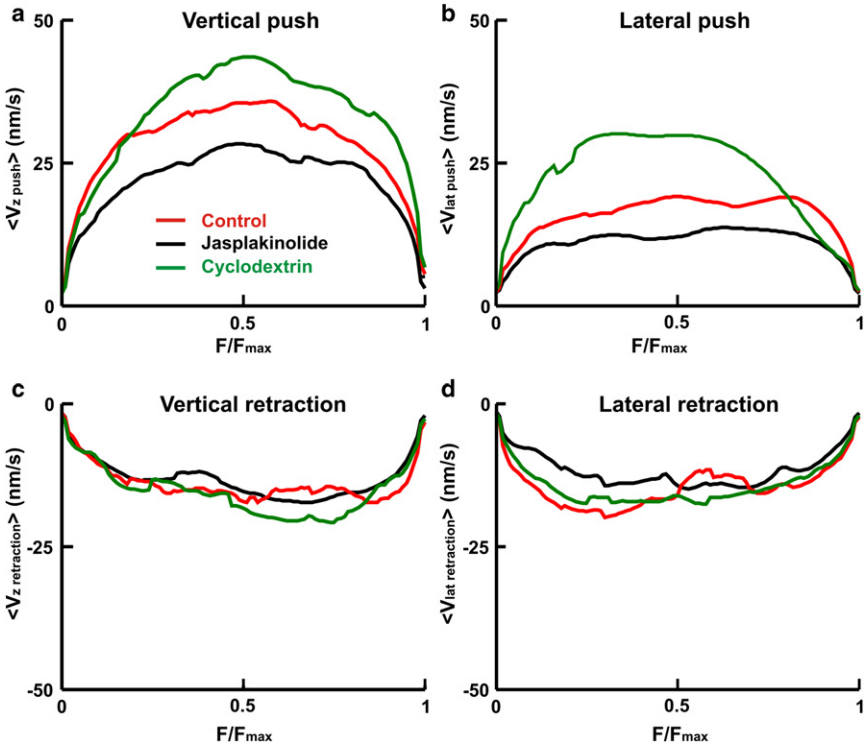


FIGURE 4 *Fv* relationships during pushes and retractions. (*a–d*) Average *Fv* relationship, $<Fv>_{0.2}$, normalized to $F_{max}$ for (*a*) vertical pushes, (*b*) lateral pushes, (*c*) vertical retractions, and (*d*) lateral retractions. The numbers of individual *Fv* relationships that were averaged in control conditions and in the presence of jasplakinolide and cyclodextrin were equal to (*a*) 23, 14, and 15, respectively; (*b*) 20, 14, and 14, respectively; (*c*) 23, 18, and 15, respectively; and (*d*) 14, 16, and 14, respectively.

(see Discussion). To verify the effect of cyclodextrin on our GCs, we measured *E* directly using the tip of the cantilever of an AFM, touching either the soma or the GC of our DRG neurons (Fig. 7 *a*) and measuring the associated indentation (Fig. 7, *b* and *c*).

The procedure of deriving *E* from indentations caused to the membrane was originally referred to as cell poking (32) and provided valuable information about the elastic properties of erythrocytes. By causing indentations with the cantilever tip of an AFM, we were able to obtain a direct measurement in situ of the effect of the used drugs on *E* of the lipid bilayer of the membrane.

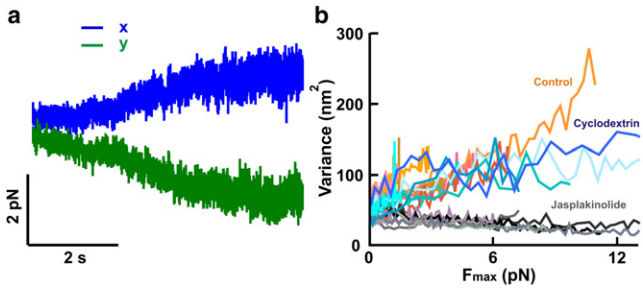


FIGURE 5 Increase of noise during pushes in control conditions and in the presence of cyclodextrin but not in the presence of jasplakinolide. (*a*) The longitudinal components of the bead displacement during a lateral push in the presence of cyclodextrin show a clear increase in noise. (*b*) Relation between force and variance for lateral pushes in control conditions in the presence of cyclodextrin and in the presence of jasplakinolide. Data for control and jasplakinolide were taken from our previous work (26).

The cantilever of the AFM was positioned under direct visual control over the soma or GC of DRG neurons (Fig. 7 *a*). Under these conditions, several hundreds of force-displacement curves (Fig. 7, *b* and *c*) were obtained in <10 min, and these individual traces were averaged to obtain average <force-displacement> curves. By fitting these <force-displacement> curves with Eq. 1, we obtained a value of *E*. We measured *E* in the soma of eight DRG neurons and 10 GCs, and the mean value of *E* was 99.18 ± 2.12 and 174.1 ± 3.7 Pa, respectively. However, the value of *E* varied rather significantly from neuron to neuron and varied from 22.8 to 188.9 Pa, with no evident correlation with either the shape or the size of the neuron. All tested neurons were alive during the measurement, as the GC filopodia and lamellipodia exhibited cyclic periods of growth and retraction. In all experiments, *E* was measured either in the soma (using method 1) or in GCs (using methods 1–3; see Materials and Methods), and then either jasplakinolide or cyclodextrin was added to the dish. After exposure for 20 min to the tested drug, *E* was measured again in the same location. Treatment with cyclodextrin caused a decrease in the value of *E* in all tested neurons ($n = 4$) in both the soma (Fig. 7 *d*) and the GCs (Fig. 7 *e*), and in the presence of cyclodextrin, *E* was 90.20 ± 3.18 and 147.10 ± 6.3 Pa in the soma and GCs (measured with method 1), respectively.

Because GCs are thin structures with a height varying between 200 to 600 nm, we also computed the value of *E* using method 2 (i.e., using the standard Hertz model for

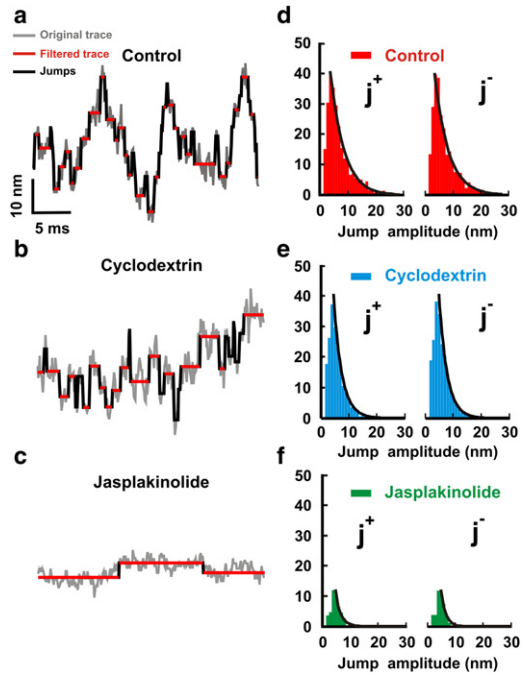


FIGURE 6 Elementary events underlying force generation in control conditions and in the presence of cyclodextrin are less pronounced in the presence of jasplakinolide. (*a–c*) Magnification of the *z* component during push in control conditions (*a*), in the presence of cyclodextrin (*b*), and in the presence of jasplakinolide (*c*). Original traces were filtered by the nonlinear diffusion algorithm (26), resulting in a smooth component and jumps. Jumps were detected infrequently during a push in the presence of jasplakinolide, but very often during a push in control conditions and in the presence of cyclodextrin. (*d–f*) Density of forward $j^+$ and backward $j^-$ jumps during pushes in control conditions (*d*), in the presence of cyclodextrin (*e*), and in the presence of jasplakinolide (*f*). (*d*) The fitting was performed with the values of 148 and 146 events/s for the jump frequency of positive and negative jumps, $A_+$ and $A_-$, respectively, and 5 and 4.8 nm for the mean size of positive and negative jumps, $j^{+*}$ and $j^{-*}$, respectively. (*e*) In the presence of cyclodextrin, the values of $A_+$, $A_-$, $j^{+*}$ and $j^{-*}$ were 226 and 224 events/s and 4.6 and 4.3 nm, respectively. (*f*) In the presence of jasplakinolide, the values of $A_+$, $A_-$, $j^{+*}$ and $j^{-*}$ were 48 and 44 events/s and 2.4 and 2.3 nm, respectively.

fitting force-displacement curves where the indentation is <50 nm) and method 3 (i.e., using the corrected Hertz model for thin samples (29) (Fig. 7 *h*). In both cases, after addition of cyclodextrin, the obtained values of *E* decreased (by 10–40% with method 2 (Fig. 7 *i*) and 10–30% with method 3 (Fig. 7 *j*)).

Jasplakinolide had a more variable effect: it increased the value of *E* in two somas and two GCs, but decreased its value in two somas and four GCs (Fig. 7, *f* and *g*). The mean fractional changes of *E* in the soma ($n = 4$) and GCs ($n = 6$) caused by jasplakinolide were $-0.16 \pm 0.3$ and $0.12 \pm 0.24$, respectively.

**TABLE 1 Jump frequency and amplitude**

| | Jasplakinolide ($n = 3$) | Control ($n = 5$) | Cyclodextrin ($n = 3$) |
|---|---|---|---|
| $j^{+*}$ (nm) | 2.5 ± 0.3 | 5.1 ± 1.3 | 4.6 ± 1.9 |
| $j^{-*}$ (nm) | 2.2 ± 0.4 | 4.9 ± 1.2 | 4.4 ± 1.7 |
| $A_+$ (event/s) | 50.0 ± 4.5 | 157.3 ± 12.0 | 226.2 ± 13.5 |
| $A_-$ (event/s) | 44.0 ± 5.3 | 155.5 ± 11.0 | 224.8 ± 14.7 |

Amplitudes of forward $j^+$ and backward $j^-$ jumps detected during pushes were exponentially distributed and fitted by the equations $A_+ e^{-j+/j+*}$ and $A_- e^{-j-/j-*}$, where $A_+$ and $A_-$ are the rates of forward and backward jumps, respectively, and $j^{+*}$ and $j^{-*}$ are the mean amplitudes of forward and backward jumps, respectively. *n* indicates the number of experiments in which jumps were analyzed.

## DISCUSSION

In this work we analyzed the effect of two drugs, jasplakinolide and cyclodextrin, on force generation in DRG lamellipodia. The drug jasplakinolide at a concentration of 25 nM reduced both $v_{max}$ and $F_{max}$ during pushes, and 2.5 mM cyclodextrin had the opposite effect. During retractions, neither $v_{max}$ nor $F_{max}$ were modified by jasplakinolide or cyclodextrin at the used concentration. Jasplakinolide reduced the amplitude and frequency of elementary jumps underlying force generation, but cyclodextrin increased their frequency. The action of both drugs, at the used concentration, was fully reversible (Fig. 3). However, at higher concentrations, these two drugs can have multiple effects, and it is useful to discuss in detail their properties and reported actions.

### Jasplakinolide

At concentrations > 200 nM, jasplakinolide disrupts actin filaments in vivo by enhancing the rate of actin filament nucleation, leading to alterations of the cytoskeleton and cellular architecture. Prolonged exposure (24–48 h) to small amounts of jasplakinolide was previously shown to reduce proliferation in human Jurkat T cells (33). A concentration of 100 nM jasplakinolide did not modify the elastic properties of fibroblast cell lines measured with AFM (34) and, as shown in Fig. 7, 25 nM jasplakinolide had only a minor effect on the membrane stiffness of DRG neurons in both the soma and GCs. Therefore, the main effect of the low concentration of jasplakinolide used in this investigation (i.e., 25 nM) was a reduction of actin turnover caused by a slowing down of filament depolymerization.

### Cyclodextrins

Depletion of cholesterol caused by cyclodextrins modifies the plasma membrane's functions and in particular the lateral mobility of membrane proteins, presumably as a consequence of the reorganization of the cell actin (35). Therefore, cholesterol not only determines membrane elasticity but also contributes to signaling, albeit in an indirect way (35). This dual action of cholesterol is likely to be at the basis of the different results reported regarding the effect of cyclodextrins on cellular membranes' mechanical properties. Cyclodextrin-impaired pressure induces

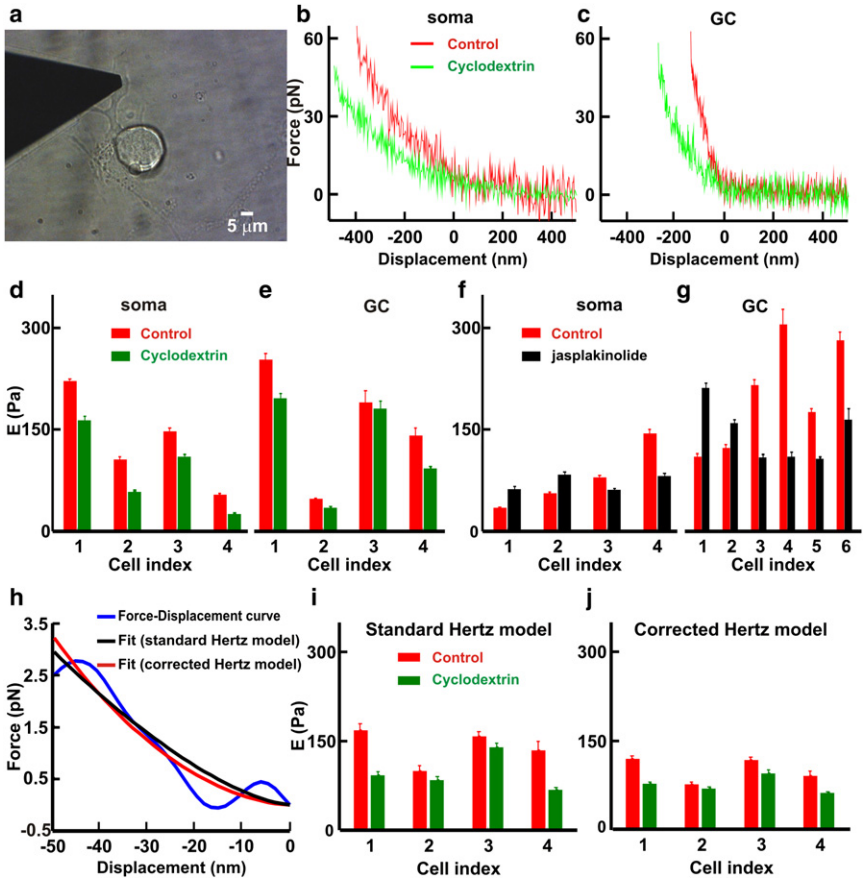


FIGURE 7 Effect of jasplakinolide and cyclodextrin on membrane stiffness. (*a*) Low-resolution image of an AFM cantilever in front of a GC emerging from the soma of a DRG neuron. (*b* and *c*) Force-displacement curves, displaying the AFM cantilever deflection as a function of its vertical *z* position when the cantilever was moved toward the soma (*b*) or GCs (*c*). (*d–g*) Bars indicate the value of Young's modulus, *E*, obtained from the best fit of the force displacement curves with the Hertz model (method 1 using Eq. 1) before and after the same neuron was treated with cyclodextrin, when the cantilever was moved toward the soma (*d*) or the GCs (*e*). Data are the mean ± SE. (*f* and *g*) As in *d* and *e*, but bars indicate the value of *E* in control conditions and in the presence of jasplakinolide. (*h*) Force-displacement curves fitted with the standard Hertz model by considering only indentations of <50 nm (method 2 using Eq. 1) and fitted with the corrected Hertz model (method 3 using Eq. 2). (*i* and *j*) Bars indicate the value of *E* for the same GCs shown in *e* obtained by using method 2 (*i*) or method 3 (*j*). Membrane stiffness obtained by the three methods decreased after addition of 2.5 mM cyclodextrin.

vasoconstriction of skeletal muscle arterioles, whereas excess cholesterol counterbalances this effect (36). Cholesterol depletion of bovine aortic endothelial cells decreases membrane deformability and increases the elastic coefficient of the membrane (37). This effect is interpreted as being due to an alteration in how the actin network inside the cells is connected to the cellular membrane. When 2.5 mM cyclodextrin was added to the extracellular medium, DRG lamellipodia moved more vigorously and cycles of protrusions and retractions similar to those observed in control conditions were observed. These cycles occurred with a frequency slightly higher than in control conditions, suggesting that the normal actin treadmilling underlying these cycles was only marginally affected. These effects of cyclodextrin were almost completely reversible. Using AFM, we determined (by a direct measurement of *E*) that 2.5 mM cyclodextrin reduced the membrane stiffness of DRG neurons both in the soma and in GCs (Fig. 7). Taken together, these observations indicate that the primary effect of cyclodextrin is to reduce the stiffness of lipid bilayers of the DRG lamellipodia.

## Molecular mechanisms of force generation

Lipid rafts are specialized membrane domains that are enriched in cholesterol and sphingomyelin, which are believed to have essential biological functions in cellular membranes (38). These rafts can have dimensions in the nanometer range (35) and lifetimes varying over several orders of magnitude (38), and this dynamics could play an important physiological role in membrane trafficking and signaling. The elastic properties of membranes are heterogeneous, and the Young's modulus *E*, characterizing membrane stiffness, varies across membrane nano/microdomains (39). Therefore, our AFM measurements of *E* based on the Hertz model and its corrections for thin substrata do not capture the heterogeneity and anisotropy of GC membranes, and our measurements must be taken as values averaged over these nanodomains.

The elastic properties of the membrane can vary in correspondence with active zones undergoing extension and/or retraction. In fibroblasts, the Young's modulus near the leading edge of active lamellipodia is 3–5 kPa, whereas it is in the order of 12 kPa in cellular regions that are not involved in push or retraction (28), suggesting that extension preferentially occurs in regions of lower cortical tension. A different observation was made in a previous study of fish migrating keratocytes (40): the stiffness of the membrane decreased from 55 kPa at the front of the leading edge of the migrating keratocyte to 10 kPa at the rear of the lamellipodia, with a profile similar to that of the actin concentration. The reported difference in the gradient stiffness

between fibroblasts and keratocytes could be caused by their different functional properties (i.e., keratocytes migrate and fibroblasts do not).

As shown in Fig. 7, 2.5 mM cyclodextrin reduced membrane stiffness both in the soma and in the lamellipodia GC the treated DRG neurons. The same drug, as shown in Figs. 2 and 4, caused the lamellipodia to protrude with a larger force and with a higher velocity, suggesting that membrane stiffness contributes to force generation. A recent theoretical investigation (41) showed that if the network of actin filaments in lamellipodia is assumed to be organized as a stiff and compact, almost two-dimensional structure, long-range mechanical stresses induced by the plasma membrane stiffness provide a selective pressure that shapes force generation and determines several of its properties (41). Our results suggest that membrane stiffness is an important factor of force generation, and support the notion that mechanical stresses inside lamellipodia have a major role. The combination of a stochastic dynamics (i.e., the alternation of random growth periods and fast retractions (25)) and mechanical interactions of the actin network with the membrane makes the system become critically self-organized (41). This provides a common theoretical framework to understand several experimental observations, such as a growth velocity that is initially insensitive to external force (25,42) and a growth velocity that is dependent on load history (43).

The effects of jasplakinolide on *Fv* relationships (Fig. 4) and on the amplitude and frequency of elementary jumps (Fig. 6) are in agreement with the essential role of actin turnover in force generation. In the presence of jasplakinolide, the mean amplitude of elementary jumps is 2.4 nm (see Table 1). This value is similar to the mean polymerization step size (2.7 nm) of actin filament polymerization (44), suggesting that when actin turnover is reduced, actin monomers are added one by one to the existing network of filaments. In control conditions, larger jumps are observed, presumably caused by the insertion of actin oligomers (45) that are present in lamellipodia as a consequence of actin filament depolymerization.

The small or almost absent effect of both jasplakinolide and cyclodextrin on *Fv* relationships (Fig. 4) during retraction was not expected, because jasplakinolide is a drug that is known to stabilize actin filaments. The absence of a significant effect of these drugs on the kinetics and dynamics of retraction shows that once initiated, lamellipodium retraction is very poorly dependent on membrane stiffness and actin turnover. Indeed, retractions could be global collapses of the overall cytoskeleton architecture overcoming the local stabilization induced by jasplakinolide.

## SUPPORTING MATERIAL

Additional information with a figure and Supporting Methods is available at http://www.biophysj.org/biophysj/supplemental/S0006-3495(12)00510-3.

This work was funded by the European Commission under the Seventh Framework Program (project CP-FP 214566-2 NanoScale, project 229375 SMD, and project 270483 FOCUS).

## REFERENCES

1. Solecki, D. J., E. E. Govek, and M. E. Hatten. 2006. mPar6 $\alpha$ controls neuronal migration. *J. Neurosci.* 26:10624–10625.
2. Ghashghaei, H. T., C. Lai, and E. S. Anton. 2007. Neuronal migration in the adult brain: are we there yet? *Nat. Rev. Neurosci.* 8:141–151.
3. Goodman, C. S. 1996. Mechanisms and molecules that control growth cone guidance. *Annu. Rev. Neurosci.* 19:341–377.
4. Song, H. J., and M. M. Poo. 2001. The cell biology of neuronal navigation. *Nat. Cell Biol.* 3:E81–E88.
5. Mongiu, A. K., E. L. Weitzke, O. Y. Chaga, and G. G. Borisy. 2007. Kinetic-structural analysis of neuronal growth cone veil motility. *J. Cell. Sci.* 120:1113–1125.
6. Mogilner, A., and G. Oster. 1996. Cell motility driven by actin polymerization 25. *Biophys. J.* 71:3030–3045.
7. Pollard, T. D., and G. G. Borisy. 2003. Cellular motility driven by assembly and disassembly of actin filaments. *Cell.* 112:453–465.
8. Pak, C. W., K. C. Flynn, and J. R. Bamburg. 2008. Actin-binding proteins take the reins in growth cones. *Nat. Rev. Neurosci.* 9:136–147.
9. Howard, J. 2001. Mechanics of Motor Proteins and the Cytoskeleton. Sinauer Associates, Sunderland, MA.
10. Raucher, D., and M. P. Sheetz. 2000. Cell spreading and lamellipodial extension rate is regulated by membrane tension. *J. Cell Biol.* 148: 127–136.
11. Fletcher, D. A., and J. A. Theriot. 2004. An introduction to cell motility for the physical scientist. *Phys. Biol.* 1:T1–T10.
12. Peskin, C. S., G. M. Odell, and G. F. Oster. 1993. Cellular motions and thermal fluctuations—the Brownian ratchet. *Biophys. J.* 65:316–324.
13. Mogilner, A., and G. Oster. 2003. Force generation by actin polymerization II: the elastic ratchet and tethered filaments 26. *Biophys. J.* 84:1591–1605.
14. Carlsson, A. E. 2003. Growth velocities of branched actin networks. *Biophys. J.* 84:2907–2918.
15. Mogilner, A. 2006. On the edge: modeling protrusion. *Curr. Opin. Cell Biol.* 18:32–39.
16. Ilangumaran, S., and D. C. Hoessli. 1998. Effects of cholesterol depletion by cyclodextrin on the sphingolipid microdomains of the plasma membrane. *Biochem. J.* 335:433–440.
17. Westover, E. J., D. F. Covey, H. L. Brockman, R. E. Brown, and L. J. Pike. 2003. Cholesterol depletion results in site-specific increases in epidermal growth factor receptor phosphorylation due to membrane level effects—studies with cholesterol enantiomers. *J. Biol. Chem.* 278:51125–51133.
18. Brown, D. A., and E. London. 2000. Structure and function of sphingolipid- and cholesterol-rich membrane rafts. *J. Biol. Chem.* 275:17221–17224.
19. Jones, D. H., K. R. Barber, E. W. VanDerLoo, and C. W. M. Grant. 1998. Epidermal growth factor receptor transmembrane domain: H-2 NMR implications for orientation and motion in a bilayer environment. *Biochemistry.* 37:16780–16787.
20. Simons, K., and E. Ikonen. 2000. Cell biology—how cells handle cholesterol. *Science.* 290:1721–1726.
21. Pollard, T. D., L. Blanchoin, and R. D. Mullins. 2000. Molecular mechanisms controlling actin filament dynamics in nonmuscle cells. *Annu. Rev. Biophys. Biomol. Struct.* 29:545–576.
22. Bubb, M. R., I. Spector, B. B. Beyer, and K. M. Fosen. 2000. Effects of jasplakinolide on the kinetics of actin polymerization. An explanation for certain in vivo observations. *J. Biol. Chem.* 275:5163–5170.

23. Wilson, C. A., M. A. Tsuchida, …, J. A. Theriot. 2010. Myosin II contributes to cell-scale actin network treadmilling through network disassembly. *Nature.* 465:373–377.

24. Cojoc, D., F. Difato, …, V. Torre. 2007. Properties of the force exerted by filopodia and lamellipodia and the involvement of cytoskeletal components. *PLoS ONE.* 2:e1072.

25. Shahapure, R., F. Difato, …, V. Torre. 2010. Force generation in lamellipodia is a probabilistic process with fast growth and retraction events. *Biophys. J.* 98:979–988.

26. Amin, L., E. Ercolini, R. Shahapure, G. Bisson, and V. Torre. 2011. The elementary events underlying force generation in neuronal lamellipodia. *Sci. Rep.* 1:153.

27. Hertz, H. 1881. Ueber die Berührung fester elastischer Körper. *J. Reine. Angew. Math.* 92:156–171.

28. Rotsch, C., K. Jacobson, and M. Radmacher. 1999. Dimensional and mechanical dynamics of active and stable edges in motile fibroblasts investigated by using atomic force microscopy. *Proc. Natl. Acad. Sci. USA.* 96:921–926.

29. Dimitriadis, E. K., F. Horkay, J. Maresca, B. Kachar, and R. S. Chadwick. 2002. Determination of elastic moduli of thin layers of soft material using the atomic force microscope. *Biophys. J.* 82:2798–2810.

30. Neuman, K. C., and S. M. Block. 2004. Optical trapping. *Rev. Sci. Instrum.* 75:2787–2809.

31. Felder, S., and E. L. Elson. 1990. Mechanics of fibroblast locomotion—quantitative-analysis of forces and motions at the leading lamellas of fibroblasts. *J. Cell Biol.* 111:2513–2526.

32. Daily, B., E. L. Elson, and G. I. Zahalak. 1984. Cell poking. Determination of the elastic area compressibility modulus of the erythrocyte membrane. *Biophys. J.* 45:671–682.

33. Odaka, C., M. L. Sanders, and P. Crews. 2000. Jasplakinolide induces apoptosis in various transformed cell lines by a caspase-3-like protease-dependent pathway. *Clin. Diagn. Lab. Immunol.* 7:947–952.

34. Rotsch, C., and M. Radmacher. 2000. Drug-induced changes of cytoskeletal structure and mechanics in fibroblasts: an atomic force microscopy study. *Biophys. J.* 78:520–535.

35. Edidin, M. 2003. The state of lipid rafts: from model membranes to cells. *Annu. Rev. Biophys. Biomol. Struct.* 32:257–283.

36. Potocnik, S. J., N. Jenkins, T. V. Murphy, and M. A. Hill. 2007. Membrane cholesterol depletion with beta-cyclodextrin impairs pressure-induced contraction and calcium signalling in isolated skeletal muscle arterioles. *J. Vasc. Res.* 44:292–302.

37. Byfield, F. J., H. Aranda-Espinoza, V. G. Romanenko, G. H. Rothblat, and I. Levitan. 2004. Cholesterol depletion increases membrane stiffness of aortic endothelial cells. *Biophys. J.* 87:3336–3343.

38. Elson, E. L., E. Fried, …, G. M. Genin. 2010. Phase separation in biological membranes: integration of theory and experiment. *Ann. Rev. Biophys.* 39:207–226.

39. Roduit, C., F. G. van der Goot, …, S. Kasas. 2008. Elastic membrane heterogeneity of living cells revealed by stiff nanoscale membrane domains. *Biophys. J.* 94:1521–1532.

40. Laurent, V. M., S. Kasas, …, J. J. Meister. 2005. Gradient of rigidity in the lamellipodia of migrating cells revealed by atomic force microscopy. *Biophys. J.* 89:667–675.

41. Cardamone, L., A. Laio, …, A. DeSimone. 2011. Cytoskeletal actin networks in motile cells are critically self-organized systems synchronized by mechanical interactions. *Proc. Natl. Acad. Sci. USA.* 108:13978–13983.

42. Prass, M., K. Jacobson, A. Mogilner, and M. Radmacher. 2006. Direct measurement of the lamellipodial protrusive force in a migrating cell. *J. Cell Biol.* 174:767–772.

43. Parekh, S. H., O. Chaudhuri, J. A. Theriot, and D. A. Fletcher. 2005. Loading history determines the velocity of actin-network growth 28. *Nat. Cell Biol.* 7:1219–1223.

44. Abraham, V. C., V. Krishnamurthi, D. L. Taylor, and F. Lanni. 1999. The actin-based nanomachine at the leading edge of migrating cells. *Biophys. J.* 77:1721–1732.

45. Okreglak, V., and D. G. Drubin. 2010. Loss of Aip1 reveals a role in maintaining the actin monomer pool and an in vivo oligomer assembly pathway. *J. Cell Biol.* 188:769–777.

## 2.4

# The role of myosin II in force generation in DRG growth cones

Ladan Amin, Wassim Sayyad, Erika Ercolini, Jelena Ban, Hiba Sheheitli, Paolo Fabris, Alejandro Valbuena & Vincent Torre

(In preparation)

# Multiple role of Myosin II in force generation in DRG growth cones

Ladan Amin[1], Wassim Sayyad[1], Erika Ercolini[1], Jelena Ban[1], Hiba Sheheitli, Paolo Fabris[1], Alejandro Valbuena[1] & Vincent Torre[1]*

[1] Neurobiology Sector, International School for Advanced Studies (SISSA), via Bonomea 265, 34136 Trieste, Italy

## Abstract

We used optical tweezers, video imaging and immunocytochemistry to analyse the role of non muscular myosin II on the force exerted by lamellipodia from developing growth cones (GCs) of isolated Dorsal Root Ganglia (DRG) neurons. The two isoforms of myosin II, A (NMIIA) and B (NMIIB), localized differently in DRG GCs: the concentration of NMIIA was approximately constant from the GC centre to its leading edge, while NMIIB was more confined in the central region of GCs. When the activity of myosin II was inhibited by 20 μM Blebbistatin cycles of lamellipodia protrusion/retraction slowed down and during retractions lamellipodia did not lift up vertically as in control conditions. Lamellipodia motion was completely abolished by 50 μM Blebbistatin. After treatment with Blebbistatin lamellipodia emerging from the soma and from GCs become “filopodish” with the clear appearance of structures reminiscent of filopodia. The force generated by lamellipodia treated with 30 μM Blebbistatin decreased by 30-50 %, but surprisingly not the force generated by filopodia, which increased by 30-50 %. Immunocytochemical analysis of filopodia emerging from GCs treated with Blebbistatin showed the presence of tubulin, in a proportion higher than in filopodia in control conditions. These results suggest that: i - contractions of the actomyosin complex formed by filaments of actin and NMIIA have an active role during “shovel-like” lamellipodia retractions; ii - myosin II is an essential component of the structural stability of GC architecture; iii - myosin II modulates the coupling of actin filaments and microtubules dynamics.

## INTRODUCTION

During development neurons are able to self-organize in precisely wired networks and are able to establish the appropriate synaptic connections. Neuronal navigation requires the existence of highly motile structures able to probe the mechanical properties of the surrounding environment and to search for the chemical cues leading to the formation of correct synaptic connections (1, 2). Neuronal exploration is guided by growth cones (GCs) located at the neurite tips (3, 4). GCs are composed of a lamellipodium with a height of 2-10 μm from which thin filopodia with a submicron diameter emerge (5). The primary source of motility in GCs is the polymerization of actin filaments (6, 7), controlled by a large set of regulatory proteins, such as Arp2/3, WASP, etc (8) and molecular motors seem to participate to the overall process by controlling several aspects of the process. Indeed non muscle myosin II has been localized in neuronal GCs, where is thought to control the retrograde flow of actin in lamellipodia (9).

The addition of actin polymers to actin filaments in close contact with the membrane pushes the cellular membrane forward exerting a protrusive force (10, 11). An important determinant of force generation is the turnover of actin filaments, during which actin monomers or small oligomers are added to the barbed end of actin filaments (polymerization) and removed from the other end (depolymerization). In this process the non muscle myosin II plays an important role: indeed myosin II controls the retrograde flow of actin monomers/oligomers by severing the actin filaments at their pointed end, providing the necessary treadmilling mechanism (9). Myosins constitute a superfamily of motor proteins with major roles in several cellular processes such as cell adhesion, migration and division (12). Myosin molecules, like all motor proteins, can walk along, propel and slide other molecules and can produce tension on actin filaments. Generation of tension and force requires metabolic energy, usually provided by ATP hydrolysis and therefore myosins have appropriate catalytic sites in their amino-terminal (head) region. The carboxy-terminal region of some myosins binds to and moves cargo in a cell, whereas the C-terminal domains of other myosins self-associate into filaments, which allows their heads to tether actin filaments forming the actomyosin complex able to exert tension. Myosins can also act indirectly through actin to bring adhesion-related proteins, such as integrins, or signal transduction molecules into close proximity. Like muscle myosin II, non-muscle myosin II (NMII)

molecules are comprised of three pairs of peptides: two heavy chains of 230 kDa, two 20 kDa regulatory light chains (RLCs) that regulate NMII activity and two 17 kDa essential light chains (ELCs) that stabilize the heavy chain structure (12). Although these myosins are referred to as 'non-muscle' myosin IIs to distinguish them from their muscle counterparts, they are also present in muscle cells, where they have distinct functions during skeletal muscle development and differentiation. In mammalian non muscle cells, two isoforms of myosin II coexist (NMIIA and NMIIB) and are involved in distinct cellular processes with different localizations (13). In fibroblasts, NMIIA produces the majority of traction forces and controls the actomyosin complex network (14), while NMIIB is responsible for collagen fibre movement (15). In neurons, NMIIB is thought to be involved in neurite outgrowth, while NMIIA plays a role in lamellipodia retraction and promotes the adhesion with formation of focal contact (16-18). A new myosin II isoform has been recently discovered and characterized (NMIIC), which is thought to regulate cell membrane extension and the formation of focal contacts showing therefore separate but coupled activities with NMIIA and NMIIB (17). The three myosin II isoforms, NMIIA, NMIIB and NMIIC have similar structural and dynamical properties but have slightly different kinetics properties. Their major difference seems to reside in their regulation properties and different proteins control them through distinct phosphorylation sites (12).

Myosin II seems to be involved in the orchestration of actin polymerization /depolymerization but also of microtrubules (MTs) dynamics. Indeed, it has been shown that actin oligomers driven by myosin II interact with growing MTs and that myosin II-dependent compressive force is necessary for MT dynamics (19). The existence of a coupling between actin and MT dynamics is also supported by the observation that inhibition of myosin II with Blebbistatin markedly accelerates axon growth and promote the reorganization of both actin and MTs in GCs (20).

The aim of the present manuscript is to analyse in more detail the role of myosin II in force generation in DRG lamellipodia and GCs, with two aims: firstly to explore the role of contractions of the actomyosin complex in the protrusion/retraction cycles observed in lamellipodia of developing neurons and secondly to better understand myosin II role in the regulation of the cytoskeleton.

# MATERIALS AND METHODS

## Neuron preparation

Wistar rats at postnatal days 10 to 12 (P10-P12) were sacrificed by decapitation after anesthesia with $CO_2$ in accordance with the Italian Animal Welfare Act. After dissection, Dorsal Root Ganglias (DRGs) were incubated with trypsin (0.5 mg/ml; Sigma-Aldrich, Milan, Italy), collagenase (1 mg/ml; Sigma-Aldrich), and DNase (0.1 mg/ml; Sigma-Aldrich) in 5 ml Neurobasal medium (Gibco, Invitrogen, Milan, Italy) in a shaking bath (37°C, 35-40 min). After mechanical dissociation, they were centrifuged at 300 rpm, resuspended in culture medium, and plated on poly-L-lysine-coated (0.5 μg/ml; Sigma-Aldrich) coverslips. Neurons were incubated for 24 h to 48 h and nerve growth factor (50 ng/ml; Alomone Labs, Jerusalem, Israel) was added before performing the measurements.

## Optical tweezers setup

The optical tweezers set-up was built as described in (21). Briefly, the trapping source was an Ytterbium fiber laser operating at 1064 nm (IPG Laser GmbH, Burbach, Germany) which was sent onto an inverted microscope (IX81, Olympus, Milan, Italy) to the focusing objective (Olympus 100X oil, NA 1.4). The dish containing the differentiating neurons and the beads (PSI-1.0NH2, G.Kisker GbR, Steinfurt, Germany) was placed on the microscope stage which could be moved by a 3 axes piezoelectric nanocube (17 MAX 301, Melles Griot, Albuquerque, NM). The temperature of the dish was kept at 37°C by a Peltier device. The bead position $\mathbf{x} = (x, y, z)$ was determined along all the axes with a lateral and vertical accuracy of 2 and 5 nm using back focal plane (BFP) detection, which relies on the interference between forward scattered light from the bead and unscattered light (21-23). The BFP of the condenser was imaged onto a quadrant photodiode (QPD; C5460SPL 6041, Hamamatsu, Milan, Italy) and the light intensity was converted to differential outputs digitized at 10 kHz and low pass filtered at 5 kHz. Bead z position was determined using the Gouy phase shift effect (22). The trap stiffness $\mathbf{K}_{x,y,z} = (k_x, k_y, k_z)$ and the detector sensitivity were calibrated using the power spectrum method (22). The force exerted by the lamellipodium $\mathbf{F}$ was taken as equal to $\mathbf{-F_{trap}}$. When the displacement of the bead from its equilibrium position inside the trap $\mathbf{d} = (d_x, d_y, d_z)$ was less than 400 nm, $\mathbf{F_{trap}} = (F_x, F_y, F_z)$

was calculated as $F_x = d_x k_x$, $F_y = d_y k_y$, and $F_z = d_z k_z$ (22). All experiments of force recordings were monitored by video imaging with a CCD camera at a frame rate of 5 Hz. Visual inspection of recorded images allowed to discard from the analysis all force recordings during which visible debris interfered with the optical determination of the bead position **x**.

**Computation of Fv relationships**

The velocity $\mathbf{v} = (v_x, v_y, v_z)$ of the bead was obtained by numerical differentiation of its sampled position $\mathbf{x} = (x(n), y(n), z(n))$ $n = 1,\ldots N$. Numerical differentiation was computed either by convolution of the position components $x(n)$, $y(n)$ and $z(n)$ with the derivative of a Gaussian filter $1/[\sigma(2\pi)^{1/2}] \exp(-t^2/\sigma^2)$ (Gaussian filtering) or by Linear regression. Gaussian filters corresponding to cut-off frequencies of 0.2, 1 and 10 Hz were used. Further details can be found in (24).

**Jumps determination by non linear diffusion filtering**

In order to detect jumps, we used an algorithm based on non linear diffusion (25, 26). The algorithm is based on the Toolbox of Frederico D'Almeida (see http://www.mathworks.com/matlabcentral/fileexchange/3710-nonlinear-diffusiontoolbox). Further details can be found in (27)

**Analysis of video sequences**

In order to quantify the kinetics of protrusion/retraction cycles of lamellipodia we acquired stacks of images at a frequency of 0.1-1 Hz. Every stack of images was composed by an image focused at the plane containing the coverslip where neurons were cultured and images focused 1,2,3,4,5, 6 and 7 microns above the coverslip. The acquisition of a stack of 8 images was obtained in 0.5 s, interval of time in which the lamellipodia motion was almost absent. We developed two algorithms: Algorithm I was designed to quantify in a semi-automatic way the time course of protrusion/retraction cycles and Algorithm II was designed to quantify the vertical motion of lamellipodia during these cycles.

Algorithm I

Images focused at the coverslip plane at different times of the protrusion/retraction cycles (Fig. 1 *a*, $t_1$-$t_3$) were analyzed: edges were extracted using standard procedures (28) and the contour of the neuron was obtained (red line in Fig. 1 *b*). A reference point on the soma or at the base of the lamellipodium was selected (red cross in Fig. 1 *b*) and an angle covering the lamellipodium was also selected (green shadow in Fig. 1 *b*). The mean distance between the red cross and the points forming the detected contour inside the green shadow was computed and plotted (Fig. 1 *c*). In this plot, representing the mean distance of the lamellipodium leading edge from a reference point, we detected local maxima and minima (green and red asterisks, respectively, in Fig. 1 *c*). The interval between a successive green and red point was taken as the period of that protrusion/retraction cycle. The reliability of the algorithm was controlled by visual inspection of the data by the operator.

Algorithm II

Algorithm II was based on classical depth-from-focus algorithms introduced in Computer Vision (29) to recover 3D information from stacks of images acquired at different focal planes. These algorithms were used in the present work to recover the lamellipodia motion also in the vertical direction. Briefly, for each pixel (i,j) and for each image intensity I(i,j,h) acquired at a focal plane h microns above the coverslip, the gradient $\nabla$ I(i,j,h) was computed. The point at location (x,y) has the height h if the feature at point (x,y) is on focus at the plane h, determined as the plane for which $\nabla$ I(i,j,h) has the maximum value. Images of the neuron taken at different focal planes separated by 1 µm are shown in Fig. 1 *d* (h=1,…,6µm) and $\nabla$ I(i,j,h) was computed.

In order to obtain a measurement of the ability of a lamellipodium to move up in the vertical direction for each value of h we computed the fraction of pixels - in a given region of interest - in focus at the height h (Fig. 1 *e*). In this way we could characterize the effect of used drugs – such as Blebbistatin and Cytochalasin D – on the ability of lamellipodia to lift up in the vertical direction. We have also developed an algorithm based on the observation that lamellipodium edges in focus at a plane above that imaged appear brighter (see red cross in Fig. 1 *d*, h=1 µm) and those in focus below appear darker (see blue arrow in Fig. 1 *d*, h=6

µm). This algorithm did not perform as well as the one based on the computation of the image gradient $\nabla$ I(i,j,h).

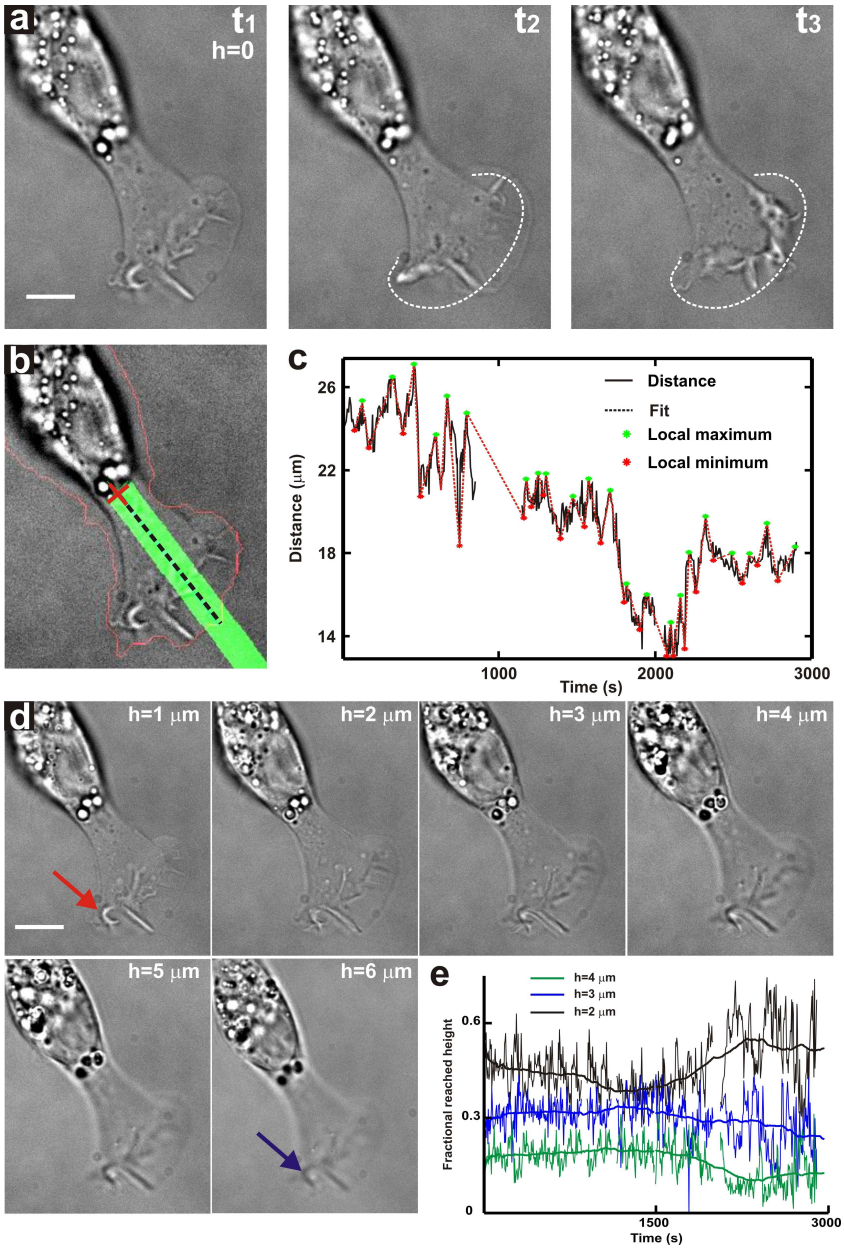


**Figure 1. Computation of lamellipodial protrusion/retraction cycles and of vertical motion.** (*a*) From left to right three images of the lamellipodium emerging from a DRG neuron undergoing cyclic waves of protrusion ($t_2$) and retraction ($t_1$ and $t_3$) in control conditions; the dotted line represents the leading edge of lamellipodia at time $t_1$. Scale bar, 5 µm. (*b*) Diagram of the method used for the semi-automatic detection of protrusion/retraction cycles. See text for technical details. (*c*) Time evolution of the distance of lamellipodium leading edge from the reference point indicated by the red cross in panel (*b*). Local maxima and minima represent maximal protrusion and retraction, respectively. (*d*) Stack of 6 images acquired at 6 focal planes at distance h from the coverslip where neurons are grown. Scale bar, 5 µm. Red and blue arrows indicate the pixels

in focus at a plane above and below the one imaged, respectively. The pixels above focus appear brighter and the pixels below appear darker. (*e*) Fractional density of lamellipodia points in focus at different focal planes (h=2, 3 and 4 µm). The continuous solid lines are a smoothing over a time window of 100 s.

**Immunostaining and imaging**

Cells were fixed in 4% paraformaldehyde containing 0.15% picric acid in phosphate-buffered saline (PBS), saturated with 0.1 M glycine, permeabilized with 0.1% Triton X-100, saturated with 0.5% BSA in PBS (all from Sigma-Aldrich, St.Louis, MO) and then incubated for 1h with primary antibodies: mouse monoclonal antibody against neuronal class III β-tubulin-TUJ1 (Covance, Berkeley, CA) and rabbit polyclonal antibodies against myosin IIA and IIB (both from Sigma-Aldrich, St.Louis, MO). The secondary antibodies were goat anti-rabbit 594 Alexa (Invitrogen, Life Technologies, Gaithersburg, MD, USA) and anti-mouse $IgG_{2a}$ biotynilated (Santa Cruz Biotechnology, Santa Cruz, CA) and the incubation time was 30 min. F-actin was marked with Alexa Fluor 488 phalloidin, whereas biotin was recognized by Marina Blue-Streptavidin (Invitrogen, Life Technologies, Gaithersburg, MD, USA) and incubated for 30 min. All the incubations were performed at room temperature (20-22°C). The cells were examined using a Leica DMIRE2 confocal microscope (Leica Microsystems GmbH, Germany) equipped with DIC and fluorescence optics, diode laser 405nm, Ar/ArKr 488nm and He/Ne 543/594nm lasers. The fluorescence images (1024x1024 pixels) were collected with a 63X magnification and 1.4 NA oil-immersion objective. Leica LCS Lite and Image J by W. Rasband (developed at the U.S. National Institutes of Health and available at http://rsbweb.nih.gov/ij/) were used for image processing.

**AFM imaging**

Atomic Force Microscopy (AFM) was performed by using a commercial AFM (Nanowizard III, JPK Berlin, Germany) combined with an inverted optical microscope (OLYMPUS IX71, 40X/1.3 NA oil immersion objective). Briefly, neurons fixed on 24 mm diameter glass coverslips were washed with PBS and mounted on the AFM liquid cell (Biocell II, JPK Berlin, Germany). All experiments were performed in PBS. For dynamic mode scanning we used cantilevers HYDRA-2R50NG (AppNano, Santa Clara, CA, USA) with a nominal spring constant of 0.08 N/m. The excitation frequency was very close to 14kHz, which corresponds to the first harmonic of the lever in liquid. Softer cantilevers

(MLCT, Bruker AFM Probes, Camarillo, CA, USA) with a nominal spring constant of 0.01 N/m were used in contact mode. After laser alignment and cantilever calibration, the system was left to settle with AFM infrared laser, optical microscope condenser and temperature controller switched on to minimize force drift during image acquisition. When the AFM was operated in contact mode the contact force of the cantilever tip was corrected during imaging to minimize the force exerted by the tip on the sample, keeping it between 200 pN and 1 nN. Images were acquired with a line rate ranging 0.2 to 1 Hz and 512 or 1024 points on the larger side of the image. For the analysis of the AFM images we used WSxM 5.0 (30). In order to estimate the average width of filopodia we calculated their area with the flooding tool of WSxM and then it was divided by the length of the filopodia.

**Localization of NMIIA and NMIIB**

Measurement of the NMIIA and NMIIB localization in respect to the actin staining has been performed on confocal fluorescence images acquired as described above (see Immunostaining and imaging). The intensity of pixels was measured over lines which were considered from the center of GC to the leading edge for NMIIA or NMIIB relative to corresponding actin staining. The final result is the average of all lines normalized to the same length, as shown in (Fig. 2 *c*-*e*).

**RESULTS**

Large and highly motile lamellipodia emerge from dissociated neurons from DRG after 6-12 hours of culture (24, 27, 31). These lamellipodia can exert forces larger than 20 pN and their leading edge can move with a speed of 30-100 nm/s (24). Motility is restricted to the lamellipodia and filopodia and dissociated neurons from DRG do not migrate and their soma remains approximately in the same location on the dish for several hours. After 2-3 days of culture dissociated neurons establish physical contacts and motility of lamellipodia and filopodia is reduced. Therefore, we have analysed the effect of inhibitors of myosin II (Blebbistatin) and of actin polymerization (Cytochalasin D) on lamellipodia and filopodia after 24-48 hours of culture, when their motility is more pronounced.

**Localization of myosin II in DRG GCs and the effect of Blebbistatin on cytoskeletal architecture**

There are three isoforms of myosin II in GCs, which have often a different localization in GCs (17, 20) possibly underlying different functions (16, 32). We examined the localization of NMIIA and NMIIB in DRG GCs by immunostaining. We determined simultaneously the cellular distribution of actin, tubulin and one of the two myosin isoforms, i.e. NMIIA and NMIIB (see Fig. 2). The staining for NMIIB (Fig. 2 *a*) was preferentially localized in the central domain and transition zone of the GC, in agreement with previous observations (9, 20) and very rarely we detected any staining in filopodia. In contrast, we observed a more diffuse staining of NMIIA (Fig. 2 *b*), present in the central and transition zone of the GC, but also in its periphery near its leading edge and occasionally also in some filopodia.

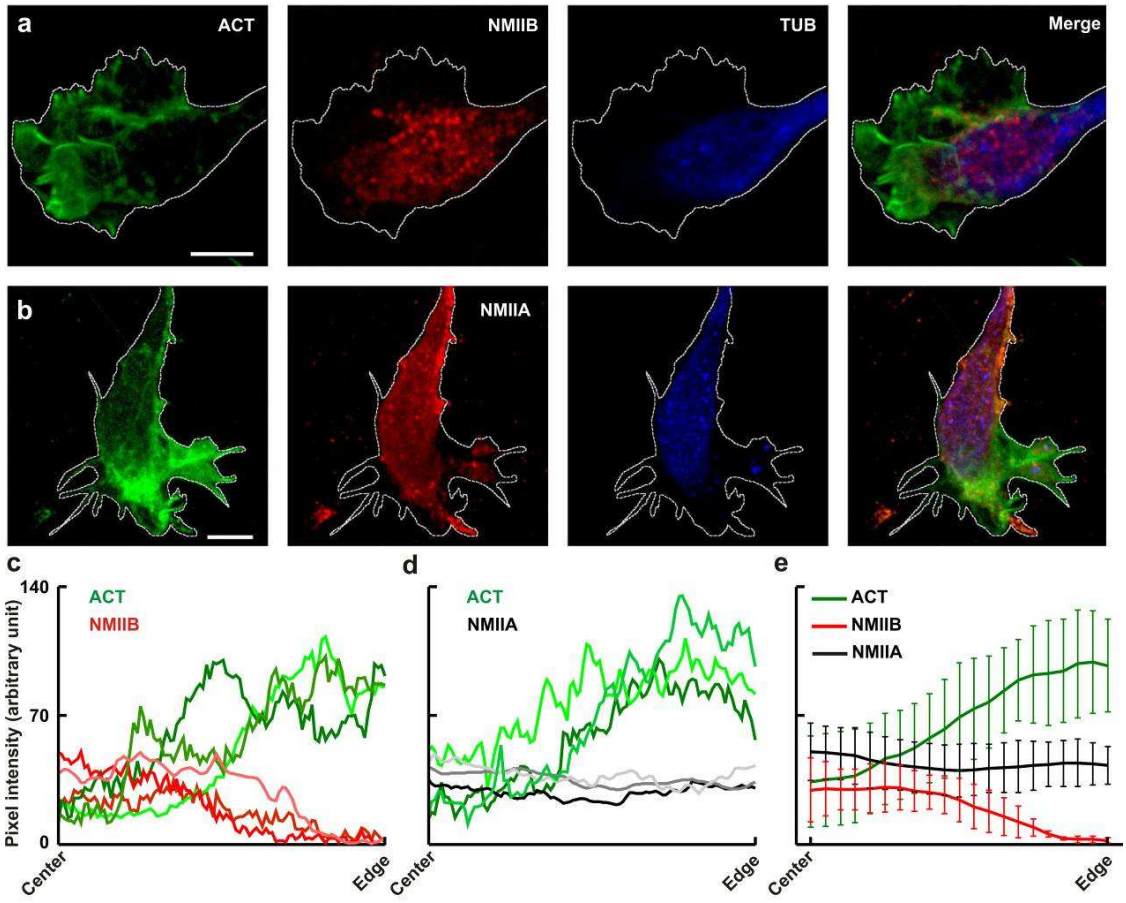


**Figure 2. Localization of NMIIA and NMIIB in DRG GCs.** (*a*) From left to right: confocal fluorescence images of a DRG GC for actin (*green*), NMIIB (*red*), and tubulin III (*blue*) and merge of the three staining. (*b*)

From left to right: confocal fluorescence images of a GC for actin, NMIIA and tubulin and merge of the three staining. Scale bar, 5µm. (*c*) Average profile of staining intensity from the GC centre to its leading edge in 3 GCs for actin (*shades of green*) and NMIIB (*shades of red*). (*d*) Average profile of staining from the GC centre to its leading edge in 3 GCs for actin (*shades of green*) and NMIIA (*shades of grey*). (*e*) Average profile of staining intensity from the GC center to its leading edge from 10 GCs for actin (*green*), NMIIB (*red*) and NMIIA (*black*).

We quantified the relative distribution of actin, NMIIA, and NMIIB by selecting a point in the centre of the GC (C) and measuring and averaging the staining intensity over rays emerging from C and reaching the GC leading edge (see Materials and Methods for further detail). As shown in Fig. 2 *c* and *d* (*shades of green*) actin concentration increased from the GC centre to its leading edge, but a different behaviour was observed for the two myosin II isoforms: NMIIB decreased consistently at the periphery (Fig. 2 *c*, *shades of red*), while NMIIA was evenly present and colocalized with actin at the GC periphery (Fig. 2 *d*, shades of grey). These observations were verified in all examined GCs (n= 10), as shown in (Fig. 2 *e*).

We analysed also the actin and tubulin distribution in lamellipodia emerging from the soma of differentiating DRG neurons. Lamellipodia sprouting from the soma had an extensive network of actin filaments interspersed with rare filaments of microtubules. Also in these lamellipodia staining of NMIIA was clearly present at their leading edge, while staining for NMIIB was more restricted near the soma and only rarely extended to the periphery of GCs (see Supplementary Information, Fig. S1).

After treatment with 20-50 µM Blebbistatin, a powerful inhibitor of both myosin isoforms (33), lamellipodia emerging from the soma and from GCs distant from the soma, changed their morphology, lost their sheet-like structure, and appeared “filopodish” (Fig. 3 *a-d*). After Blebbistatin treatment (Fig. 3 *d-f*) sparse actin filaments were clearly visible which did not appear to be joined by the usual actin network. Untreated GCs at the tip of long neurites had the core of microtubules surrounded by a mesh of actin filaments and very rarely microtubules entered in filopodia, which were primarily composed by actin filaments. After treatment with Blebbistatin, the terminal end of neurites was composed by actin filaments but also microtubules at the most distant GC tips (Fig. 3 *e* and *f*). The average number of filopodia per GC in untreated DRG neurons was 3.2±0.6 and was 4.6±0.5 after treatment with 30 µM Blebbistatin (Fig. 3 *g*).

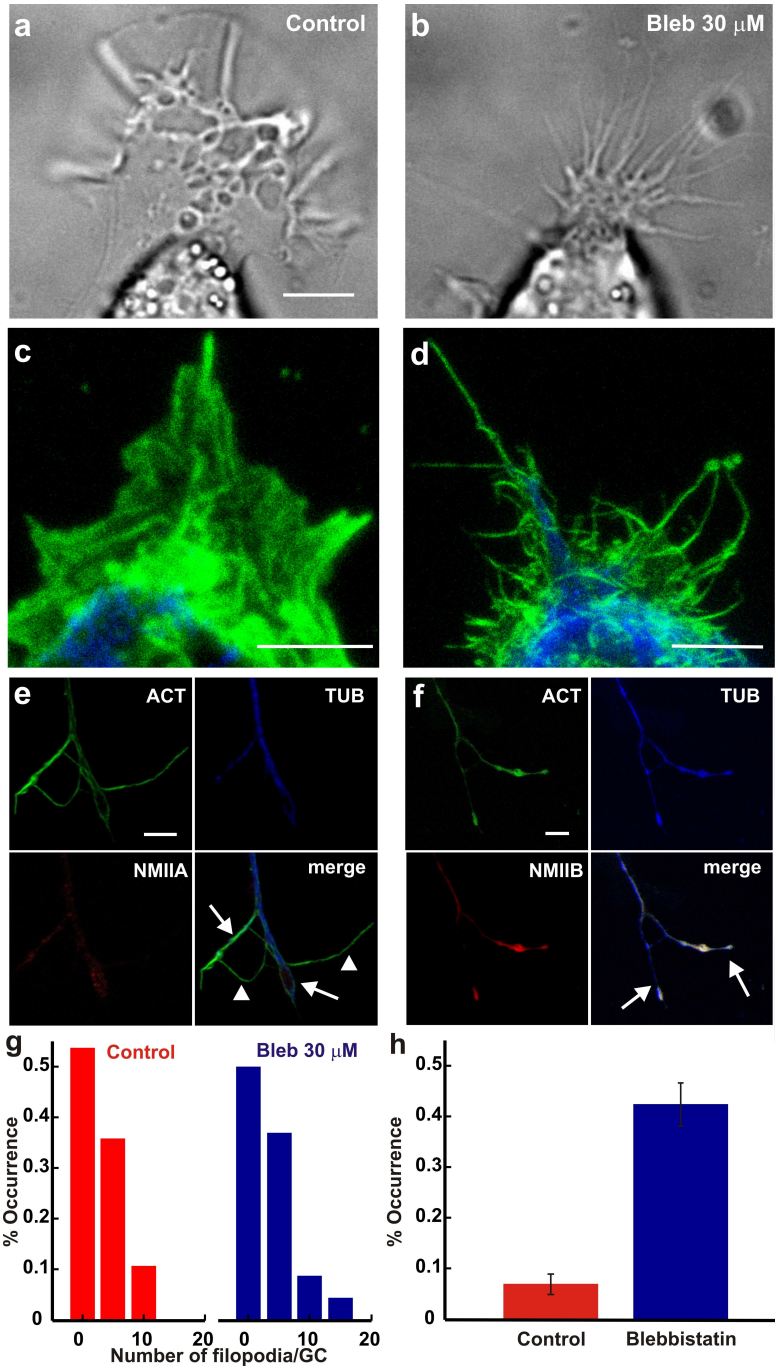


**Figure 3. The effect of Blebbistatin on GC morphology.** (*a-b*) Lamellipodium emerging from a DRG neuron in control conditions and after treatment with 30 μM Blebbistatin, respectively. Note the "filopodish" appearance of the lamellipodia after Blebbistatin treatment. (*c*) Immunostaining of DRG lamellipodium in control conditions for actin (*green*) and tubulin (*blue*) staining (*d*) As in (*c*) but in the presence of 30 μM Blebbistatin. Scale bar, 5 μm. (*e*) Immunostaining of a GC after Blebbistatin treatment for actin, NMIIB and tubulin and merge of the three staining. Arrows and arrowheads indicate filopodia with and without a clear

staining for tubulin, respectively. Scale bar, 5µm. (*f*) Immunostaining of a GC after Blebbistatin treatment for actin, NMIIA and tubulin and merge of the three staining. (*g*) Histograms of filopodia number per GC before (*red histogram*) and after treatment with blebbistatin (*blue histogram*). (*h*) The fraction of filopodia with a staining for microtubules in control conditions (*red bar*) and after Blebbistatin treatment (*blue bar*).

If the mean number of filopodia per GC was not significantly affected by myosin II inhibition, treatment with Blebbistatin had a profound effect on the distribution of microtubules inside filopodia: in control conditions the fraction of filopodia emerging from GCs exhibiting a staining for microtubules was 0.07± 0.02 (Fig. 3 *h, red bar*) but after Blebbistatin treatment increased to 0.42±0.04 (Fig. 3 *h, blue bar*), showing that inhibition of NMII elevated the presence of microtubules inside filopodia.

**The ultrastructure of GCs treated with Blebbistatin**

The "filopodish" morphology of GC treated with Blebbistatin (Fig. 3 *a* and *b*) and the concomitant increased presence of microtubules inside filopodia suggested us to investigate in more detail the ultrastructure of untreated GCs and after treatment with Blebbistatin. Therefore, we used AFM, with the aim of establishing whether morphology - at a nm resolution - of filopodia in untreated and treated GC was similar or not.

Lamellipodia emerging from the soma or from GCs at the tip of neurites could have the corrugated surface previously described (34) with holes and a maximal height up to 900 nm (Fig. 4 *a*). After treatment with 30 µM Blebbistatin lamellipodia emerging from the soma were fragmented (Fig. 4 *b*) and GCs at the tip of long neurites GCs did not have a flat and extended surface and terminated with 2-4 thin terminal neurites. The shape and geometrical properties of these neurites were similar to those of filopodia from untreated GCs. Indeed, collected data show that the length (Fig. 4 *c*), height (Fig. 4 *d*) and width (Fig. 4 *e*) of untreated filopodia (*red histograms*) were very similar to those of terminal neurites of GCs treated with Blebbistatin (*blue histograms*). Lamellipodia of treated GCs had an height similar to that of untreated neurons with less holes rarely reaching the coverslip (Fig. 4 *b*). Analysis of fluorescence images show that the average area of treated GCs was 45.48±10.53 $\mu m^2$ when in untreated GCs was 109.5±21.0 $\mu m^2$. Therefore, Blebbistatin did not alter the structure at a nm resolution of filopodia emerging from GCs or from the tip of terminal neurites, but reduced at some extent lamellipodium area.

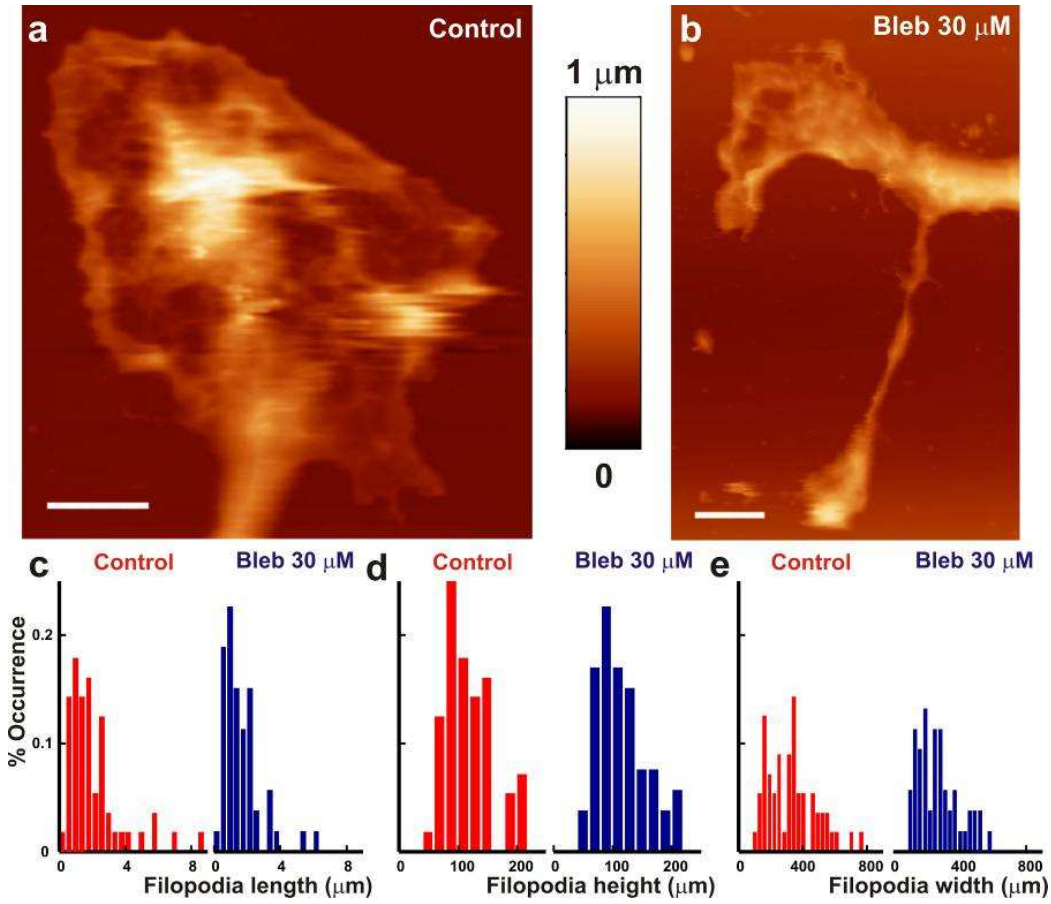


**Figure 4. The effect of Blebbistatin on GCs ultrastructure.** (*a-b)* AFM images of an untreated GC and of a GC treated with 30 μM Blebbistatin, respectively. Untreated lamellipodia are often fragmented with holes reaching the coverslip. Filopodia emerging from lamellipodia are visible after Blebbistatin treatment, but these lamellipodia have a more compact structure, with less holes. Scale bar, 3 μm. *(c)* Distribution of filopodia length for untreated and Blebbistatin treated GCs (*blue* and *red histogram*, respectively). Average length is 2.1 ± 1.7 μm and 1.6 ± 1.2 μm for untreated and Blebbistatin treated GCs. *(d)* Distribution of filopodia average height for untreated and Blebbistatin treated GCs (*blue* and *red histogram*, respectively). Both histograms have the same distribution with similar average values: 120 ± 30 and 115 ± 24 nm for untreated and Blebbistatin treated GCs. *(e)* Distribution of filopodia average width for untreated and Blebbistatin treated GCs (*blue* and *red histogram*, respectively). Both histograms have the same distribution with similar average values: 333 ± 154 nm and 285 ± 160 nm for untreated and Blebbistatin treated GCs.

## The effect of Blebbistatin and Cytochalasin D on protrusion/retraction cycles

Lamellipodia emerging from the soma of DRG neurons protrude and collapse continuously and we followed their protrusion/retraction cycles by videoimaging (Fig. 1 *a*). By analysing these image sequences with Algorithm I described in the Materials and

Methods section, we followed the average distance of the lamellipodium leading edge (Fig. 5 *a*) from a reference point (C) usually chosen in the center of the DRG soma or at the base of the lamellipodium (see Fig. 1 *b*) and we could measure the period of protrusion/retraction cycles (*red bars* in Fig. 5 *b*). When 30 μM Blebbistatin was added to the medium bathing the neuronal culture, within 5 minute or so lamellipodia shrank (Fig. 3 *b*) and cycles of protrusion/retraction could still be observed in some lamellipodia but with a period 30-50 % longer than in control conditions (Fig. 5 *a* and *b*). When a higher concentration of Blebbistatin was used, such as 50 μM, lamellipodia shrank within 2-5 minutes and motility was suppressed.

In control conditions during protrusion/retraction cycles lamellipodia move also upwards by 2-5 μm and indeed at a focal plane 3 or 4 μm higher than the coverslip their leading edge could be seen well on focus. By using Algorithm II described in the Materials and Methods section, we counted the number of pixels of moving lamellipodium becoming well in focus at different heights, i.e. at 2,3 and 4 μm above the coverslip (Fig. 5 *c*). After addition of 30 μM Blebbistatin to the bathing medium, lamellipodia prolonged the duration of their protrusion/retraction cycles (Fig. 5 *a* and *b*) but also reduced the average height reached during these cycles (Fig. 5 *c*). Indeed, the fraction of pixels on focus at 2 μm above the coverslip increased, while those on focus at 3 and 4 μm above decreased (Fig. 5 *c*).

Treatment with a concentration of 50 μM Blebbistatin invariably led to the suppression of motility of analysed lamellipodia, therefore, we investigated the effect of other drugs known to affect and abolish motility, but acting on a different biochemical target. Cytochalasin D is a well known and specific inhibitor of actin filament polymerization (35). Cytochalasin D binds to the barbed end actin filaments blocking the addition of new actin monomers or oligomers. Concentrations of Cytochalasin D, such as 25 or 50 nM caused lamellipodia to shrink completely and abolished almost entirely GC motility, confirming the fundamental role of actin filament polymerization. Both Blebbistatin and Cytochalasin D reduce lamellipodia motility but do not have the same effect of lamellipodia and filopodia morphology: lamellipodia treated with Cytochalasin D shrink but do not acquire the “filopodish“ appearance observed in lamellipodia treated with Blebbistatin. The addition of 12.5 nM Cytochalasin D clearly affected lamellipodia motility but did not abolish it and therefore we studied in greater detail the effect of 12.5 nM Cytochalasin D on

protrusion/retraction cycles. The leading edge of untreated lamellipodia in control conditions have repetitive cycles of protrusion/retraction (Fig. 5 *d* and *e*) and their leading edge could move by 2-3 µm in 1 or 2 minutes and the addition of 12.5 nM Cytochalasin D caused the lamellipodium shaft to shrink but did not abolish completely the protrusion/retraction cycles, which could be still observed (Fig. 5 *f*).

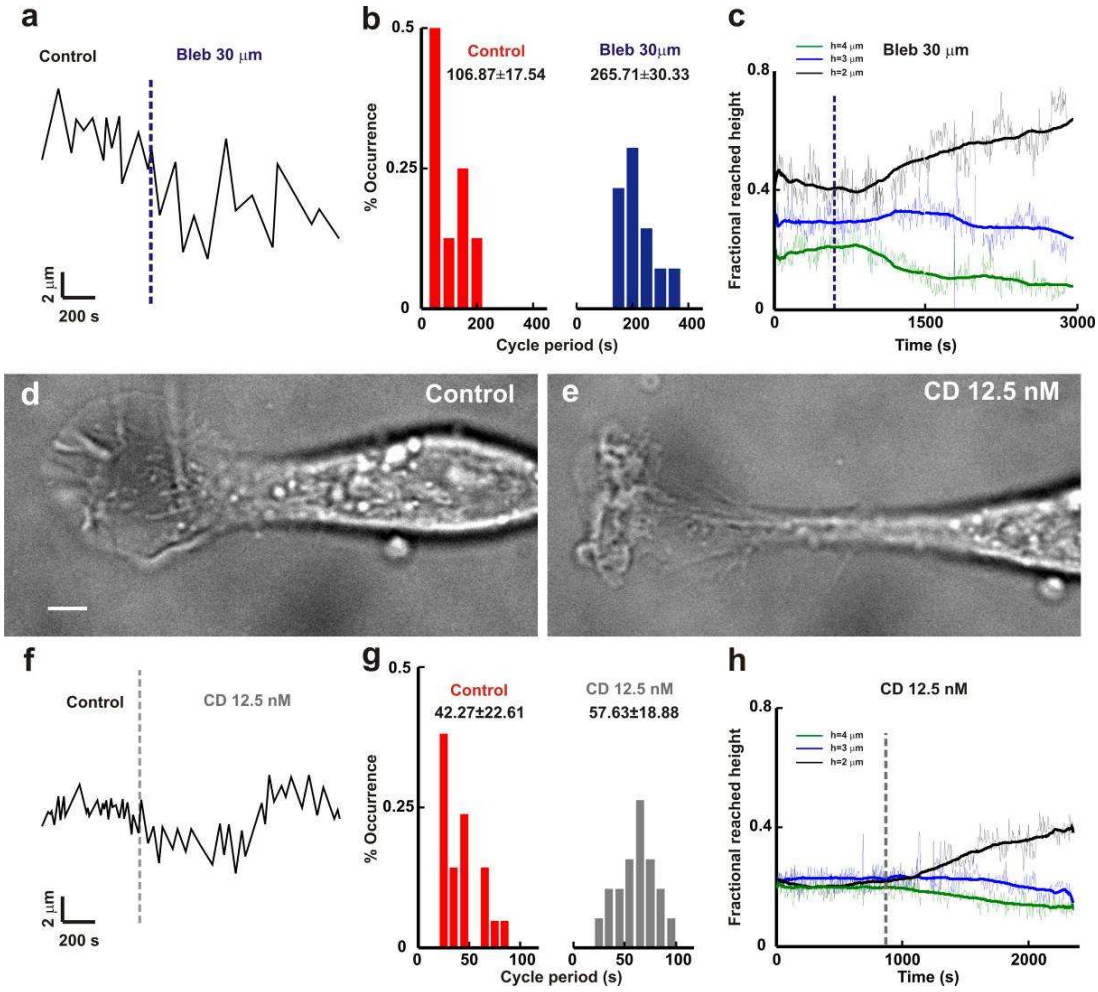


**Figure 5. The effect of Blebbistatin and Cytochalasin D on protrusion/retraction cycles.** (*a*) Maximal protrusion/retraction of lamellipodia vs time. Dotted line represents the time of drug addition. (*b*) Histogram of cycle periods in control conditions (*red histogram*) and in the presence of 30 µM Blebbistatin (*blue histogram*). (*c*) Fractional density of lamellipodia points in focus at different focal planes (h=2, 3 and 4 µm). After addition of Blebbistatin lamellipodia are not able to move up more than 3 µm. (*d-e*) Images of lamellipodia emerging from DRG neuron in control conditions (*d*) and after treatment with 12.5 nM Cytochalasin D (*e*) Scale bar, 2 µm. (*f-h*) As in (*a-c*) but in the presence of 12.5 nM Cytochalasin D.

The period of protrusion/retraction cycles increased from an average of 49.1±17.5 in control conditions to 70.7±20.4 in the presence of 12.5 nM Cytochalasin D (Fig. 5 *g*). The same concentration of Cytochalasin D also reduced the ability of treated lamellipodia to lift up along the vertical direction during these protrusion/retraction cycles: the fraction of edges seen in focus at focal planes higher than 3 μm significantly decreased and lamellipodia edges seen on focus at a plane 2 μm above the coverslip became much more frequent (Fig. 5 *h*).

**The effect of Blebbiststin and Cytochalasin D on the force exerted by lamellipodia**

Having analysed the effect of Blebbistatin and Cytocalsin D on the kinetics of protrusion/retraction cycles with videoimaging, we used optical tweezers to analyse changes of the force exerted by lamellipodia and filopodia caused by these two inhibitors. Untreated lamellipodia pushed trapped beads (Fig. 6 *a-c*) exerting forces up to 10-20 pN as previously described (21) and often bead could be displaced out of the optical trap (Fig. 6 *d*). Lamellipodia of DRG treated with 30 μM Blebbistatin shrank (Fig. 6 *e*) and occasionally could still pull and push a trapped bead (Fig. 6 *e-g*) but with a lower force and velocity (Fig. 6 *h*).

The addition of 25 nM Cytochalasin D caused lamellipodia to shrink and often neurons died after some tens of minutes, but in several occasions they could still exert a force during the initial phase of drug treatment (Fig. 6 *i-k*) but measured forces were significantly reduced (Fig. 6 l). In many experiments we were able to measure the force exerted by lamellipodia in control conditions and we were able to measure the force from the same lamellipodia after the addition of 25 nM Cytochalasin D (n=24, Fig. 6 *o*) or of 30 μM Blebbistatin (n=18, Fig. 6 *n*). These experiments show that the two drugs reduced the force exerted during lateral push (LP) (compare Fig. 6 *m*, *n* and *o*) but at a lower extent during lateral retractions (LR). Both drugs reduced by 50-80 % the force exerted during both vertical push and retractions (compare Fig. 6 *m*, *n* and *o*). Lateral refers to the (*x*,*y*) plane of the coverslip and vertical refers to the *z* axis (perpendicular to the coverslip). The analysis of the Force-velocity (*Fv*) relationships (Fig. 6 *p-s*) shows that both drugs do not modify the shape of the *Fv* relationships but reduced the maximal velocity *v* for both vertical and lateral pushes and retractions. Lamellipodia velocity was reduced more potently by 25 nM Cytochalasin D than by 30 μM Blebbistatin (compare black and blue traces in Fig. 6 *p-s*). We computed average *Fv* relationships, <*Fv*>, from the measured displacements and forces for vertical and

lateral pushes and retractions (see Material and Methods). *Fv* relationships obtained from a single experiment were normalized to $F_{max}$ and were averaged to obtain average *Fv* relationships, <*Fv*> (24). At the beginning bead is in the trap far from lamellipodia and its velocity is zero. During push lamellipodia leading edge moves toward the trapped bead with constant velocity. Before reaching to a solid contact with bead, the bead velocity increase but later on after contact is complete bead and lamellipodia move with the same constant velocity. Therefore <Fv> relationships after an initial rise of *v* exhibited a flat shape, during which the mean velocity remained constant while the force increased (Fig. 6 *p*-*s*). The analysis of the Force-velocity (*Fv*) relationships (Fig. 6 *p*-*s*) shows that both drugs do not modify the shape of the *Fv* relationships but reduced the maximal velocity *v* for both vertical and lateral pushes and retractions. Lamellipodia velocity was reduced more potently by 25 nM Cytochalasin D than by 30 μM Blebbistatin (compare black and blue traces in Fig. 6 *p*-*s*).

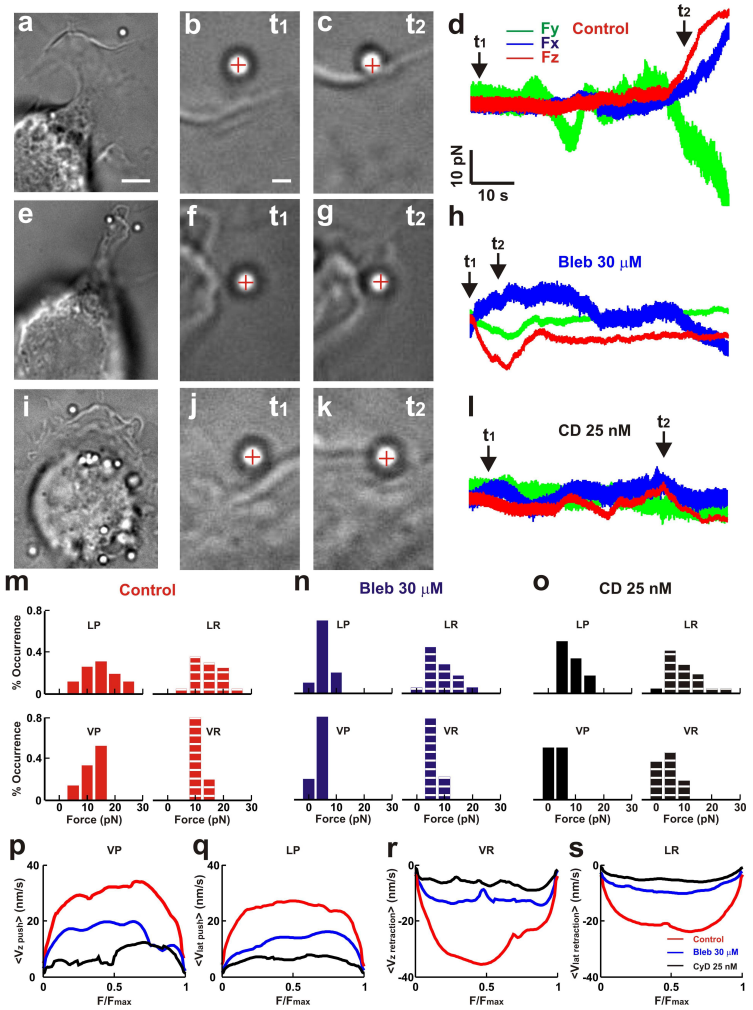


**Figure 6. The effect of Blebbistatin and Cytochalasin D on the force generated by lamellipodia.** (*a*) Low-resolution image of a bead trapped in front of a lamellipodium emerging from the soma of a DRG neuron in

control conditions. Scale bar, 5µm (*b-c*) High-resolution images during a push. At $t_1$ the bead is in the optical trap (*b*), and when the lamellipodium grows, at $t_2$, it pushes the bead (*c*).The cross indicates the center of the optical trap. Scale bar, 1µm. (d) The three components $F_x$, $F_y$, and $F_z$ of the force exerted when the lamellipodium pushes the bead. (*e-h*) As in (*a-d*) but in the presence of Blebbistatin. (*i-l*) As in (*a-c*) but in the presence of Cytochalasin D. The trap stiffness is $k_{x,y} = 0.1$, $k_z = 0.03$ pN/nm. (*m-o*) Histogram of force exerted by lamellipodia during push (solid histograms) and retraction (stripped histograms) in control conditions (*m*), in the presence of Blebbistatin (*n*), and in the presence of Cytochalasin D (*o*). Four different stereotyped behaviors were considered: vertical push (VP), vertical retraction (VR), lateral push (LP) and lateral retraction (LR). (*p-s*) Average *Fv* relationship, $\langle Fv \rangle_{0.2}$, normalized to $F_{max}$ for vertical pushes (p), lateral pushes (q), vertical retractions (r), and lateral retractions (s).

These results show that both Blebbistatin and Cytochalasin D reduce the maximal force that can be exerted by protruding lamellipodia and the maximal velocity of its leading edge.

**Changes of noise during force generation with Blebbistatin and Cytochalasin D**

A remarkable feature of force generation during vertical and lateral push is a concomitant increase of noise when the lamellipodia push the bead (27). This increase of noise is not present when the lamellipodium retracts, pulling the bead away from the optical trap. We have previously shown that in untreated GCs, the relation between the variance of the measured displacement $\sigma^2$ and the exerted force F is upward convex and $\sigma^2$ increases from about 50 $nm^2$ to 150 $nm^2$ for forces exceeding 15 pN (Fig. 7 *a* and *b*, red traces) and that this increase of $\sigma^2$ is abolished by the drug Jasplakinolide, inhibiting actin filament depolymerisation (36). In GCs treated with 12.5 and 25 nM Cytochalasin D the relation between F and $\sigma^2$ is flat and almost no increase of $\sigma^2$ is observed even when the force exceeds 8 pN (compare grey and black traces in Fig. 7 *a*). In the presence of 30 µM Blebbistatin a small increase of $\sigma^2$ from about 40 to 60 $nm^2$ was observed (compare blue trace in Fig. 7 *b*).

Following bead adhesion to the lamellipodium membrane (27), $\sigma^2$ could decrease to less than 6 $nm^2$ and subsequently, when the lamellipodium pushed the bead forward and backward jumps constituting the elementary events underlying force generation appeared. In the presence of 25 nM Cytochalasin D, forward and backward jumps could still be observed but were less frequent than in control conditions (Fig. 7 *c* and *e*). Also in the presence of 30

μM Blebbistatin forward and backward jumps were observed and were more frequent (Fig. 7 *d* and *f*) than those observed in the presence of Cytochalasin D. The amplitude of forward $j^+$ and backward jumps $j^-$ were exponentially distributed (Fig. 7 *e* and *f*) and were fitted by the equations $A_+ e^{-j+/j+*}$ and $A_- e^{-j-/j-*}$ where $A_+$ and $A_-$ are the frequency of forward and backward jumps, respectively, and $j^{+*}$ and $j^{-*}$ are the mean amplitude of forward and backward jumps, respectively. Mean values of these parameters obtained in control conditions and in the presence of Cytochalasin D and Blebbistatin are shown in Table 1. In control conditions the mean values of $j^{+*}$ and $j^{-*}$ were 5.1±1.3 and 4.9±1.2 nm respectively with corresponding rates $A_+$ and $A_-$ of 157.3±12.2 and 155.5±11.1 events/s respectively. In the presence of both Blebbistatin and Cytochalasin D the mean values of mean amplitude of forward and backward jumps $j^{+*}$ and $j^{-*}$ decreased by about 50 % in agreement with the reduced or absent noise increase during force generation caused by the addition of the two drugs ( see Fig. 7 *a* and *b*). The two drugs, however, had a different action on the jump frequency: larger concentrations of Cytochalasin D progressively reduced $A_+$ , i.e. the rate of the appearance of forward jumps but not of backward jumps, in agreement with the known effect of Cytochalasin D to block actin filament polymerization (35). Blebbistatin reduced both the forward and backward rates $A_+$ and $A_-$.

| | Control (n=4) | Blebbistatin 30 μM (n=4) | CytochalasinD 12.5nM (n=3) | CytochalasinD 25nM (n=4) |
|---|---|---|---|---|
| $j_+$ (nm) | 5.1 | 3.05 | 3.6 | 2.46 |
| $j_-$ (nm) | 4.9 | 2.96 | 3.6 | 2.35 |
| $A_+$ event/s | 157.3 | 135.10 | 138.26 | 110.99 |
| A- event/s | 155.5 | 125.68 | 157.74 | 153.25 |

**Table 1. Jump frequency and amplitude.** Amplitudes of forward $j^+$ and backward $j^-$ jumps detected during pushes were exponentially distributed and fitted by the equations $A_+ e^{-j+/j+*}$ and $A_- e^{-j-/j-*}$, where $A_+$ and $A_-$ are the rates of forward and backward jumps, respectively, and $j^{+*}$ and $j^{-*}$, are the mean amplitudes of forward and backward jumps, respectively. *n* indicates the number of experiments in which jumps were analyzed.

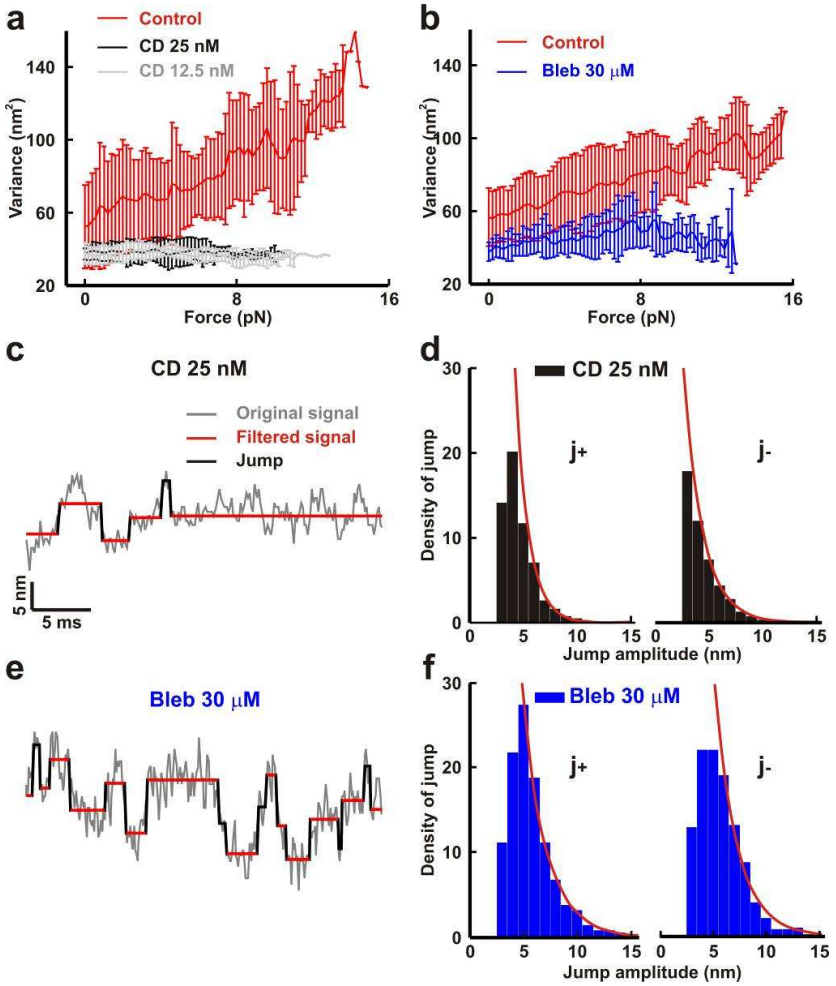


**Figure 7. The effect of Blebbistatin and Cytochalasin D on the elementary events underlying force generation.** (*a*) Average force – variance relationship for lateral pushes in control conditions (*red curve*) and in the presence of Cytochalasin D (*black and grey curves*). (*b*) As in (*a*) but in the presence of Blebbistatin (*blue curve*). (*c-d*) Magnification of the z component during push in the presence of Cytochalasin D (*c*) and in the presence of Blebbistatin (*e*). Original traces were filtered by the nonlinear diffusion algorithm (27), resulting in a smooth component and jumps. Jumps were detected infrequently during a push in the presence of Cytochalasin D, but more often during a push and in the presence of Blebbistatin. (*d-f*) Density of forward $j^+$ and backward $j^-$ jumps during pushes in the presence of Cytochalasin D (*e*) and in the presence of Blebbistatin (*f*). Because of a residue noise, jumps with an amplitude lower than 2-3 nm could not be detected.

## Blebbistatin makes filopodia able to exert a larger force

Both Blebbistatin and Cytochalasin D reduced the amplitude of the force exerted by DRG lamellipodia, but rather surprisingly we found the unexpected result that the force exerted by filopodia treated with Blebbistatin is larger than in untreated filopodia.

In control conditions filopodia emerging from lamellipodia (Fig. 8 *a*) during their protrusion could push a trapped bead exerting forces very rarely exceeding 4 pN (Fig. 8 *b*). We have measured from the same neurons the force exerted by filopodia after the addition of 30 µM Blebbistatin (Fig. 8 *d*). In these conditions, filopodia emerging from lamellpodia which have shrinked (see also Fig. 3) are still able to exert a force which very often was larger (Fig. 8 *e*) and are also able to exert a significant force along the vertical direction (compare red traces in Fig. 8 *b* and *e*). Collected data from 12 neurons show that the average force exerted by filopodia was 2.7±1.2 pN in control conditions and increased to 4.2±1.3 pN in the presence of 30 µM Blebbistatin (Fig. 8 *c* and *f*).

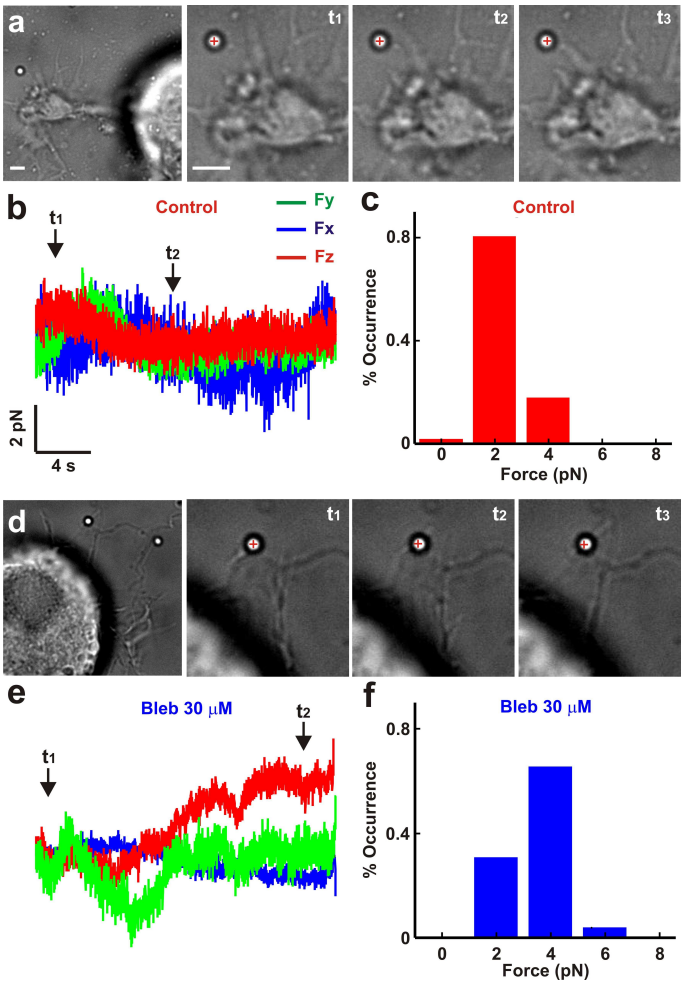


**Figure 8. The effect of Blebbistatin on the force exerted by DRG filopodia.** (*a*) Images of a bead trapped in front of a filopodium emerging from a GC of DRG neuron. At $t_1$ the bead is in the optical trap and at $t_2$-$t_3$ filopodium pushes the bead. The cross indicates the center of the optical trap. Scale bar, 3 µm. (*b*) The three

components $F_x$, $F_y$, and $F_z$ of the force exerted by filopodium. (*c*) Histogram of force exerted by filopodia measured during push. (*d-f*) As in (*a-c*) but in the presence of Blebbistatin. The trap stiffness is $k_{x,y}$=0.1, $k_z$=0.03 pN/nm.

These results show that Blebbistatin reduces the amplitude of the force exerted by lamellipodia but increases the force exerted by filopodia of the DRG neurons.

## DISCUSSION

The present manuscript describes in detail the effect of the inhibition of myosin on the morphology, kinetics and dynamics of lamellipodia and filopodia emerging from the soma and GCs from DRG neurons. Our results suggest a possible role of myosin II in force generation and in particular during "shovel-like" lamellipodia retractions and confirm its role in the coupling between actin and MT dynamics. Myosin II seems also an essential component of GC architectural stability linking together actin filaments. Let us discuss these issues in more detail.

### Localization of NMIIA and NMIIB in lamellipodia

Most nonmuscle cells express the three myosin II isoforms, NMIIA, NMIIB and NMIIC. These myosin II proteins share 60–90% similarity in the amino acid sequences (17) and some cellular functions are isoform-specific, while others are redundant (12). NMIIB has been proposed to play a role in neurite outgrowth (17, 32, 37) and NMIIA has been implicated in neurite retraction and adhesion (17, 32, 38). NMIIB has been localized both in the GC periphery (39, 40) as well as in the central domain and the transition zone (9, 41). We found that in DRG GCs, NMIIB is primarily localized in the central domain of GC and its concentration falls near the leading edge of GCs (see Fig. 2 *a*). In contrast, we found a more even distribution of NMIIA in DRG GCs and staining for NMIIA is also clearly seen near lamellipodia leading edges (Fig. 2 *b*). Actin is primarily concentrated at the periphery of GCs and we found that near the leading edge actin and NMIIA colocalized rather well suggesting the presence of an actomyosin complex, i.e. of interacting actin and myosin filaments. A similar localization of NMIIA in neuronal GCs was already observed by (20, 41).

Differential localization of NMIIA and NMIIB depends on the cellular specificity and possibly also on the developmental stage of the cell (17, 32). Moreover, the alternative splicing of NMIIB and NMIIC heavy and light chain pre-mRNAs, increases the total number of expressed NMII proteins and this alternative splicing occurs predominantly in neurons. Therefore all these isoforms of NMII proteins can be differentially controlled resulting in a complex orchestration of myosin functional roles.

**Cycles of protrusion/retraction and the effect of Blebbistatin and Cytochalasin D**

Lamellipodia emerging from the soma of DRG neurons after 6-24 hours of culture have a very high motility and undergo clear cycles of protrusion and retraction. This motility is attenuated after 2 days of culture, when long neurites emerge from the soma and establish physical contacts with other neurons. This oscillatory behavior requires the existence of a positive feedback from either actin itself or upstream activators, in combination of a delayed inhibition (42, 43), but the biochemical nature of this positive feedback has not yet been identified.

The two compounds used in the present investigation, Blebbistatin and Cytochalasin D, reduce GC motility and at a high concentration – 50 μM for Blebbistatin and 50 nM for Cytochalasin D – completely abolish cellular motility.

Blebbistatin is known to inhibit myosin II (33, 44) and Cytochalasin D (35) prevents the addition of new actin monomers/oligomers to protruding actin filaments. A low dose of both drugs reduce motility without abolishing it and prolong the period of protrusion/retraction cycles. Both drugs attenuate the height reached by lamellipodia during "shovel-like" events (Fig. 5) and drastically reduce the increase of noise associated to force generation (Fig. 7).

As shown in Figs 2 and 3, application of Blebbistatin causes lamellipodia to have a "filopodish" morphology, which is not the case when Cytochalasin D is added to the extracellular medium. The "filopodish" morphology induced by Blebbistatin is likely to be caused by removal of the crosslinkage of actin filaments mediated by NMII filaments. These observations show that a rather complex biochemical machinery underlie the observed

protrusion/retraction cycles and that the resulting dynamics changes during differentiation and could be cell specific. The identification and characterization of the positive feedback (42, 43) underlying these cycles will be a major issue for future investigations.

**Role of contractions of the actomyosin complex during "shovel-like" events**

Contractions of the actomyosin complex play a fundamental role in several cellular processes such changes of the cellular shape (45) , cell migration (32, 46) cell-cell and cell-matrix adhesion (47), cell division and cell differentiation (12).

During the cycles of protrusion/retraction here analysed (Fig. 5) lamellipodia following their maximal protrusion undergo "shovel-like" events, which we were able to follow in time with a temporal resolution of 5-10 s by acquiring stacks of images at different focal planes (Fig. 9 *a*). By using algorithms used in Computer Vision to derive the shape of objects (Fig. 1) from image stacks we obtained the 3D reconstruction of the lamellipodium shown in Fig. 9 *b* and *c*. The vertical motion of the lamellipodium is represented in Fig. 9 *b* in a color coded manner, in which dark red points have an height of 6 μm and those in dark blue move up by 1 μm. Fig. 9 *c* represents the same data but with a 3D rendering in which the upward motion of the lamellipodium can be visually appreciated. At time $t_1$ the lamellipodium is fully extended over the coverslip and essentially a flat surface. At times $t_2$ and $t_3$ the lamellipodium leading edge lifts up by 3-5 μm and at times $t_4$ and $t_5$ moves towards its center. As shown in Fig. 9 *c* when the lamellipodium lifts up and its leading edge curls this global motion appears as a deformation of the lamellipodium structure not evidently associated to a clear retraction of it. Lamellipodium retraction appears at a later time and is followed by a global collapse of the lamellipodium on itself.

These "shovel-like" events seem to precede the usual lamellipodium retraction and given the localization of NMIIA at the lamellipodium periphery are most likely to originate from contractions of the actomyosin. These observations suggest a dual and complementary role for the two myosin II isoforms: NMIIA located also at the periphery of lamellipodia, undergoing "shovel-like" events, could mediate a contraction of the actomyosin complex initiating retraction and NMIIB located more centrally near the transition region of the lamellipodium could control actin turnover (9). Numerical simulations of the actomyosin

complex have shown that generate stresses are overwhelmingly contractile and force chains play a major role (48).

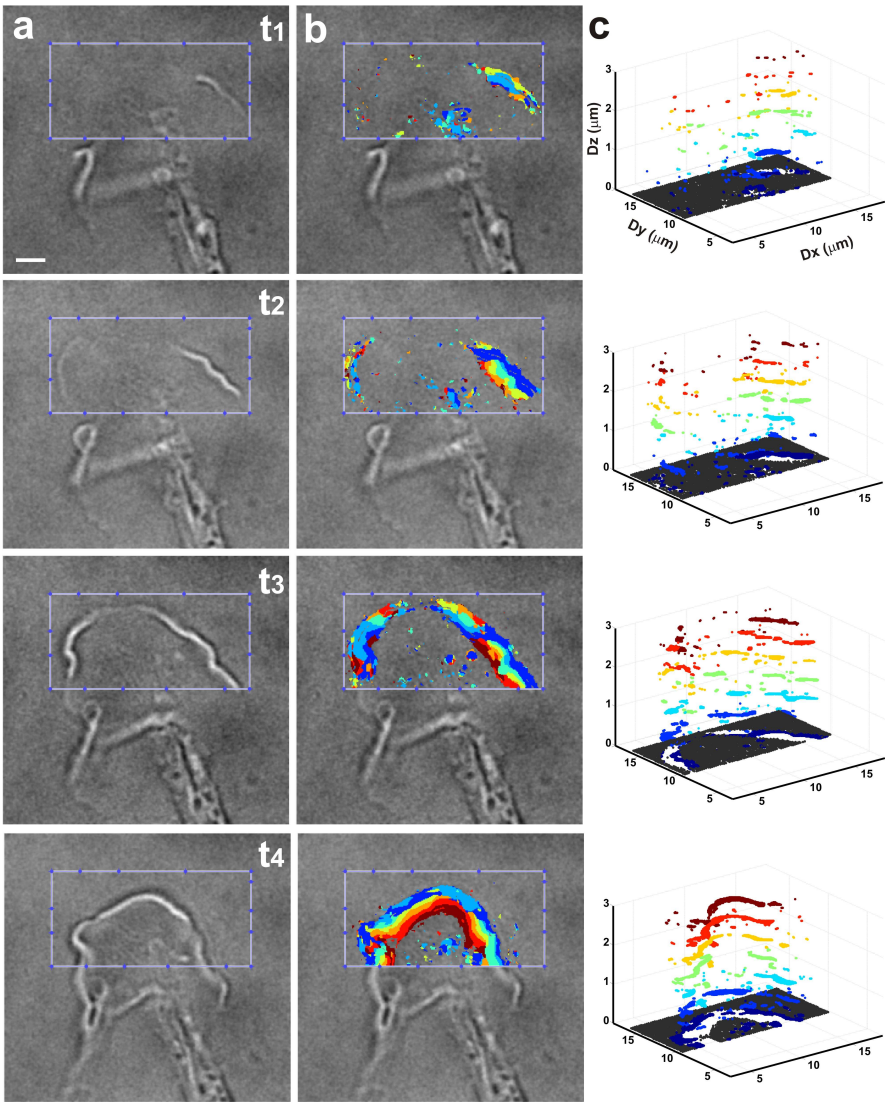


**Figure 9. The 3D reconstruction of the lamellipodium.** (*a*) From top to bottom four consecutive images of the lamellipodia emerging from a DRG GC following a 3D motion called "shovel-like" event. This event was recorded by acquiring 9 stacks of images at different focal planes. Scale bar, 2 μm. (*b*) Same images shown in panel (a) superimposed to the color coded height. Each color correspond to a focal plane and the distance between focal planes is h=0.5 μm. (*c*) 3D reconstruction of the lamellipodium shown in panel (*a*) obtained by using Algorithm II (see Materials and Methods section).

The complicated lamellipodia 3D motion seems the result of the complex dynamical behavior of the underling actin cytoskeleton, sustained through polymerization,

depolymerization and crosslinking of actin filaments. It has been suggested that the actin cytoskeleton can be thought of as an “active” polar gel (49); where the “active” property highlights the fact that the actin polymeric network is under constant remodeling through energy consuming processes that include the action of motor proteins such as myosin. Particularly, it has been proposed in (50) that both isoforms of myosin II, A and B, are capable of forming bipolar filaments that can cause localized contractions on the actin network. These contractions could cause a local change in distances between points of the actin gel. Interestingly, it has been shown experimentally (51) that thin sheets of polymeric gels, when undergoing non-uniform local shrinking or swelling, can exhibit a range of complex three-dimensional shapes ranging from large scale buckling configurations to multiscale wrinkling structures. Differential shrinking or swelling changes distances between points on the surface (51), so that from a mechanical point of view, the flat configuration is no longer the equilibrium position that allows the sheet to have a minimum elastic potential energy; this drives the sheet to buckle into a three dimensional shape. This same mechanism for shaping thin elastic sheets of polymer gels has been proposed to be at play in the generation of complex folded shapes of biological organisms like lichens, sea slugs and orchids (52). We propose that this mechanism acts also in the lamellipodia GCs and that myosin and particularly NMIIA, could be acting to generate local contractions of the actin network leading to local changes in distances between points of the lamellipodium, in a way that drives lamellipodia into large amplitude buckling configurations such as the ones displayed in Fig. 9.

**Role of myosin II in lamellipodia architectural integrity**

GCs treated with Blebbistatin lose their usual sheet-like morphology and acquire a “filopodish” appearance, as shown in Fig. 3 *a-d*. The same result is observed when actin is stained with the appropriate antibody. As shown in Fig. 3 *c*, actin staining in lamellipodia emerging from the soma of DRG neurons has the usual sheet-like appearance. When neurons are treated with 30 μM Blebbistatin, lamellipodia do not always have the usual sheet-like appearance and the actin staining is less diffuse (Fig. 3 *d*). In some neurons, the actin staining has the “filopodish” appearance (Fig. 3 *d*) observed in DIC images (Fig. 3 *b*).

Filaments of NMII could cross-link actin filaments providing to the network a diffuse lateral connectivity gluing together the sparse actin filaments resulting in a sheet-like overall

structure. Inhibition of NMII destroys this connectivity leading the observed “filopodish” appearance.

**Coupling of actin and MT dynamics**

When NMII was inhibited by Blebbistatin, we observed two significant – and at some extent unexpected – morphological changes: lamellipodia lose their sheet-like appearance and become “filopodish” and filopodia emerging from GCs have a higher proportion of microtubules inside (Fig. 3 *c* and *d*) in agreement with previous findings (53). These morphological changes are mirrored by the observation that filopodia treated with Blebbistatin exert a larger force (Fig. 8). The mean flexural rigidity of microtubules is 2.2 x $10^{-23}$ $Nm^2$ which is almost 1000 times larger than that of actin filaments equal to 7.3 $10^{-26}$ $Nm^2$ (54) and therefore filopodia from GCs treated with Blebbistatin are expected to have a larger stiffness and to exert a larger force.

These observations are consistent with the emerging view that inhibition of NMII promotes axon regeneration (20). Chondroitin sulfate proteoglycans (CSPGs), one of the major components of the extracellular matrix in the CNS, inhibit axonal regeneration after injury, through the activation of NMII by phosphorylation of RLC remodelling ultimately cytoskeletal dynamics (18). Inhibition of NMII by Blebbistatin promotes axon outgrowth irrespective of the presence of CSPGs in both CNS and PNS neurons (18, 20) providing therefore a promising pharmacological/chemical treatment for neuronal regeneration.

These observations reported in the present manuscript confirm the essential role of NMII in cytoskeletal dynamics and in the orchestration of both actin and MT dynamics in GCs (18-20). As shown in Fig. 3 after Blebbistatin treatment, the proportion of filopodia with MTs inside them, increases from 0.07 to 0.42 suggesting that Blebbistatin has stimulated the growth of MTs filaments. The biochemical pathway through which NMII affects MT dynamics is not known and is likely not to involve the Rho-kinase (ROCK) (20): indeed inhibition of NMII promotes axon growth but not inhibition of the Rho-ROCK pathway. On the other hand, repulsive guidance molecule (RGMa) induces neurite outgrowth inhibiton through RhoA and Rho-kinase dependent phosphorylation of NMIIA RLC resulting with F-actin reduction (55). These findings suggest therefore mechanistically distinct actin- and MT-based GC responses.

# Supplementary Information

**Localization of myosin in DRG lamellipodia emerging from soma.**

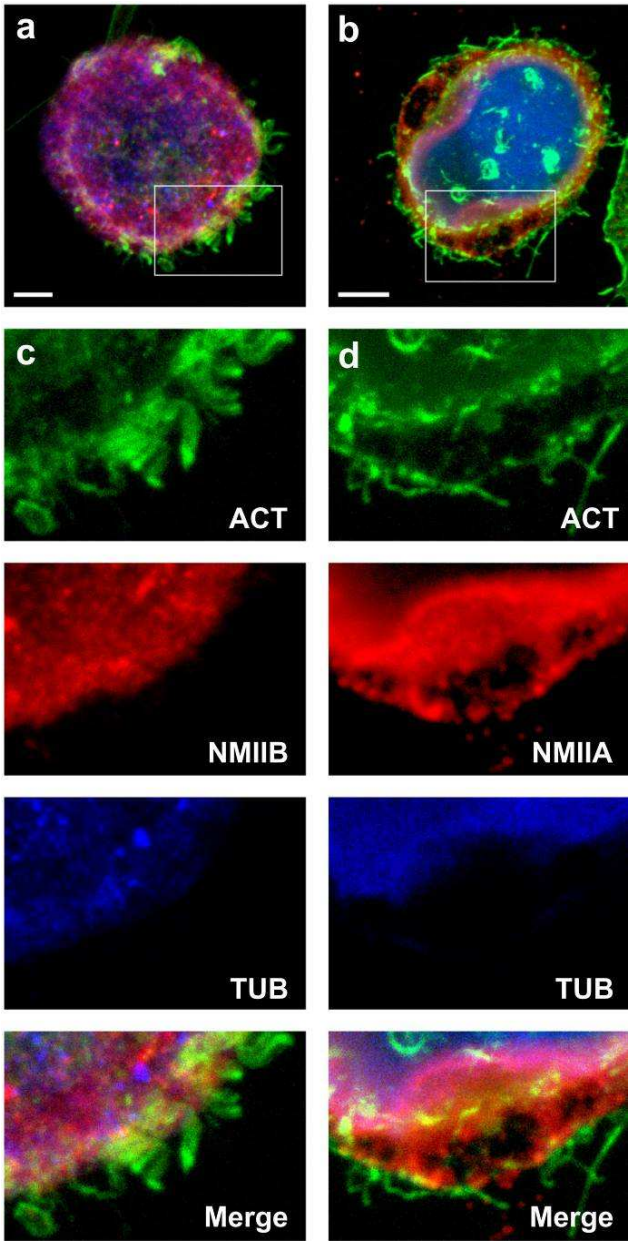


**Figure S1. Localization of NMIIA and NMIIB in DRG lamellipodia.** (*a*-*b*) Confocal fluorescence images of lamallipodia emerging from DRG neurons (*c*) From top to bottom: high resolution images of a DRG lamellipodia shown in (*a*) labeled for actin (*green*), NMIIB (*red*), and tubulin III (*blue*) and merge of the three staining. (*d*) high resolution images of a DRG lamellipodia shown in (*b*) labeled for actin (*green*), NMIIA (*red*), and tubulin III (*blue*) and merge of the three staining Scale bar, 5μm.

## REFERENCES


1. Solecki, D. J., E. E. Govek, and M. E. Hatten. 2006. mPar6 alpha controls neuronal migration. J Neurosci 26: 10624-10625 ISI:000241727300003.

2. Ghashghaei, H. T., C. Lai, and E. S. Anton. 2007. Neuronal migration in the adult brain: are we there yet? Nat Rev Neurosci 8: 141-151 PM:17237805.

3. Goodman, C. S. 1996. Mechanisms and molecules that control growth cone guidance. Annu Rev Neurosci 19: 341-377 PM:8833447.

4. Song, H. J., and M. M. Poo. 2001. The cell biology of neuronal navigation. Nat. Cell Biol. 3: E81-E88 ISI:000167365800006.

5. Mongiu, A. K., E. L. Weitzke, O. Y. Chaga, and G. G. Borisy. 2007. Kinetic-structural analysis of neuronal growth cone veil motility. J Cell Sci 120: 1113-1125 ISI:000244759500020.

6. Mogilner, A., and G. Oster. 1996. Cell motility driven by actin polymerization 25. Biophys. J. 71: 3030-3045 PM:8968574.

7. Pollard, T. D., and G. G. Borisy. 2003. Cellular motility driven by assembly and disassembly of actin filaments. Cell 112: 453-465 ISI:000181252600005.

8. Pak, C. W., K. C. Flynn, and J. R. Bamburg. 2008. Actin-binding proteins take the reins in growth cones. Nat Rev Neurosci 9: 136-147 ISI:000252503300015.

9. Medeiros, N. A., D. T. Burnette, and P. Forscher. 2006. Myosin II functions in actin-bundle turnover in neuronal growth cones. Nat Cell Biol 8: 215-226 ISI:000235708000007.

10. Howard, J. 2001. *Mechanics of Motor Proteins and the Cytoskeleton*. Sinauer Associates, Inc, Sunderland, MA.

11. Raucher, D., and M. P. Sheetz. 2000. Cell spreading and lamellipodial extension rate is regulated by membrane tension. J Cell Biol 148: 127-136 ISI:000084795300017.

12. Vicente-Manzanares, M., X. F. Ma, R. S. Adelstein, and A. R. Horwitz. 2009. Non-muscle myosin II takes centre stage in cell adhesion and migration. Nature Reviews Molecular Cell Biology 10: 778-790 ISI:000271071200012.

13. Conti, M. A., and R. S. Adelstein. 2008. Nonmuscle myosin II moves in new directions. Journal of Cell Science 121: 11-18 ISI:000252243400005.

14. Cai, Y. F., O. Rossier, N. C. Gauthier, N. Biais, M. A. Fardin, X. Zhang, L. W. Miller, B. Ladoux, V. W. Cornish, and M. P. Sheetz. 2010. Cytoskeletal coherence requires myosin-IIA contractility. Journal of Cell Science 123: 413-423 ISI:000274337800012.

15. Meshel, A. S., Q. Wei, R. S. Adelstein, and M. P. Sheetz. 2005. Basic mechanism of three-dimensional collagen fibre transport by fibroblasts. Nature Cell Biology 7: 157-U70 ISI:000226719500012.

16. Wylie, S. R., and P. D. Chantler. 2001. Separate but linked functions of conventional myosins modulate adhesion and neurite outgrowth. Nature Cell Biology 3: 88-92 ISI:000166146400025.

17. Wylie, S. R., and P. D. Chantler. 2008. Myosin IIC: A third molecular motor driving neuronal dynamics. Molecular Biology of the Cell 19: 3956-3968 ISI:000259183200030.

18. Yu, P. P., L. Y. Santiago, Y. Katagiri, and H. M. Geller. 2012. Myosin II activity regulates neurite outgrowth and guidance in response to chondroitin sulfate proteoglycans. Journal of Neurochemistry 120: 1117-1128 ISI:000301112500023.

19. Burnette, D. T., L. Ji, A. W. Schaefer, N. A. Medeiros, G. Danuser, and P. Forscher. 2008. Myosin II activity facilitates microtubule bundling in the neuronal growth cone neck. Developmental Cell 15: 163-169 ISI:000257566600018.

20. Hur, E. M., I. H. Yang, D. H. Kim, J. Byun, Saijilafu, W. L. Xu, P. R. Nicovich, R. Cheong, A. Levchenko, N. Thakor, and F. Q. Zhou. 2011. Engineering neuronal growth cones to promote axon regeneration over inhibitory molecules. Proceedings of the National Academy of Sciences of the United States of America 108: 5057-5062 ISI:000288712200069.

21. Cojoc, D., F. Difato, E. Ferrari, R. B. Shahapure, J. Laishram, M. Righi, E. M. Di Fabrizio, and V. Torre. 2007. Properties of the force exerted by filopodia and lamellipodia and the involvement of cytoskeletal components. PLoS ONE 2: e1072 PM:17957254.

22. Neuman, K. C., and S. M. Block. 2004. Optical trapping. Rev. Sci. Instrum. 75: 2787-2809 ISI:000224754800001.

23. Gittes, F., and C. F. Schmidt. 1998. Interference model for back-focal-plane displacement detection in optical tweezers. Opt. Lett. 23: 7-9 ISI:000071271100003.

24. Shahapure, R., F. Difato, A. Laio, G. Bisson, E. Ercolini, L. Amin, E. Ferrari, and V. Torre. 2010. Force generation in lamellipodia is a probabilistic process with fast growth and retraction events. Biophys. J. 98: 979-988 PM:20303855.

25. Perona, P., and J. Malik. 1990. Scale-Space and Edge-Detection Using Anisotropic Diffusion. Ieee Transactions on Pattern Analysis and Machine Intelligence 12: 629-639 ISI:A1990DK89400002.

26. Weickert, J. 2001. Applications of nonlinear diffusion in image processing and computer vision. ACTA MATHEMATICA UNIVERSITATIS COMENIANAE 70: 33-50.

27. Amin, L., E. Ercolini, R. Shahapure, G. Bisson, and V. Torre. 2011. The elementary events underlying force generation in neuronal lamellipodia. Scientific Reports 1 ISI:000300556400001.

28. Bertero, M., T. A. Poggio, and V. Torre. 1988. Ill-Posed Problems in Early Vision. Proc IEEE 76: 869-889 ISI:A1988Q311100002.

29. Krotkov, E. 1987. Focusing. International Journal of Computer Vision 1: 223-237 ISI:A1987M205000003.

30. Horcas, I., R. Fernandez, J. M. Gomez-Rodriguez, J. Colchero, J. Gomez-Herrero, and A. M. Baro. 2007. WSXM: A software for scanning probe microscopy and a tool for nanotechnology. Review of Scientific Instruments 78 ISI:000243892300028.

31. Amin, L., E. Ercolini, R. Shahapure, E. Migliorini, and V. Torre. 2012. The Role of Membrane Stiffness and Actin Turnover on the Force Exerted by DRG Lamellipodia. Biophysical Journal 102: 2451-2460 ISI:000305003100007.

32. Betapudi, V. 2010. Myosin II Motor Proteins with Different Functions Determine the Fate of Lamellipodia Extension during Cell Spreading. Plos One 5 ISI:000273338500007.

33. Kovacs, M., J. Toth, C. Hetenyi, A. Malnasi-Csizmadia, and J. R. Sellers. 2004. Mechanism of blebbistatin inhibition of myosin II. Journal of Biological Chemistry 279: 35557-35563 ISI:000223303400051.

34. Laishram, J., S. Kondra, D. Avossa, E. Migliorini, M. Lazzarino, and V. Torre. 2009. A morphological analysis of growth cones of DRG neurons combining Atomic Force and Confocal Microscopy. Journal of Structural Biology 168: 366-377 ISI:000271665900002.

35. Cooper, J. A. 1987. Effects of Cytochalasin and Phalloidin on Actin. Journal of Cell Biology 105: 1473-1478 ISI:A1987K595800001.

36. Bubb, M. R., I. Spector, B. B. Beyer, and K. M. Fosen. 2000. Effects of jasplakinolide on the kinetics of actin polymerization. An explanation for certain in vivo observations. J. Biol. Chem. 275: 5163-5170 PM:10671562.

37. Bridgman, P. C., S. Dave, C. F. Asnes, A. N. Tullio, and R. S. Adelstein. 2001. Myosin IIB is required for growth cone motility. Journal of Neuroscience 21: 6159-6169 ISI:000170318200037.

38. Conti, M. A., S. Even-Ram, C. Y. Liu, K. M. Yamada, and R. S. Adelstein. 2004. Defects in cell adhesion and the visceral endoderm following ablation of nonmuscle myosin heavy chain II-A in mice. Journal of Biological Chemistry 279: 41263-41266 ISI:000224075500002.

39. Cheng, T. P. O., N. Murakami, and M. Elzinga. 1992. Localization of Myosin-Iib at the Leading-Edge of Growth Cones from Rat Dorsal-Root Ganglionic Cells. Febs Letters 311: 91-94 ISI:A1992JT76500003.

40. Miller, M., E. Bower, P. Levitt, D. Q. Li, and P. D. Chantler. 1992. Myosin-Ii Distribution in Neurons Is Consistent with A Role in Growth Cone Motility But Not Synaptic Vesicle Mobilization. Neuron 8: 25-44 ISI:A1992HB18500003.

41. Rochlin, M. W., K. Itoh, R. S. Adelstein, and P. C. Bridgman. 1995. Localization of myosin II A and B isoforms in cultured neurons. J Cell Sci. 108 ( Pt 12): 3661-3670 PM:8719872.

42. Carlsson, A. E. 2010. Actin Dynamics: From Nanoscale to Microscale. Annual Review of Biophysics, Vol 39 39: 91-110 ISI:000278959400006.

43. Carlsson, A. E. 2012. Self-Feedback in Actin Polymerization. Advances in Systems Biology 736: 397-406 ISI:000300257900023.

44. Straight, A. F., A. Cheung, J. Limouze, I. Chen, N. J. Westwood, J. R. Sellers, and T. J. Mitchison. 2003. Dissecting temporal and spatial control of cytokinesis with a myosin II inhibitor. Science 299: 1743-1747 ISI:000181519500049.

45. Roh-Johnson, M., G. Shemer, C. D. Higgins, J. H. McClellan, A. D. Werts, U. S. Tulu, L. Gao, E. Betzig, D. P. Kiehart, and B. Goldstein. 2012. Triggering a Cell Shape Change by Exploiting Preexisting Actomyosin Contractions. Science 335: 1232-1235 ISI:000301225100047.

46. Solecki, D. J., N. Trivedi, E. E. Govek, R. A. Kerekes, S. S. Gleason, and M. E. Hatten. 2009. Myosin II Motors and F-Actin Dynamics Drive the Coordinated Movement of the Centrosome and Soma during CNS Glial-Guided Neuronal Migration. Neuron 63: 63-80 ISI:000268189900009.

47. Pasapera, A. M., I. C. Schneider, E. Rericha, D. D. Schlaepfer, and C. M. Waterman. 2010. Myosin II activity regulates vinculin recruitment to focal adhesions through FAK-mediated paxillin phosphorylation. Journal of Cell Biology 188: 877-890 ISI:000275862800013.

48. Dasanayake, N. L., P. J. Michalski, and A. E. Carlsson. 2011. General Mechanism of Actomyosin Contractility. Physical Review Letters 107 ISI:000294783200035.

49. Kruse, K., J. F. Joanny, F. Julicher, J. Prost, and K. Sekimoto. 2005. Generic theory of active polar gels: a paradigm for cytoskeletal dynamics. European Physical Journal e 16: 5-16 ISI:000226766900001.

50. Bridgman, P. C. 2002. Growth cones contain myosin II bipolar filament arrays. Cell Motility and the Cytoskeleton 52: 91-96 ISI:000176014100004.

51. Klein, Y., E. Efrati, and E. Sharon. 2007. Shaping of elastic sheets by prescription of non-Euclidean metrics. Science 315: 1116-1120 ISI:000244387600034.

52. Sharon, E., M. Marder, and H. L. Swinney. 2004. Leaves, flowers and garbage bags: Making waves. American Scientist 92: 254-261 ISI:000220792000022.

53. Rosner, H., W. Moller, T. Wassermann, J. Mihatsch, and M. Blum. 2007. Attenuation of actinomyosinII contractile activity in growth cones accelerates filopodia-guided and microtubule-based neurite elongation. Brain Research 1176: 1-10 ISI:000251203800001.

54. Gittes, F., B. Mickey, J. Nettleton, and J. Howard. 1993. Flexural Rigidity of Microtubules and Actin-Filaments Measured from Thermal Fluctuations in Shape. J. Cell Biol. 120: 923-934 ISI:A1993KL80200008.

55. Kubo, T., M. Endo, K. Hata, J. Taniguchi, K. Kitajo, S. Tomura, A. Yamaguchi, B. K. Mueller, and T. Yamashita. 2008. Myosin IIA is required for neurite outgrowth inhibition produced by repulsive guidance molecule. Journal of Neurochemistry 105: 113-126 ISI:000254383800010.

## 2.5

# Comparison of the force exerted by hippocampal and DRG growth cones

L. Amin, E. Ercolini, J. Ban, and V. Torre

(In preparation)

# Comparison of the force exerted by hippocampal and DRG growth cones

Ladan Amin, † Erika Ercolini, † Jelena Ban† and Vincent Torre†*

†*Neurobiology Sector, International School for Advanced Studies (SISSA), IT-34136 Trieste, Italy.*

## Abstract

We have used optical tweezers to compare the force exerted by lamellipodia and filopodia from developing growth cones of isolated Dorsal Root Ganglia (DRG) neurons and hippocampal neurons. DRG and hippocampal neurons were obtained from P1-P2 and P10-P12 rats. Lamellipodia of DRG neurons were usually larger than those from hippocampal neurons and the number of filopodia with inner microtubules was higher in hippocampal than in DRG neurons. The force exerted by filopodia of DRG growth cones was in the order of 1-2 pN and never exceeded 5 pN, while filopodia from hippocampal growth cones exerted a larger force, often in the order of 5 pN. Lamellipodia of hippocampal and DRG growth cones exerted lateral forces up to 20 pN, but lamellipodia of DRG neurons could exert a vertical force larger than lamellipodia of hippocampal neurons. Therefore, the lateral force exerted by lamellipodia of the peripheral nervous system (PNS) and of the central nervous system (CNS) neurons at different developmental stages is similar, but, in some cases, hippocampal filopodia are able to exert a larger force.

## INTRODUCTION

Neuronal motility is at the basis of several major functions, such as neuronal development, memory, repair and cell migration (1). During the realization of these functions, neurons protrude neurites, highly motile structures which explore the environment searching of the appropriate chemical or mechanical cues guiding the formation of correct connections (1, 2). Neurite exploration is guided by growth cones (GCs) located at their tip (3-5), formed by an extended lamellipodium from which thin filopodia emerge (6). Filopodia tips can move at a velocity that can reach 0.8-1 μm/s (7-9) and their motility is at the basis of the efficient formation of neural networks.

The primary source of motility in growth cones is the polymerization of actin filaments (7-9), a process controlled by a variety of regulatory proteins (10). The addition of actin polymers to actin filaments in close contact with the membrane pushes the cellular membrane forward exerting a protrusive force (11, 12). By using optical tweezers (13, 14), we previously measured the force exerted by lamellipodia and filopodia from developing growth cones of isolated Dorsal Root Gaglia neurons (DRG) (15-18). The force exerted by filopodia was in the order of 1-2 pN and never exceeded 5 pN, while lamellipodia exerted large forces up to 20 pN.

It is now well established that several properties of cells and neurons are altered by the mechanical properties of the environment (19, 20) and, for instance, differentiation of stem cells and of neuronal precursors is influenced by the stiffness of the substrate over which they are cultivated (21). In the central nervous system (CNS) neurons develop and navigate over glial cells, which constitute a rather soft substrate (20, 22, 23) but neurons in the peripheral nervous system (PNS) navigate through a different environment (24, 20), suggesting that their biomechanics may differ from those of CNS neurons and possibly the force exerted by lamellipodia and filopodia of Growth Cones (GCs) of CNS and PNS neurons could be different.

DRG neurons are part of the PNS and we asked whether the force exerted by neurons of CNS was different. DRG neurons investigated in previous analyses were obtained from P10-P12 rats and it is possible that neurons isolated from rats at different developmental stages exert a force with a different strength. The aim of the present investigation is to measure and compare the force exerted by filopodia and lamellipodia of DRG and hippocampal neurons obtained from P1-P2 and from P10-P12 rats. In this way we obtain a

comparison of the force exerted by growth cones from PNS and CNS neurons at different developmental stages.

## MATERIALS AND METHODS

### Cell culture preparation

**DRG neurons.** DRG neurons were obtained as previously described (16, 17). Briefly, Wistar rats 1-2 days old (P1-P2) and 10 to 12 days old (P10-P12) were sacrificed by decapitation after being anesthetized by $CO_2$ in accordance with the Italian Animal Welfare Act. Dissociated neurons were plated on poly-L-lysine-coated coverslips and incubated for 24 h to 48 h. Nerve growth factor (50 ng/ml; Alomone Labs, Jerusalem, Israel) was added before performing the measurements.

**Hippocampal neurons.** After decapitation, hippocampi of P1-P2 or P10-P12 Winstar rats were dissected, cut in slices and washed twice with the dissection medium (25). The enzymatic dissociation was performed treating the slices with 5 mg/ml trypsin (Sigma-Aldrich, St.Louis, MO) and 0.75 mg/ml DNAseI (Sigma-Aldrich, St.Louis, MO) in digestion medium (5 min, room temperature). Then, trypsin was neutralized by 1 mg/ml trypsin inhibitor (Sigma-Aldrich, St.Louis, MO) in the dissection medium for 10 minutes in ice. After a wash in the dissection medium, mechanical dissociation was performed in the same dissection medium with 0.6 mg/ml DNAseI by approximately 50 passages through a Gilson P1000 tip. The cell suspension was then centrifuged at 800 rpm for 5 min, and the pellet re-suspended in the culture medium. Finally, hippocampal neurons were plated on pretreated polyornithine (50 µg/ml, Sigma-Aldrich, St.Louis, MO) coverslips. The hippocampal neuronal cultures were incubated (5% $CO_2$, 37 C) for 24-48 hours in minimum essential medium with Earle's salts and Glutamax I with 10% FBS, 2.5 µg/ml gentamycin (all from Invitrogen, Life Technologies, Gaithersburg, MD, USA), 6 mg/ml D-glucose, 3.6 mg/ml Hepes, 0.1 mg/ml apo-tranferrine, 30 µg/ml insulin, 0.1 µg/ml biotin, 1.5 µg/ml vitamin B12 (all from Sigma-Aldrich, St.Louis, MO).

### Optical tweezers setup

The optical tweezers set-up was built as described in (15) and it was extensively described in (16, 17) .the trapping source was an Ytterbium fiber laser operating at 1064 nm (IPG Laser GmbH, Burbach, Germany) which was sent onto an inverted microscope (IX81, Olympus, Milan, Italy) to the focusing objective (Olympus 100X oil, NA 1.4). The dish

containing the differentiating neurons and the beads (PSI-1.0NH2, G.Kisker GbR, Steinfurt, Germany) was placed on the microscope stage and its temperature was kept at 37 C by a Peltier device. The bead position $\mathbf{x} = (x, y, z)$ was determined with a lateral and vertical accuracy of 2 and 5 nm, respectively, by using back focal plane detection (13, 26, 27). The trap stiffness $\mathbf{K}_{x,y,z} = (k_x, k_y, k_z)$ and the detector sensitivity were calibrated using the power spectrum method (13). The force exerted by the lamellipodium or by the filopodium **F** was considered equal to $-\mathbf{F}_{\mathbf{trap}}$. When the displacement of the bead from its equilibrium position inside the trap $\mathbf{d} = (d_x, d_y, d_z)$ was less than 400 nm and 250 nm vertically and laterally, respectively, $\mathbf{F}_{\mathbf{trap}} = (F_x, F_y, F_z)$ was calculated as $F_x = k_x\, d_x$, $F_y = k_y\, d_y$, and $F_z = k_z\, d_z$ (13). All force recording experiments were monitored by video imaging with a CCD camera at a frame rate of 5 Hz. The determination of the linear range and the sensitivity of the optical trap are described in detail in (17)

**Computation of Fv relationships**

Details of the computation of *Fv* relationships as well as of the determination of the bandwidth of biological events underlying force generation can be found in (16). The velocity $\mathbf{v} = (v_x, v_y, v_z)$ of the bead was obtained by numerical differentiation of its sampled position $\mathbf{x} = (x(n), y(n), z(n))$ $n = 1,\ldots N$. Numerical differentiation was computed either by convolution of the position components $x(n)$, $y(n)$ and $z(n)$ with the derivative of a Gaussian filter $1/[\sigma(2\pi)^{1/2}] \exp(-t^2/\sigma^2)$ (Gaussian filtering) or by Linear regression. Gaussian filters corresponding to cut-off frequencies of 0.2, 1 and 10 Hz were used.

**Immunostaining and imaging**

Cells were fixed in 4% paraformaldehyde containing 0.15% picric acid in phosphate-buffered saline (PBS), saturated with 0.1 M glycine, permeabilized with 0.1% Triton X-100, saturated with 0.5% BSA (all from Sigma-Aldrich, St.Louis, MO) in PBS and then incubated for 1hour with primary antibodies: mouse monoclonal antibodies against neuronal class III β-tubulin-TUJ1 and SMI 312 neurofilament marker (all from Covance, Berkeley, CA) followed by the 30min incubation with secondary antibodies: goat anti-mouse immunoglobulin (Ig) $G_1$-FITC and $IgG_{2a}$-TRITC (Southern Biotech, Birmingham, AL), goat anti-mouse 594 Alexa (Invitrogen, Life Technologies, Gaithersburg, MD, USA). Alexa Fluor 488 phalloidin (Invitrogen, Life Technologies, Gaithersburg, MD, USA) was used to stain F-actin. All the incubations were performed at room temperature (20-22 C). The cells were examined using a Leica DMIRE2 confocal microscope (Leica Microsystems GmbH, Germany) equipped with

DIC and fluorescence optics, diode laser 405nm, Ar/ArKr 488nm and He/Ne 543/594nm lasers. The fluorescence images (1024x1024 pixels) were collected with a 63X magnification and 1.4 NA oil-immersion objective. For the neurite's length analysis Leica DM6000 or Zeiss Axioskop 2 MOT microscopes equipped with CCD camera, DIC and fluorescence optics were used. Images were acquired with 40X magnification (1.0 or 1.3 NA) oil-immersion objectives.

**Neurite and filopodia length and lamellipodia area measurement**

The length of the neurites and of the filopodia was measured from the confocal images showing actin staining by using the following software: NeuriteTracer (ImageJ plugin) (28), Volume 168, Issue 1, Pages 134-139

(http://dx.doi.org/10.1016/j.jneumeth.2007.08.029).

**RESULTS**

Neurons from DRG and hippocampi of P10-P12 and of P1-P2 Wistar rats were isolated and plated on poly-L-lysine-coated and poly-ornithine coated coverslips. After 24-48 h of culture, coverslips containing either DRG or hippocampal neurons were positioned on the stage of an inverted microscope used for imaging and force measurement (16) (see also Materials and Methods). Silica beads with a diameter of 1 μm were trapped with an infrared (IR) optical tweezer in front of growth cones and it was possible to measure the force exerted by neuronal filopodia and lamellipodia with sub pN sensitivity at 10 kHz resolution.

## Geometrical properties of hippocampal and DRG growth cones

The morphology and geometrical properties of hippocampal and DRG neurons are rather different and when cultivated in a dish they can be easily recognized. After 6-12 hours of culture, as previously observed (29), thin neurites emerge from the soma of hippocampal neurons (Fig. 1 *a*) but extended lamellipodia sprout from the soma of DRG neurons (Fig. 1 *b*). Neurites emerging from hippocampal neurons can grow extensively up to some tens of μm and occasionally could retract. After 12 hours of culture, neurites start to emerge also from the soma of DRG neurons and follow a dynamics similar to that observed in hippocampal neurons.

To quantitatively describe the differences in the geometry of DRG and hippocampal neurites and GCs, both cultures were fixed at 24-29 hours after plating. These times were sufficiently short to prevent neurites from forming a network. Morphological differences were analyzed by immounofluorescence with different probes for actin (phalloidin) and microtubule (III β-tubulin-TUJ1). Quantitative details are summarized in Table 1.

The number of neurites emerging from hippocampal and DRG neurons is different. In DRG cultures (P10-P12 and P1-P2) most of the observed neurons have 1 (63%), 2 (28%) or 3 (6%) neurites and only occasionally neurons show up to 6 (3%) neurites (Fig. 2 *a*, *red histograms*). Most of the plated hippocampal neurons (P1-P2) generate either one or two neurites (44% and 40% respectively), 16% of cells have three or more neurites. But the number of neurites generated from P10-P12 hippocampal neurons is significantly higher and almost 80% of these neurons have more than 3 neurites (Fig. 2 *a, green histograms*). Neurites from DRG neurons of both P1-P2 and P10-P12 rats are longer (65.6±8.0 and 50.7±5.8 µm, respectively) than those from hippocampal neurons (22.2±2.0 and 28.2±2.4 µm, respectively) (Fig. 2 *b*). Growth cones (GCs) emerge from the neurites tips of both DRG and hippocampal neurons and these GCs have different morphology and motility. Although the size of GCs can vary widely, the average size of a DRG GC is several times larger than the size of an hippocampal GC. In hippocampal GCs several filopodia emerging from a lamellipodium are shown to be significantly less extended than those from a DRG lamellipodium (Fig. 1 *c* and *d*). In hippocampal neurons, the GC size is almost constant at different development stages (P1-P2 and P10-P12 rats). But in DRG neurons, P10-P12 GC lamellipodia are larger than those of P1-P2 GCs (Fig. 2 *e*). The ratio between the number of filopodia and the GC area is larger in hippocampal GCs (0.4±0.1 $\mu m^{-2}$ for hippocampal GCs versus 0.10± 0.02 $\mu m^{-2}$) (Fig. 2 *d*). Therefore, hippocampal neurons seem to be more “filopodish” while GCs have a more bundle-like structure. Filopodia characterizations were determined by measuring filopodia number and length (Fig. 2 *c* and *d*). Hippocampal GCs present slightly shorter filopodia and the length of filopodia remains constant in both P1-P2 and P10-P12 GCs (Fig. 2 *c*).

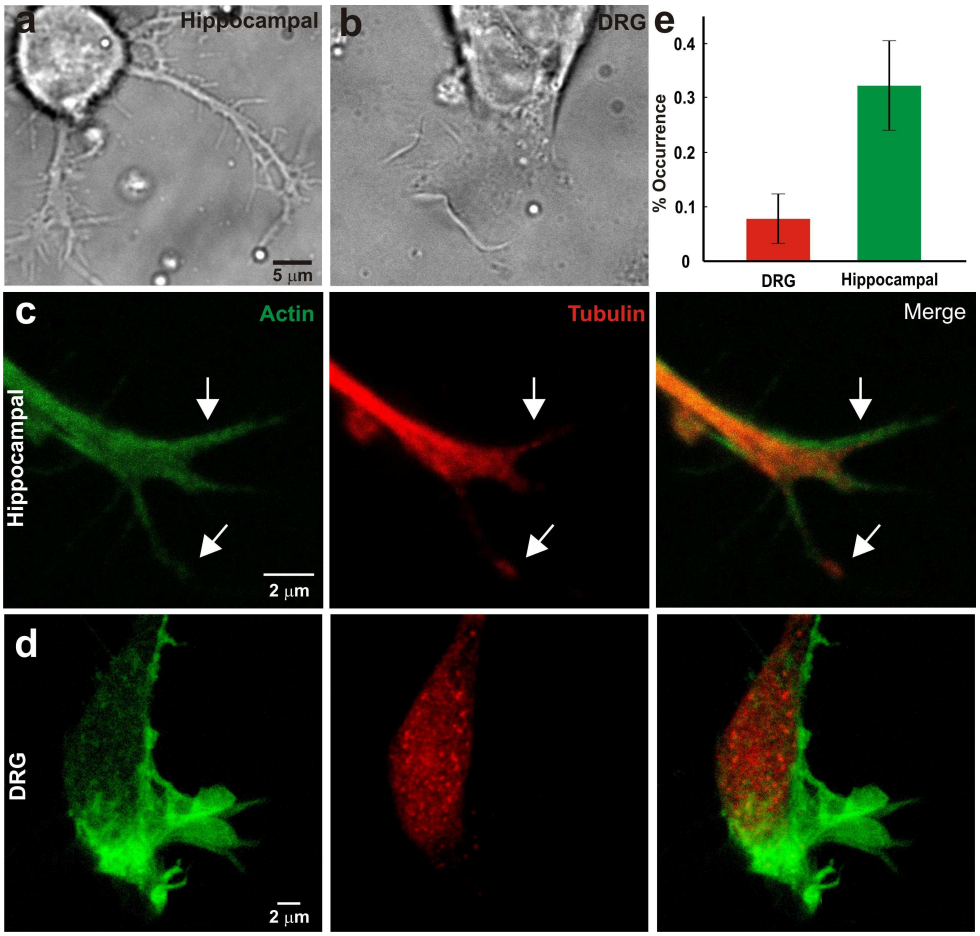


**Figure 1. Geometrical properties of hippocampal and DRG growth cones**. (*a*-*b*) Low resolution image of neurites emerging from the soma of hippocampal (*a*) and DRG (*b*) neuron. (*c*) From left to right: confocal fluorescence images of a hippocampal GC stained for actin (*green*), tubulin (*red*) and merge of the two staining. Arrows indicate a filopodium with microtubules inside. (*d*) As in (*c*) but for DRG GC. (*e*) The fraction of filopodia with a staining for microtubules in DRG (*red bar*) and hippocampal (*blue bar*) GC.

GCs from DRG and hippocampal neurons, not only differ in their geometrical properties, but also in the organization of their cytoskeleton. Immunostaining of GCs for actin and tubulin shows that in hippocampal GCs microtubules extend into the periphery domain (P domain) and even penetrate inside filopodia (Fig. 1 *c*). In DRG GCs microtubules usually terminate at the central domain (C domain) and only rarely (less than 10%) protrude into the P domain (Fig. 1 *e*).

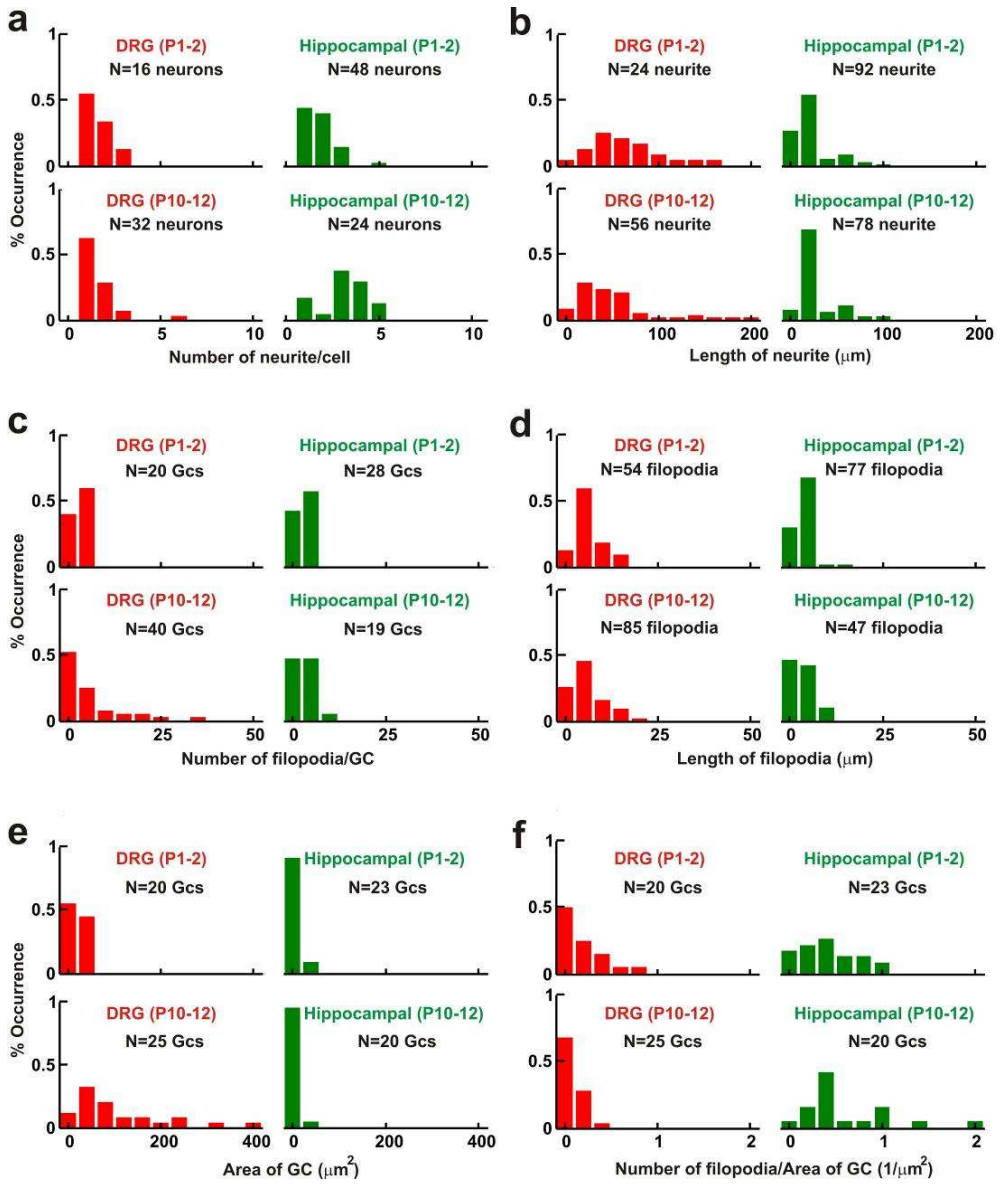


**Figure 2. Differences in the geometry of DRG and hippocampal neurites and GCs.** (*a*) Number of neurites emerging from DRG neurons (*red histograms*) and hippocampal (*green histogram*) soma. (*b*) Measurement of individual neurite lengths from the tip of each neurite to the edge of the DRG (*red histogram*) and hippocampal (*green histogram*) soma. (*c*) Number of filopodia emerging from DRG (*red histogram*) and hippocampal (*green histogram*) GCs. (*d*) Measurement of individual filopodium lengths from the tip of each filopodia to the edge of the DRG (*red histogram*) and hippocampal (*green histogram*) GCs. (*e*) Area of DRG (*red histogram*) and hippocampal (*green histogram*) GCs. (*f*). Ratio of number of filopodia and area of GC in DRG (*red histogram*) and hippocampal (*green histogram*) GCs.

| | Hippocampal | | DRG | |
|---|---|---|---|---|
| | (P1-P2) | (P10-P12) | (P1-2) | (P10-P12) |
| Neurite length (µm) | 22.2±2.0 | 28.2±2.4 | 65.6±8.0 | 50.7±5.8 |
| Number of filopodia/GC | 2.7±0.4 | 2.9±0.5 | 3.0±0.5 | 5.5±1.3 |
| Filopodia length (µm) | 3.6±0.2 | 3.7±0.4 | 6.2±0.5 | 5.9±0.6 |
| GC Area ($\mu m^2$) | 7.0±1.5 | 10.9±1.3 | 24.3±3.2 | 109.5±21.0 |
| Number of filopodia/GC area (1/ $\mu m^2$) | 0.4±0.1 | 0.6±0.5 | 0.2±0.04 | 0.1± 0.02 |

**Table 1**: Geometrical differences of DRG and hippocampal GCs

We have not observed any statistical significant difference in neurons dissociated from P1-P2 and from P10-P12 rats except for the number of neurites in hippocampal neurons and the size of GCs in DRG neurons which are higher in more mature rats. The time of culture seems to be the major determinant of neurites length and not the rat age.

## Force measurements in hippocampal and DRG filopodia and lamellipodia

Filopodia of hippocampal and DRG GCs have a similar and elongated shape with a diameter varying from 80 to 400 nm and an average length of 2.7±0.4 and 5.5±1.3 µm, respectively. In order to measure the force they exert, we positioned a silica bead trapped with an IR laser beam in front of filopodia tips (Fig. 3 *a* and *e*). Protruding filopodia pushed trapped beads and displaced them from their equilibrium position inside the optical trap both for hippocampal (Fig. 3 *b* and *c*) and DRG filopodia (Fig. 3 *f* and *g*). During these protrusions, filopodia exerted a lateral force up to 2-4 pN and often also along the vertical axis but rarely exceeding 2 pN (Fig. 3*d* and *h*). Collected data indicate that DRG filopodia during protrusions exerted an average force of 2.2 ±0.1 pN (n=58) lower than the force exerted by hippocampal filopodia equal to 3.0 ±0.1 pN (n=64) (Fig. 3 *i*). Often filopodia could seal on the silica bead, so that when they retracted they pulled the bead away from the optical trap, exerting a force during their retraction. During retractions both DRG and hippocampal filopodia exerted a force significantly larger than during protrusion, equal to 4.9±0.5 (n=31) and 5.3±0.7 pN (n=23), respectively (Fig. 3 *j*).

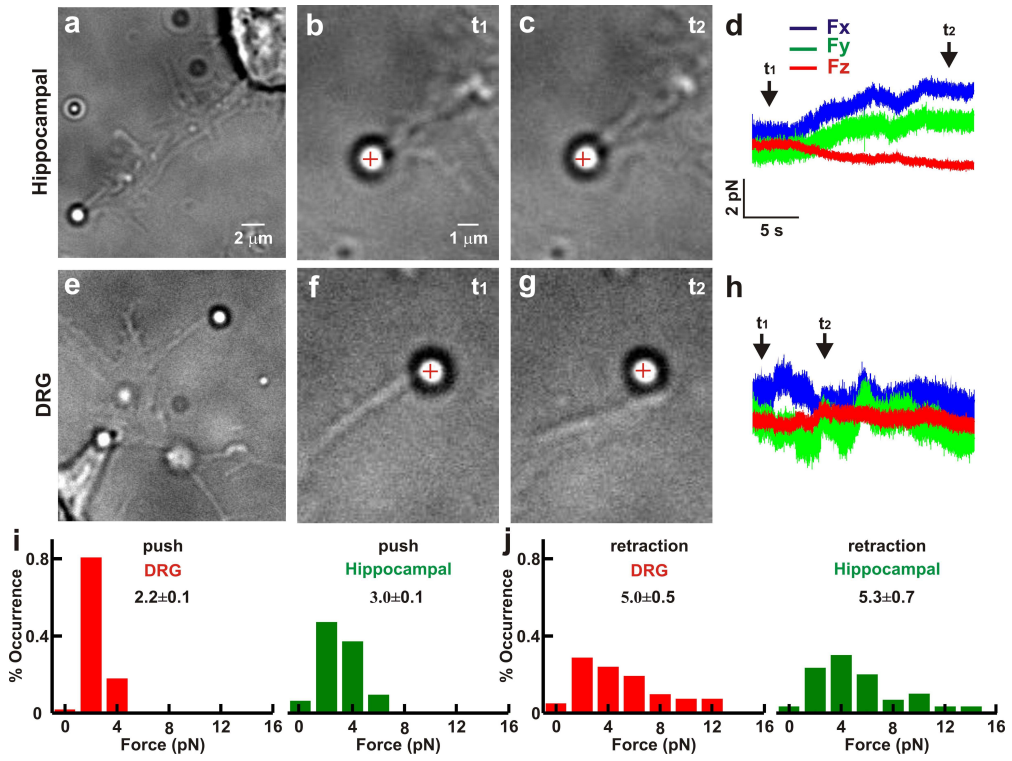


**Figure 3. Comparison of the force exerted by filopodia from hippocampal and DRG growth cones.** (*a*) Low resolution image of a bead trapped in front of a filopodium emerging from a GC of hippocampal neuron. (*b-c*) High resolution images during a push by a filopodium. At $t_1$ the bead is in the optical trap (*b*) and at $t_2$ the filopodium pushes the bead (*c*). The cross indicates the center of the optical trap. (*d*) The three components $F_x$, $F_y$, and $F_z$ of the force exerted by the filopodium. (*e-h*) As in (*a-d*) for a filopodium emerging from a GC of DRG neuron. (*i*) Histogram of the force measured during a push in DRG (*red histogram*) and hippocampal (*green histogram*) neurons. (*j*) As in (*i*) but during retraction. The trap stiffness is $k_{x,y}$=0.1, $k_z$=0.03 pN/nm.

During their exploratory motion often filopodia pivot and push beads aside, possibly as a consequence of shearing movements of the lamellipodial actin network where the filopodial shaft emerges. We refer to the first case as lateral collisions (Fig. 4 *a-b* and *i-j*) and to the latter case, where the filopodium pushes the bead, as protrusion (Fig. 4 *e-f* and *m-n*). The amplitude of exerted force and their time course was similar for DRG and hippocampal filopodia both for lateral collisions (Fig. 4 *c* and *k*) and protrusions (Fig. 4 *g* and *o*). The force exerted during lateral collisions depends on the geometry of the collision, since a filopodium, during its exploratory motion, can hit the bead by slightly touching it with its tip (as in Fig. 4 *b*) or hitting it with an intermediate part of the shaft (as in Fig. 4 *j*). Histograms of the force measured during lateral collisions are shown in Fig. 4 *d* and *l*, and during protrusions in Fig. 4 *h* and *p* (hippocampal and DRG filopodia, respectively).

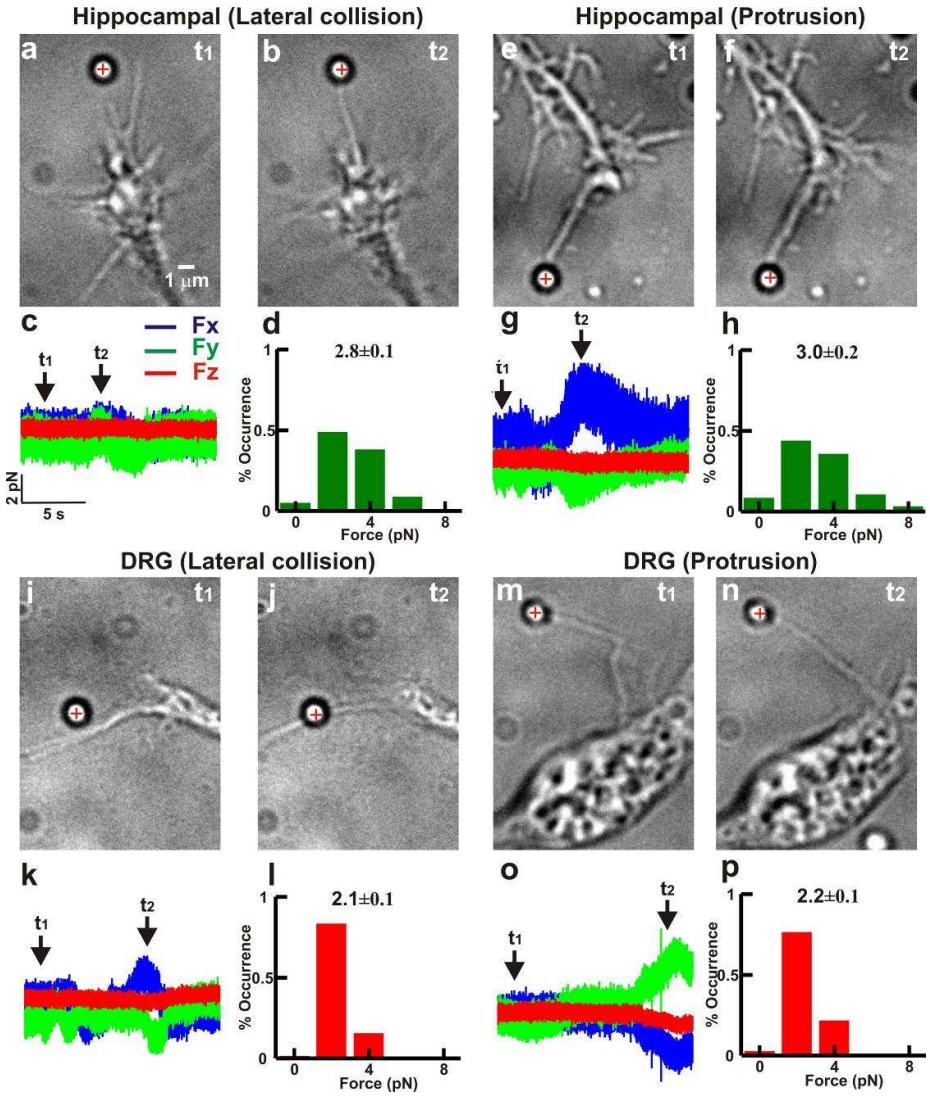


**Figure 4. Lateral collision and protrusion of filopodia.** (*a*-*b*) Lateral collision between a filopodium from hippocampal neuron and a trapped bead. The cross indicates the bead's equilibrium position inside the optical trap. (*c*) $F_x$, $F_y$, and $F_z$ during the lateral collision shown in (*a*–*b*). (*d*) Histogram of force measured during lateral collision in hippocampal neurons. (*e*-*f*) Collision between a protruding filopodium from hippocampal neuron and a trapped bead. (f) $F_x$, $F_y$, and $F_z$ during the filopodial protrusion shown in (e–*f*). (g–h) Histograms of forces measured during protrusions. (*i*-*l*) As in (*a*-*d*) for a filopodium from a DRG neuron. (*m*-*p*) As in (*e*-*h*) for a protruding filopodium from a DRG neuron.

Simple mechanical considerations show that the force exerted by a wandering filopodium during a lateral collision as discuss in (15) can be accounted for by the elastic force expected from its flexural rigidity (11, 37) and its bending or buckling. No additional contribution from other force-generating mechanisms is required.

As in the case of filopodia, silica beads were trapped in front of lamellipodia (Fig. 5 *a*) and when the lamellipodia grew, they displaced the bead (Fig. 5 *b* and *c*) exerting a force up to 20 pN. Growing lamellipodia could displace beads almost entirely in the lateral direction (Fig. 5 *b-d*) and more often they displaced beads both laterally and vertically (Fig. 5 *f-h*). Collected data show that DRG lamellipodia exerted an average force of 9.7 ±0.5 (n=51) significantly larger than the average force of 4.8 ±0.4 pN (n=33) exerted by hippocampal lamellipodia (Fig. 5 *i*, *red and green histogram*, respectively).

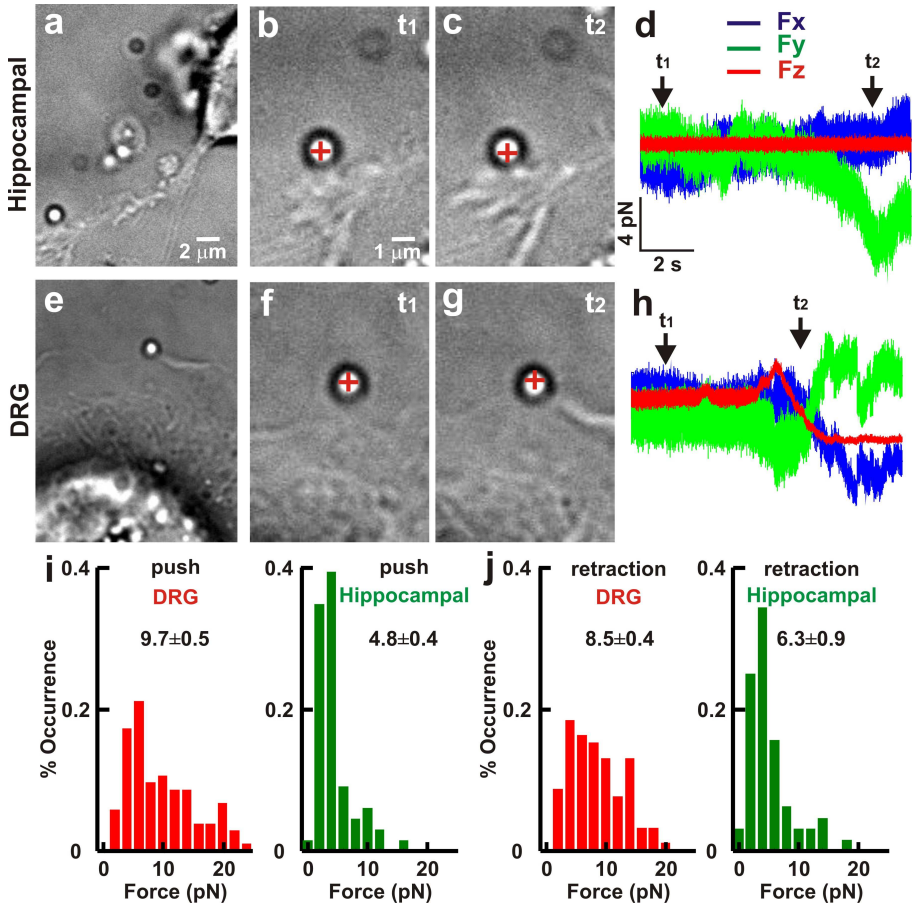


**Figure 5. Comparison of the force exerted by lamellipodia from hippocampal and DRG growth cones.** (*a*) Low resolution image of a bead trapped in front of a lamellipodium emerging from a hippocampal neuron. (*b-c*) High resolution images during a push by a lamellipodium. At $t_1$ the bead is in the optical trap (*b*) and at $t_2$ lamellipodium grows and pushes the trapped bead (*c*). The cross indicates the center of the optical trap. (*d*) The three components $F_x$, $F_y$, and $F_z$ of the force exerted by the lamellipodium from hippocampal neuron. (*e-h*) As in (*a-d*) but for a lamellipodium emerging from a DRG neuron. (*i*) Histogram of force measured during push in DRG (*red histogram*) and hippocampal (*green histogram*) neurons. (*j*) As in (*i*) but during retraction. The trap stiffness is $k_{x,y}$=0.1, $k_z$=0.03 pN/nm.

When the lamellipodium retracted, if the bead was attached to the membrane it was possible to measure the force exerted by the lamellipodium during the retraction (Fig. 5 *e-g*). Force recordings (Fig. 5 *h*) show that the bead was displaced in x, y, and z and that at time $t_2$ the lamellipodium is performing a retraction (both in the lateral and vertical directions). The adhesion of the bead to the lamellipodial membrane is confirmed by the fact that the bead does not jump back into the trap and that the variance of the trace decreases.

In DRG lamellipodia, measured forces for vertical pushes are larger than hippocampal lamellipodia with mean values of 3.9±0.3 pN and 1.0±0.2 pN, respectively (Table 2). Forces during retraction have slightly larger values in DRG lamellipodia, and span approximately the same range of values both for DRG (Fig. 5 *j, red histogram*) and hippocampal (Fig. 5 *j, green histogram*) lamellipodia, having mean values of 8.5±0.4 pN and 6.3±0.9 pN, respectively (see Table 2 for details). During vertical retraction, the measured pulling force reaches values up to 10 pN in DRG lamellipodia while in hippocampal lamellipodia the maximum value was up 4 pN with mean values of 4.1±0.3 and 2.0±0.30 pN, respectively (Table 2). In hippocampal neurons there is no significant difference in the force exerted by filopodia or lamellipodia of P1-P2 or P10-P12 neurons.

| | | Hippocampal | | DRG | |
|---|---|---|---|---|---|
| | | $F_{x,y}$ (pN) | $F_z$ (pN) | $F_{x,y}$ (pN) | $F_z$ (pN) |
| filopodia | push | 3.0±0.1 | 0.7 ± 0.1 | 2.2±0.1 | 0.6±0.1 |
| | retraction | 5.3±0.7 | 1.5 ± 0.2 | 5.0±0.5 | 1.3±0.2 |
| lamellipodia | push | 4.8±0.4 | 1.0 ± 0.2 | 9.7±0.5 | 3.9±0.3 |
| | retraction | 6.3±0.9 | 2.0 ± 0.30 | 8.5±0.4 | 4.1±0.3 |

**Table 2:** force generated by filopodia and lamellipodia of hippocampal and DRG neurons

## Force-velocity relationships from hippocampal and DRG lamellipodia

We computed average *Fv* relationships, <*Fv*>, from the measured displacements and forces for vertical and lateral pushes and retractions (16, 17) both for hippocampal and DRG lamellipodia from P10-P12 rats. Vertical refers to the direction perpendicular to the coverslip (*z* axis) and lateral refers to the plane of the coverslip (*x,y*). *Fv* relationships obtained from a single experiment (see Materials and Methods and (16)) were normalized to $F_{max}$ and were averaged so to obtain average *Fv* relationships, <*Fv*>. At the beginning bead is in the trap far from lamellipodia and its velocity is zero. During push lamellipodia leading edge moves

toward the trapped bead with constant velocity (41). Before reaching to a solid contact with bead, the bead velocity increase but later on after contact is complete bead and lamellipodia move with the same constant velocity. Therefore during vertical pushes <*Fv*> were characterized by an initial rise of *v* reaching the value of ~ 35 nm/s for DRG lamellipodia (Fig. 6 *a*, *red line*) and ~ 15 nm/s for hippocampal lamellipodia (Fig. 6 *a*, *green line*). <*Fv*> relationships during lateral pushes (Fig. 6 *b*) and retractions (Fig. 6 *d*) were very similar for hippocampal (*green lines*) and DRG lamellipodia (*red lines*). For vertical retractions (Fig. 6 *c*) the shape of <*Fv*> relationships was very similar but had a higher velocity for DRG lamellipodia up to 19 nm/s while in hippocampal lamellipodia it was not higher than 12 nm/s.

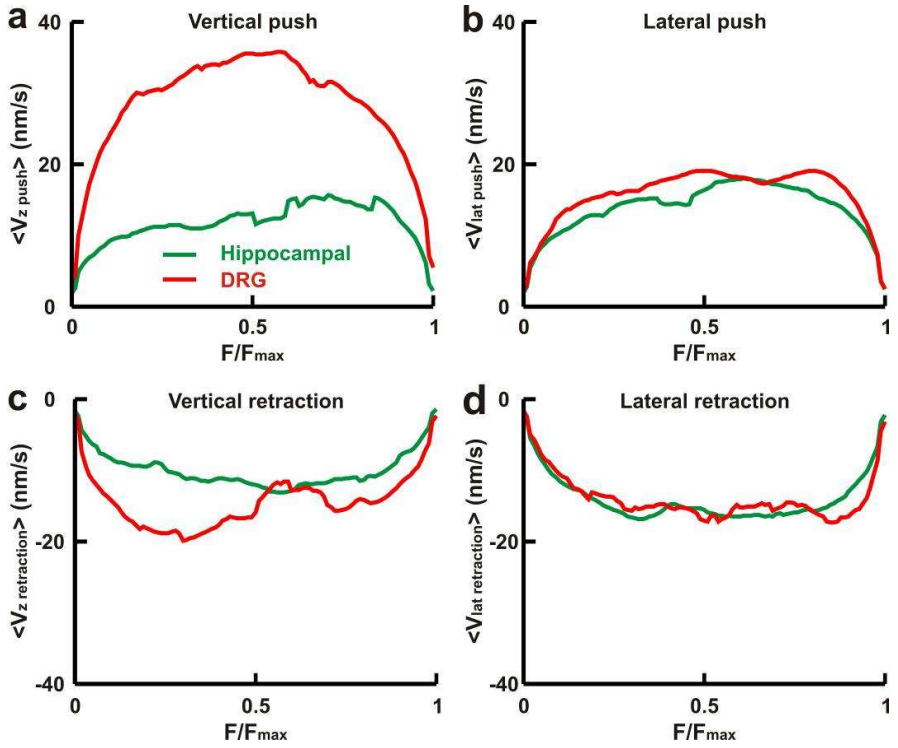


**Figure 6. *Fv* relationships during pushes and retractions from hippocampal and DRG lamellipodia.** (*a-d*) Average *Fv* relationships, $\langle Fv \rangle_{0.2}$, normalized to $F_{max}$ for vertical pushes (*a*), lateral pushes (*b*), vertical retractions (*c*) and lateral retractions (*d*) for hippocampal (*green lines*) and DRG (*red lines*) lamellipodia

## Axonic and dendritic GCs

We investigated also possible differences between the force exerted by axonic and dendritic GCs in DRG neurites. After 1 and even 2 days of culture, neurites are rather immature and it is difficult to distinguish between axons and dendrites in a reliable way, but after 3 days of culture neurofilaments can be clearly identified in axons by using antibodies for the SMI protein (30). In some experiments (n=7), after obtaining force recordings with

our optical setup, neurons were fixed and were stained for actin, tubulin and SMI so to identify whether the tested GC came from an axonic or a dendritic neurite. Neurons were cultivated on a gridded coverslip with numbered meshes so to allow a precise identification and localization of tested GCs. By using this procedure, we verified that the force recorded from axonic and dendritic GCs was similar and we did not observe any major differences (see Supplementary Information, Figs. S1 and S2).

## DISCUSSION

The present manuscript show that filopodia and lamellipodia from GCs of CNS - hippocampal neurons - and PNS - DRG neurons - exert forces with a broadly similar amplitude, developing following a very similar time course. Both types of neurons exert forces varying from 1 up to 20 pN and occasionally higher. At a more quantitative level, two main differences appear: firstly, filopodia from hippocampal growth cones exert a force larger than from DRG growth cones; secondly, lamellipodia from DRG growth cones exert a larger force and can reach a higher speed if they move in a vertical direction. We have not observed any substantial differences between the force exerted by axonic and dendritic GCs. Let us discuss in detail what these differences might be (or) are.

### Hippocampal and DRG filopodia

Hippocampal neurons are more spiny and the number of filopodia per area of GC is higher than in DRG neurons (Table 1) but the length of DRG filopodia is higher than that of hippocampal filopodia (Table 1). The filament length is an important factor in determining the amplitude of its thermal fluctuations and of the exerted force. The effective elastic constant of an actin filament is inversely proportional to the length of the filament, so if the filament is too long, it becomes too "soft" and it buckles under load forces of less than a picoNewton (7).

The most important morphological differences between hippocampal and DRG filopodia is the higher presence of microtubules inside hippocampal filopodia. Our immunostaining experiments indicates that in hippocampal GCs a higher number of MTs extends into the P domain of GCs and enters the proximal part of a filopodia (Fig. 1).

Microtubules are not just passive players, but they are one of the important cytoskeletal components during neuronal development and play an active role in neurite growth and axon specification (31, 32, 33). Individual MTs penetrating the filopodia are highly dynamic and they play an important role in guidance decisions (31). MTs inside filopodia undergo cycles of growth and catastrophe, dynamic instability, and they can also have direct effect on membrane protrusion (34, 35) Therefore, actin filaments and microtubules can move and undergo dramatic changes in their organization and location within the P domain of the growth cone due to "dynamic instability" of MTs. It is believed that dynamic instability enables MTs to quickly remodel their organization and selectively grow in response to extracellular signals (34). It has been shown that maximum polymerization and depolymerisation forces for MTs is much larger than actin filament polymerization force (11). This can be understood by assuming that a filament behaves as a homogeneous elastic rod and that the magnitude of buckling forces is proportional to the flexural rigidity of the filament (36). The mean flexural rigidity of microtubules is $2.2 \times 10^{-23}$ $Nm^2$ which is almost 1000 times larger than that of actin filaments equal to $7.3\ 10^{-26}$ $Nm^2$ (37). Taken all these considerations together, we conclude that the existence of microtubules inside filopodia of hippocampal GC is the main reason why hippocampal filopodia exert a larger force than DRG filopodia.

The number of neurites in hippocampal neurons is significantly higher than DRG neurons and it increases in more mature rats (P10-P12). After one day of culture, 63% of DRG neurons have only one neurite and the number of neurites remains constant in both preparations of P1-P2 and P10-P12 DRG. After the same hours of culture, DRG neurites grow longer than those from hippocampal neurons.

**Hippocampal and DRG lamellipodia**

DRG lamellipodia can displace beads from the trap even when the maximum trapping force is more than 20 pN (Fig. 5 *i* and *j*). Our experimental data indicate that the maximal measured force depends on the contact area between the bead and the lamellipodium leading edge (16, 17). In these experiments, the bead diameter was 1 µm and the area in contact with the silica bead, $A_c$, obtained from videomicrographs, varied from less than 0.1 up to 1.5 $\mu m^2$. Therefore, we expected that the contact area between a bead and a larger lamellipodium would be on average higher than with a smaller lamellipodium. This could be one of the

reasons why lamellipodia from DRG neurons exert a larger force than from hippocampal neurons. Another possibility is that larger lamellipodia are more rigid than smaller lamellipodia, as a consequence of a more global structural stability caused by an extensive crosslinking of connecting proteins (38), such as myosins and other regulatory proteins. Our results show that the mean size of DRG GCs (P10-P12) is almost 10 times larger than hippocampal GCs (Table 1) and the lamellipodia area of DRG neurons are much larger than the hippocampal ones. Interestingly, the mean size of a hippocampal GC obtained from P1-P2 and P10-P12 rats remains constant, which suggests that the maximal exerted force by lamellipodia in hippocampal neurons must not change and this hypothesis is confirmed by our experimental data.

Video tracking observations from very early stages show that in DRG cultures, vigorous lamellipodia emerge directly from the soma protrude and collapse continuously and undergo three dimensional motions. Using algorithms used in computer vision processing (39) we were able to obtain a 3D reconstruction of the lamellipodia. Our results indicate that DRG lamellipodia leading edges are able to lift up by 3-5 µm and exert a larger vertical force than hippocampal lamellipodia (Table 2). On the other hand, in most of the force measurement experiments very thin hippocampal lamellipodia grow below the bead without pushing it. In these kinds of experiments, no significant bead displacement was observed. Therefore, lamellipodia from DRG neurons are expected to exert larger vertical forces.

The outcome of the present manuscript is in agreement with recent studies (40) that showed that the DRG GCs exert a larger traction force in comparison to hippocampal GCs. Moreover it has been shown that density of paxillin is significantly higher in DRG than in hippocampal GCs (40), suggesting that the difference in force generation by lamellipodia could also be due to stronger adhesions in DRG GCs.

Our results indicate that the different morphology of GCs, which could vary widely among neuronal cell types and species, can affect their motility and force generation. These morphological differences in CNS and PNS neurons are probably due to their functionality. Moreover, different substrate stiffness can have an effect on outgrowth and traction forces of DRG GCs but hippocampal GCs are independent of substrate stiffness (40). CNS neurons grow on the softest tissues in the body (glial cells), a different environment from where PNS neurons grow (40, 20). This suggests that also the location has an important role in the mechanisms underlying force generation in neurons.

## Supplementary Information

*Comparison of axonic and dendritic growth cones*

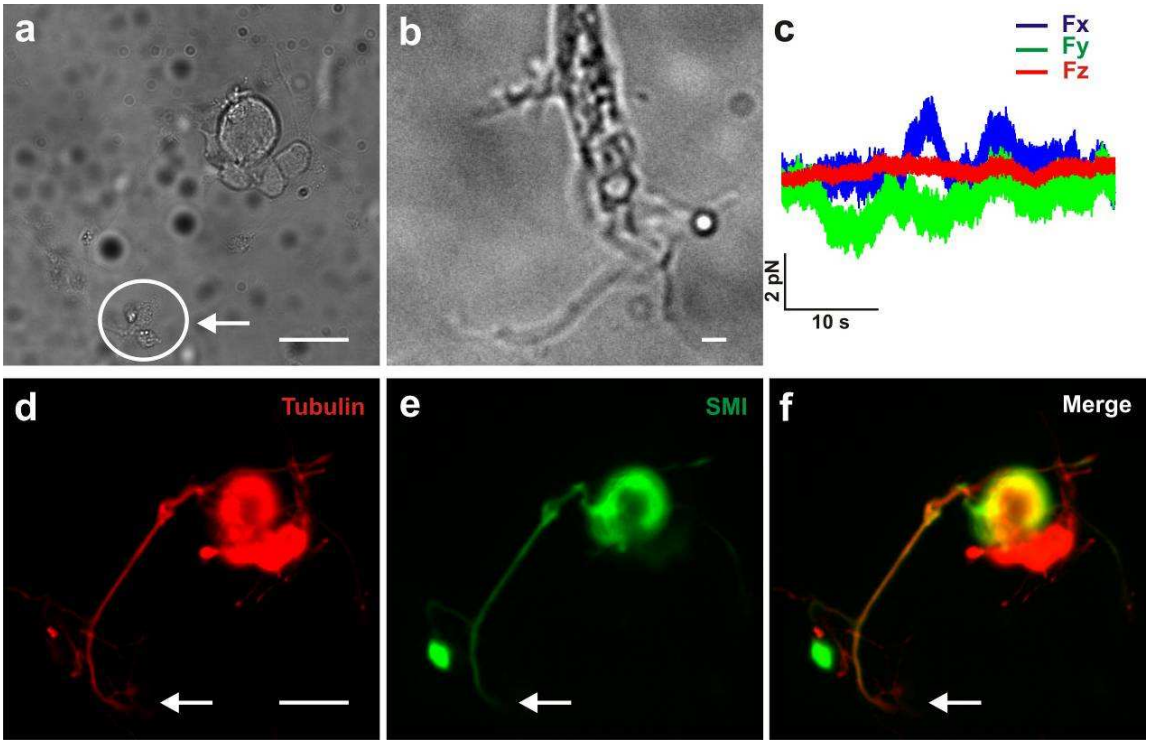


**Figure S1. Axonic growth cone.** (*a*) Low resolution image of DRG neurons and GC indicated by an arrow. Scale bar, 5 µm. (*b*) High resolution image of the GC shown in panel (*a*). Scale bar, 2 µm. (*c*) The three components $F_x$, $F_y$, and $F_z$ of the force exerted by filopodia emerging from the GC shown in (*b*). (*d-f*) Fluorescence images of the same neuron and GC indicated in (*a*) stained for tubulin (*red*), (*d*), and SMI (*green*), (*e*). The green staining indicates that the neurite is an axon. Merge of the two staining is shown in (*f*). Scale bar, 5 µm.

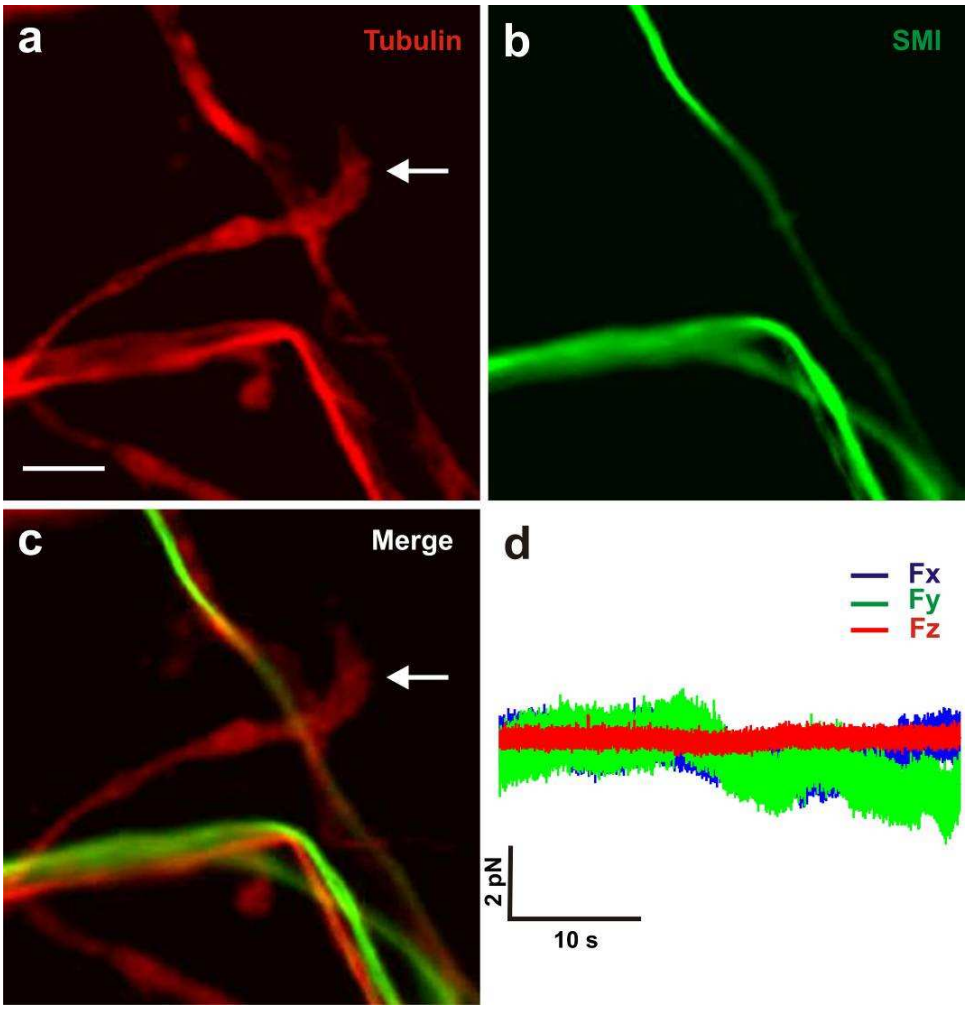


**Figure S1. Dendritic growth cone.** (*a*-*c*) Fluorescence image of GC indicated by an arrow. Tubulin is marked in *red* (*a*) and SMI in *green* (*b*). In (*c*) the merge of the two staining. The absence of green staining indicates that the GC is a dendritic GC. Scale bar, 3 µm. (*d*) The three components $F_x$, $F_y$, and $F_z$ of the force exerted by filopodia emerging from GC shown in (*a*-*c*).

## REFERENCES


1. Ghashghaei, H. T., C. Lai, and E. S. Anton. 2007. Neuronal migration in the adult brain: are we there yet? Nat Rev Neurosci 8: 141-151 PM:17237805.

2. Solecki, D. J., E. E. Govek, and M. E. Hatten. 2006. mPar6 alpha controls neuronal migration. J Neurosci 26: 10624-10625 ISI:000241727300003.

3. Bray, D., C. Thomas, and G. Shaw. 1978. Growth cone formation in cultures of sensory neurons. Proc. Natl. Acad. Sci. U. S. A 75: 5226-5229 PM:283427.

4. Goodman, C. S. 1996. Mechanisms and molecules that control growth cone guidance. Annu Rev Neurosci 19: 341-377 PM:8833447.

5. Song, H. J., and M. M. Poo. 2001. The cell biology of neuronal navigation. Nat. Cell Biol. 3: E81-E88 ISI:000167365800006.

6. Mongiu, A. K., E. L. Weitzke, O. Y. Chaga, and G. G. Borisy. 2007. Kinetic-structural analysis of neuronal growth cone veil motility. J Cell Sci 120: 1113-1125 ISI:000244759500020.

7. Mogilner, A., and G. Oster. 1996. Cell motility driven by actin polymerization 25. Biophys. J. 71: 3030-3045 PM:8968574.

8. Suter, D. M., and P. Forscher. 2000. Substrate-cytoskeletal coupling as a mechanism for the regulation of growth cone motility and guidance. J Neurobiol 44: 97-113 ISI:000088622800002.

9. Pollard, T. D., and G. G. Borisy. 2003. Cellular motility driven by assembly and disassembly of actin filaments. Cell 112: 453-465 ISI:000181252600005.

10. Pak, C. W., K. C. Flynn, and J. R. Bamburg. 2008. Actin-binding proteins take the reins in growth cones. Nat Rev Neurosci 9: 136-147 ISI:000252503300015.

11. Howard, J. 2001. *Mechanics of Motor Proteins and the Cytoskeleton*. Sinauer Associates, Inc, Sunderland, MA.

12. Raucher, D., and M. P. Sheetz. 2000. Cell spreading and lamellipodial extension rate is regulated by membrane tension. J Cell Biol 148: 127-136 ISI:000084795300017.

13. Neuman, K. C., and S. M. Block. 2004. Optical trapping. Rev. Sci. Instrum. 75: 2787-2809 ISI:000224754800001.

14. Bustamante, C., J. C. Macosko, and G. J. L. Wuite. 2000. Grabbing the cat by the tail: Manipulating molecules one by one. Nat Rev Mol Cell Biol 1: 130-136 ISI:000165765300017.

15. Cojoc, D., F. Difato, E. Ferrari, R. B. Shahapure, J. Laishram, M. Righi, E. M. Di Fabrizio, and V. Torre. 2007. Properties of the force exerted by filopodia and lamellipodia and the involvement of cytoskeletal components. PLoS ONE 2: e1072 PM:17957254.

16. Shahapure, R., F. Difato, A. Laio, G. Bisson, E. Ercolini, L. Amin, E. Ferrari, and V. Torre. 2010. Force generation in lamellipodia is a probabilistic process with fast growth and retraction events. Biophys. J. 98: 979-988 PM:20303855.

17. Amin, L., E. Ercolini, R. Shahapure, G. Bisson, and V. Torre. 2011. The elementary events underlying force generation in neuronal lamellipodia. Scientific Reports 1 ISI:000300556400001.

18. Amin, L., E. Ercolini, R. Shahapure, E. Migliorini, and V. Torre. 2012. The Role of Membrane Stiffness and Actin Turnover on the Force Exerted by DRG Lamellipodia. Biophysical Journal 102: 2451-2460 ISI:000305003100007.

19. Discher, D. E., P. Janmey, and Y. L. Wang. 2005. Tissue cells feel and respond to the stiffness of their substrate. Science 310: 1139-1143 ISI:000233437300033.

20. Moore, S. W., P. Roca-Cusachs, and M. P. Sheetz. 2010. Stretchy Proteins on Stretchy Substrates: The Important Elements of Integrin-Mediated Rigidity Sensing. Developmental Cell 19: 194-206 ISI:000281090000006.

21. Engler, A. J., S. Sen, H. L. Sweeney, and D. E. Discher. 2006. Matrix elasticity directs stem cell lineage specification. Cell 126: 677-689 ISI:000240276700017.

22. Lu, Y. B., K. Franze, G. Seifert, C. Steinhauser, F. Kirchhoff, H. Wolburg, J. Guck, P. Janmey, E. Q. Wei, J. Kas, and A. Reichenbach. 2006. Viscoelastic properties of individual glial cells and neurons in the CNS. Proceedings of the National Academy of Sciences of the United States of America 103: 17759-17764 ISI:000242464900034.

23. Christ, A. F., K. Franze, H. Gautier, P. Moshayedi, J. Fawcett, R. J. M. Franklin, R. T. Karadottir, and J. Guck. 2010. Mechanical difference between white and gray matter in the rat cerebellum measured by scanning force microscopy. Journal of Biomechanics 43: 2986-2992 ISI:000285122900018.

24. Franze, K., and J. Guck. 2010. The biophysics of neuronal growth. Reports on Progress in Physics 73 ISI:000282092500001.

25. Ruaro, M. E., P. Bonifazi, and V. Torre. 2005. Toward the neurocomputer: Image processing and pattern recognition with neuronal cultures. Ieee Transactions on Biomedical Engineering 52: 371-383 ISI:000227139500004.

26. Gittes, F., and C. F. Schmidt. 1998. Interference model for back-focal-plane displacement detection in optical tweezers. Opt. Lett. 23: 7-9 ISI:000071271100003.

27. Kress, H., E. H. K. Stelzer, G. Griffiths, and A. Rohrbach. 2005. Control of relative radiation pressure in optical traps: Application to phagocytic membrane binding studies. Phys. Rev. E 71: 061927-1-061927-10 ISI:000230274500077.

28. Pool, M., J. Thiemann, A. Bar-Or, and A. E. Fournier. 2008. NeuriteTracer: A novel ImageJ plugin for automated quantification of neurite outgrowth. Journal of Neuroscience Methods 168: 134-139 ISI:000253062300018.

29. Dotti, C. G., C. A. Sullivan, and G. A. Banker. 1988. The Establishment of Polarity by Hippocampal-Neurons in Culture. Journal of Neuroscience 8: 1454-1468 ISI:A1988M969400033.

30. Choi, Y. J., A. Di Nardo, I. Kramvis, L. Meikle, D. J. Kwiatkowski, M. Sahin, and X. He. 2008. Tuberous sclerosis complex proteins control axon formation. Genes & Development 22: 2485-2495 ISI:000259221000005.

31. Schaefer, A. W., N. Kabir, and P. Forscher. 2002. Filopodia and actin arcs guide the assembly and transport of two populations of microtubules with unique dynamic parameters in neuronal growth cones. J. Cell Biol. 158: 139-152 ISI:000176876700013.

32. Dent, E. W., S. L. Gupton, and F. B. Gertler. 2011. The Growth Cone Cytoskeleton in Axon Outgrowth and Guidance. Cold Spring Harbor Perspectives in Biology 3 ISI:000287846200009.

33. Vitriol, E. A., and J. Q. Zheng. 2012. Growth Cone Travel in Space and Time: the Cellular Ensemble of Cytoskeleton, Adhesion, and Membrane. Neuron 73: 1068-1081 ISI:000301998700006.

34. Buck, K. B., and J. Q. Zheng. 2002. Growth cone turning induced by direct local modification of microtubule dynamics. Journal of Neuroscience 22: 9358-9367 ISI:000179031600026.

35. Mack, T. G. A., M. P. Koester, and G. E. Pollerberg. 2000. The microtubule-associated protein MAP1B is involved in local stabilization of turning growth cones. Molecular and Cellular Neuroscience 15: 51-65 ISI:000085030600005.

36. Dogterom, M., and B. Yurke. 1997. Measurement of the force-velocity relation for growing microtubules. Science 278: 856-860 ISI:A1997YD47900045.

37. Gittes, F., B. Mickey, J. Nettleton, and J. Howard. 1993. Flexural Rigidity of Microtubules and Actin-Filaments Measured from Thermal Fluctuations in Shape. J. Cell Biol. 120: 923-934 ISI:A1993KL80200008.

38. Laurent, V. M., S. Kasas, A. Yersin, T. E. Schaffer, S. Catsicas, G. Dietler, A. B. Verkhovsky, and J. J. Meister. 2005. Gradient of rigidity in the lamellipodia of migrating cells revealed by atomic force microscopy. Biophysical Journal 89: 667-675 ISI:000230114500065.

39. Bertero, M., T. A. Poggio, and V. Torre. 1988. Ill-Posed Problems in Early Vision. Proc IEEE 76: 869-889 ISI:A1988Q311100002.

40. Koch, D., W. J. Rosoff, J. J. Jiang, H. M. Geller, and J. S. Urbach. 2012. Strength in the Periphery: Growth Cone Biomechanics and Substrate Rigidity Response in Peripheral and Central Nervous System Neurons. Biophysical Journal 102: 452-460 ISI:000300122500010.

41. Carlsson,A.E. (2003). Growth velocities of branched actin networks. Biophys J *84*, 2907-2918.

# 3

# DISCUSSION

Experimental tools such as optical tweezers, video imaging, immunocytochemistry and AFM enable us to provide a precise characterization of the molecular mechanism underlying force generation in DRG growth cones. My PhD thesis aimed at describing in detail the role of actin turnover, membrane stiffness and myosin II in force generation by DRG growth cones. Using optical tweezers, I measured force generated by DRG and hippocampal lamellipodia and filopodia during neuronal differentiation with high temporal resolution and force sensitivity (picoNewton) without causing any photodamage. These are the main conclusions of my PhD work:

*1 – Dynamical properties of force Generation.*

I found that force generation in lamellipodia is a probabilistic process in which fast growths alternate with local transient retractions of the lamellipodium leading edge. Experimental characterization of Fv relationships in neuronal growth cones shows that <Fv> relationships exhibited a flat shape, during which the mean velocity remained constant while the force increased (Shahapure et al., 2010). Therefore, autocatalytic model (Carlsson, 2001; Carlsson, 2003) correctly describe force generation in a mean approximation. In individual

experiments, the velocity does not remain constant but oscillates and can change its direction. During these events, occurrence of local catastrophes seems the most likely biological mechanisms underlying local transient retractions controlled by cofilin and other severing proteins. Transient increase in rate of retrograde actin flow over protrusion rate at leading edge (Lin and Forscher, 1995) can effect a transient retraction of lamellipodium leading edge. These results give new insight on dynamical properties of force generation in neuronal growth cone lamellipodia (Lacayo et al., 2007; Pak et al., 2008; Weiner et al., 2007).

*2 – Detection of elementary events during force Generation.*

A detailed analysis of Brownian fluctuations of an optically trapped bead when it seals on the lamellipodia leading edge can provide insights into the underlying kinetics of the force generation process. My results indicate that force generation in neuronal lamellipodia is composed by elementary events corresponding to forward and backward jumps ranging from 2 to 20 nm (Amin et al., 2011). This suggests that force generation occurs at different rates. At the slowest rate the lamellipodium leading edge advances smoothly with small jumps and the amplitude of these jumps correspond to size of actin monomer (2.7 nm) which can be explained by the addition of the actin monomers to the existing actin filaments. At the fastest rate, larger jumps are observed and they are likely to be caused by the insertion of small actin oligomers (Okreglak and Drubin, 2010) and by the occurrence of a burst of actin polymerization in single or neighboring actin filaments. These jumps are not observed when GCs were fixed with paraformaldehyde, suppressing all cellular motility, but when actin turnover is reduced by treating the neurons with Jasplakinolide (Bubb et al., 2000) or Cytochakasin D (Cooper, 1987), force generation still occurs but at a slower rate (Amin et al., 2012).

3 – *Role of actin turnover and membrane stiffness during force generation*

In the presence of jasplakinolide, the amplitude and frequency of elementary jumps underlying force generation is reduced (Amin et al., 2012) with the mean amplitude of 2.4 nm similar to the mean polymerization step size (2.7 nm) of actin filament, suggesting that when actin turnover is reduced and force generation occurs at the slowest rate and jasplakinolide prevents the addition of small actin oligomers to protruding actin filaments therefore larger jumps were not observed. Higher concentrations of jasplakinolide completely

block the force generation. On the contrary, Cyclodextrin had the opposite effect and increased the frequency of elementary events. DRG lamellipodia treated with 2.5 mM cylodextrin moved more vigorously by showing cycles of protrusions and retractions similar to those observed in control conditions with slightly higher frequencies, suggesting that the normal actin treadmilling underlying these cycles was only marginally affected. By using AFM, I determined that cyclodextrin reduced the membrane stiffness of DRG neurons both in the soma and in GCs. Taken together; my results indicate that actin turnover is a fundamental factor of force generation and the membrane stiffness provides a selective pressure which shape force generation.

*4 – Role of Myosin II during force Generation.*

Another part of my Thesis addressed the role of myosin II, as an important factor in the force generation by growth cones. I observed that inhibition of myosin II has an opposite effect on the force generation by lamellipodia and filopodia. In the presence of Blebbistatin force exerted by lamellipodia drastically reduced, but surprisingly force exerted by filopodia increased by 30-50 %. My experimental data indicates that in DRG GCs, NMIIB is primarily localized in the central domain of GC and rarely extended to the periphery of GCs. In contrast, NMIIA was clearly present at GCs leading edge. Actin and NMIIA colocalized rather well, suggesting the presence of an actomyosin complex formed by Actin and NMIIA which may have an active role during 3D buckling of lamellipodia. When NMII is inhibited, by application of Blebbistatin, two significant morphological changes were observed. Firstly, lamellipodia lose their sheet-like appearance and become “filopodish” and they are not able to lift up during retraction which is likely to be caused by removal of the crosslinkage of actin filaments caused by NMII filaments and secondly, filopodia emerging from GCs have a higher proportion of microtubules inside. These morphological changes could explain my unexpected observation that filopodia treated with Blebbistatin exert a larger force than in untreated filopodia. My results suggest a possible role of myosin II in force generation and in particular during lamellipodia retractions and confirm a coupling between actin and MT dynamics.

*5 –Comparison of force generation in GCs form the CNS and PNS.*

I also provided an experimental comparison of force exerted by growth cones emerging from DRG and hippocampal neurons. I found that filopodia and lamellipodia of both types of neurons can exert force with an amplitudes varying between 1-20 pN developing with a similar time course. At a more quantitative level two main differences was observed: firstly, filopodia from hippocampal growth cones exert a force larger than from DRG growth cones; secondly, lamellipodia from DRG growth cones exert larger force and can move up at a higher speed in axial direction. By using immunocytochemical analysis I summarized the morphological differences of these neurons. My results show that the morphological properties of GC vary widely between neuronal cell types and these differences can affect their motility and force generation properties. These morphological differences in CNS (hippocampal) and PNS (DRG) neurons could be related to their differences in functionality. Moreover, different substrate stiffness can effect on outgrowth and traction force (Koch et al., 2012) suggesting that the environment of neurons has an important role in mechanism underlying force generation.

This study shows that a rather complex biochemical machinery underlie the observed protrusion/retraction cycles of neuronal lamellipodia and This dynamics changes during differentiation and could be cell specific. The identification and characterization of the positive feedback (Calsson, 2010b) underlying these cycles will be a major issue for future investigations. There are several theoretical predictions about positive and negative feedback as the main mechanisms of actin waves and patches (Calsson, 2012). These include the role of the myosin II in the actin wave motion, the distribution of the Arp2/3 complex throughout the wave and the acting filament orientations along the motion direction. Each of these can be tested experimentally using proper devices and techniques including optical tweezers, fluorescence imaging techniques. Moreover GC is the source of plenty of molecules, regulators and inhibitors including those that target the microtubule and actin dynamics, such as WASP which is responsible for activating Arp2/3 complex. These proteins regulate many other fundamental cellular processes and have the potential to affect axon regeneration and neurites outgrowth (Dent et al., 2011). In future it will be interesting and fundamental to investigate the role of them in force generation and axon regeneration.

The study of developmental axon growth and guidance will continue to reveal fundamental mechanisms that may further our understanding of axon regeneration in the adult nervous system.

# REFERENCES


1. Allard, J., and Mogilner, A. (2012). Traveling waves in actin dynamics and cell motility. Current Opinion in Cell Biology *25*, *1-9*

2. Amin,L., Ercolini,E., Shahapure,R., Bisson,G., and Torre,V. (2011). The elementary events underlying force generation in neuronal lamellipodia. Scientific Reports *1*.

3. Amin,L., Ercolini,E., Shahapure,R., Migliorini,E., and Torre,V. (2012). The Role of Membrane Stiffness and Actin Turnover on the Force Exerted by DRG Lamellipodia. Biophysical Journal *102*, 2451-2460.

4. Betapudi,V. (2010). Myosin II Motor Proteins with Different Functions Determine the Fate of Lamellipodia Extension during Cell Spreading. PLoS ONE *5*.

5. Bonanomi,D., Fornasiero,E.F., Valdez,G., Halegoua,S., Benfenati,F., Menegon,A., and Valtorta,F. (2008). Identification of a developmentally regulated pathway of membrane retrieval in neuronal growth cones. Journal of Cell Science *121*, 3757-3769.

6. Bridgman,P.C., Dave,S., Asnes,C.F., Tullio,A.N., and Adelstein,R.S. (2001). Myosin IIB is required for growth cone motility. Journal of Neuroscience *21*, 6159-6169.

7. Bubb,M.R., Spector,I., Beyer,B.B., and Fosen,K.M. (2000). Effects of jasplakinolide on the kinetics of actin polymerization. An explanation for certain in vivo observations. J.Biol.Chem. *275*, 5163-5170.

8. Buck,K.B. and Zheng,J.Q. (2002). Growth cone turning induced by direct local modification of microtubule dynamics. Journal of Neuroscience *22*, 9358-9367.

9. Burnette,D.T., Ji,L., Schaefer,A.W., Medeiros,N.A., Danuser,G., and Forscher,P. (2008). Myosin II activity facilitates microtubule bundling in the neuronal growth cone neck. Developmental Cell *15*, 163-169.

10. Carlsson,A.E. (2001). Growth of branched actin networks against obstacles. Biophys J *81*, 1907-1923.

11. Carlsson,A.E. (2003). Growth velocities of branched actin networks. Biophys J *84*, 2907-2918.

12. Carlsson,A.E. (2010a). Actin Dynamics: From Nanoscale to Microscale. Annual Review of Biophysics, Vol 39 *39*, 91-110.

13. Carlsson,A.E. (2010b). Dendritic Actin Filament Nucleation Causes Traveling Waves and Patches. Physical Review Letters *104*.

14. Carlsson,A.E. (2012). Self-Feedback in Actin Polymerization. Advances in Systems Biology *736*, 397-406.

15. Charras, G.T., Yarrow, J.C., Horton, M.A., Mahadevan, L., and Mitchison, T.J. (2005). Non-equilibration of hydrostatic pressure in blebbing cells. Nature 435, 365–369.

16. Conti,M.A. and Adelstein,R.S. (2008). Nonmuscle myosin II moves in new directions. Journal of Cell Science *121*, 11-18.

17. Conti,M.A., Even-Ram,S., Liu,C.Y., Yamada,K.M., and Adelstein,R.S. (2004). Defects in cell adhesion and the visceral endoderm following ablation of nonmuscle myosin heavy chain II-A in mice. Journal of Biological Chemistry *279*, 41263-41266.

18. Cooper,J.A. (1987). Effects of Cytochalasin and Phalloidin on Actin. Journal of Cell Biology *105*, 1473-1478.

19. Dasanayake,N.L., Michalski,P.J., and Carlsson,A.E. (2011). General Mechanism of Actomyosin Contractility. Physical Review Letters *107*.

20. Dent,E.W. and Gertler,F.B. (2003). Cytoskeletal dynamics and transport in growth cone motility and axon guidance. Neuron *40*, 209-227.

21. Dent,E.W., Gupton,S.L., and Gertler,F.B. (2011). The Growth Cone Cytoskeleton in Axon Outgrowth and Guidance. Cold Spring Harbor Perspectives in Biology *3*.

22. Dent,E.W. and Kalil,K. (2001). Axon branching requires interactions between dynamic microtubules and actin filaments. J Neurosci *21*, 9757-9769.

23. Fackler, O.T., and Grosse, R. (2008). Cell motility through plasma membrane blebbing. The Journal of Cell Biology 181, 879–884.

24. Forscher,P., Buchanan,J., and Smith,S. (1987). Modulation of Organelle Transport in Neuronal Growth Cones. Journal of Cellular Biochemistry 164.

25. Forscher,P. and Smith,S.J. (1988). Actions of Cytochalasins on the Organization of Actin-Filaments and Microtubules in A Neuronal Growth Cone. Journal of Cell Biology *107*, 1505-1516.

26. Gallo,G. and Letourneau,P.C. (2000). Neurotrophins and the dynamic regulation of the neuronal cytoskeleton. J.Neurobiol. *44*, 159-173.

27. Ghashghaei,H.T., Lai,C., and Anton,E.S. (2007). Neuronal migration in the adult brain: are we there yet? Nat Rev Neurosci *8*, 141-151.

28. Gittes,F., Mickey,B., Nettleton,J., and Howard,J. (1993). Flexural Rigidity of Microtubules and Actin-Filaments Measured from Thermal Fluctuations in Shape. J.Cell Biol. *120*, 923-934.

29. Goodman,C.S. (1996). Mechanisms and molecules that control growth cone guidance. Annu Rev Neurosci *19*, 341-377.

30. Hines,J.H., Abu-Rub,M., and Henley,J.R. (2010). Asymmetric endocytosis and remodeling of beta(1)-integrin adhesions during growth cone chemorepulsion by MAG. Nature Neuroscience *13*, 829-U68.

31. Hirokawa,N., Niwa,S., and Tanaka,Y. (2010). Molecular Motors in Neurons: Transport Mechanisms and Roles in Brain Function, Development, and Disease. Neuron *68*, 610-638.

32. Howard,J. (2001). *Mechanics of Motor Proteins and the Cytoskeleton*. (Sunderland, MA: Sinauer Associates, Inc).

33. Hur,E.M., Saijilafu, and Zhou,F.Q. (2012). Growing the growth cone: remodeling the cytoskeleton to promote axon regeneration. Trends in Neurosciences *35*, 164-174.

34. Hur,E.M., Yang,I.H., Kim,D.H., Byun,J., Saijilafu, Xu,W.L., Nicovich,P.R., Cheong,R., Levchenko,A., Thakor,N., and Zhou,F.Q. (2011). Engineering neuronal growth cones to promote axon regeneration over inhibitory molecules. Proceedings of the National Academy of Sciences of the United States of America *108*, 5057-5062.

35. Koch,D., Rosoff,W.J., Jiang,J.J., Geller,H.M., and Urbach,J.S. (2012). Strength in the Periphery: Growth Cone Biomechanics and Substrate Rigidity Response in Peripheral and Central Nervous System Neurons. Biophysical Journal *102*, 452-460.

36. Kolpak,A.L., Jiang,J., Guo,D.R., Standley,C., Bellve,K., Fogarty,K., and Bao,Z.Z. (2009). Negative Guidance Factor-Induced Macropinocytosis in the Growth Cone Plays a Critical Role in Repulsive Axon Turning. Journal of Neuroscience *29*, 10488-10498.

37. Lacayo,C.I., Pincus,Z., VanDuijn,M.M., Wilson,C.A., Fletcher,D.A., Gertler,F.B., Mogilner,A., and Theriot,J.A. (2007). Emergence of large-scale cell morphology and movement from local actin filament growth dynamics. PLoS Biol *5*, 2035-2052.

38. Lin,C.H., Thompson,C.A., and Forscher,P. (1994). Cytoskeletal reorganization underlying growth cone motility. Curr.Opin.Neurobiol. *4*, 640-647.

39. Lowery,L.A. and Van Vactor,D. (2009). The trip of the tip: understanding the growth cone machinery. Nature Reviews Molecular Cell Biology *10*, 332-343.

40. Maccioni,R.B. and Cambiazo,V. (1995). Role of Microtubule-Associated Proteins in the Control of Microtubule Assembly. Physiological Reviews *75*, 835-864.

41. Mack,T.G.A., Koester,M.P., and Pollerberg,G.E. (2000). The microtubule-associated protein MAP1B is involved in local stabilization of turning growth cones. Molecular and Cellular Neuroscience *15*, 51-65.

42. Medeiros,N.A., Burnette,D.T., and Forscher,P. (2006). Myosin II functions in actin-bundle turnover in neuronal growth cones. Nat Cell Biol *8*, 215-226.

43. Meldolesi,J. (2011). Neurite outgrowth: This process, first discovered by Santiago Ramon y Cajal, is sustained by the exocytosis of two distinct types of vesicles. Brain Research Reviews *66*, 246-255.

44. Mitchison,T. and Kirschner,M. (1988). Cytoskeletal dynamics and nerve growth 9. Neuron *1*, 761-772.

45. Mogilner,A. (2009). Mathematics of cell motility: have we got its number? Journal of Mathematical Biology *58*, 105-134.

46. Mogilner,A. and Oster,G. (1996). Cell motility driven by actin polymerization 25. Biophys.J. *71*, 3030-3045.

47. Mogilner,A. and Oster,G. (2003). Force generation by actin polymerization II: the elastic ratchet and tethered filaments 26. Biophys.J. *84*, 1591-1605.

48. Okreglak,V. and Drubin,D.G. (2010). Loss of Aip1 reveals a role in maintaining the actin monomer pool and an in vivo oligomer assembly pathway. J.Cell Biol. *188*, 769-777.

49. Paluch, E., Sykes, C., Prost, J., and Bornens, M. (2006). Dynamic modes of the cortical actomyosin gel during cell locomotion and division. Trends in Cell Biology 16, 5–10.

50. Pak,C.W., Flynn,K.C., and Bamburg,J.R. (2008). Actin-binding proteins take the reins in growth cones. Nat Rev Neurosci *9*, 136-147.

51. Pantaloni,D., Le Clainche,C., and Carlier,M.F. (2001). Mechanism of actin-based motility. Science *292*, 1502-1506.

52. Peskin,C.S., Odell,G.M., and Oster,G.F. (1993). Cellular Motions and Thermal Fluctuations - the Brownian Ratchet. Biophys J *65*, 316-324.

53. Pollard,T.D. and Borisy,G.G. (2003). Cellular motility driven by assembly and disassembly of actin filaments. Cell *112*, 453-465.

54. Rochlin,M.W., Dailey,M.E., and Bridgman,P.C. (1999). Polymerizing microtubules activate site-directed F-actin assembly in nerve growth cones. Mol.Biol.Cell *10*, 2309-2327.

55. Schaefer,A.W., Kabir,N., and Forscher,P. (2002). Filopodia and actin arcs guide the assembly and transport of two populations of microtubules with unique dynamic parameters in neuronal growth cones. J.Cell Biol. *158*, 139-152.

56. Shahapure,R., Difato,F., Laio,A., Bisson,G., Ercolini,E., Amin,L., Ferrari,E., and Torre,V. (2010). Force generation in lamellipodia is a probabilistic process with fast growth and retraction events. Biophys.J. *98*, 979-988.

57. Smith,S.J. (1988). Neuronal Cytomechanics - the Actin-Based Motility of Growth Cones. Science *242*, 708-715.

58. Solecki,D.J., Govek,E.E., and Hatten,M.E. (2006). mPar6 alpha controls neuronal migration. J Neurosci *26*, 10624-10625.

59. Song,H.J. and Poo,M.M. (2001). The cell biology of neuronal navigation. Nat.Cell Biol. *3*, E81-E88.

60. Suter,D.M. and Forscher,P. (1998). An emerging link between cytoskeletal dynamics and cell adhesion molecules in growth cone guidance. Current Opinion in Neurobiology *8*, 106-116.

61. Tojima,T., Akiyama,H., Itofusa,R., Li,Y., Katayama,H., Miyawaki,A., and Kamiguchi,H. (2007). Attractive axon guidance involves asymmetric membrane transport and exocytosis in the growth cone. Nature Neuroscience *10*, 58-66.

62. Tojima,T., Itofusa,R., and Kamiguchi,H. (2010). Asymmetric Clathrin-Mediated Endocytosis Drives Repulsive Growth Cone Guidance. Neuron *66*, 370-377.

63. Vicente-Manzanares,M., Ma,X.F., Adelstein,R.S., and Horwitz,A.R. (2009). Non-muscle myosin II takes centre stage in cell adhesion and migration. Nature Reviews Molecular Cell Biology *10*, 778-790.

64. Vitriol,E.A. and Zheng,J.Q. (2012). Growth Cone Travel in Space and Time: the Cellular Ensemble of Cytoskeleton, Adhesion, and Membrane. Neuron *73*, 1068-1081.

65. Weiner,O.D., Marganski,W.A., Wu,L.F., Altschuler,S.J., and Kirschner,M.W. (2007). An actin-based wave generator organizes cell motility. PLoS Biol *5*, 2053-2063.

66. Wylie,S.R. and Chantler,P.D. (2001). Separate but linked functions of conventional myosins modulate adhesion and neurite outgrowth. Nature Cell Biology *3*, 88-92.

67. Wylie,S.R. and Chantler,P.D. (2008). Myosin IIC: A third molecular motor driving neuronal dynamics. Molecular Biology of the Cell *19*, 3956-3968.

68. Yu,P.P., Santiago,L.Y., Katagiri,Y., and Geller,H.M. (2012). Myosin II activity regulates neurite outgrowth and guidance in response to chondroitin sulfate proteoglycans. Journal of Neurochemistry *120*, 1117-1128.

69. Zhou,F.Q. and Cohan,C.S. (2004). How actin filaments and microtubules steer growth cones to their targets. Journal of Neurobiology *58*, 84-91.

# ACKNOWLEDGMENTS

I would like to express my deep and sincere gratitude to my supervisor, Prof. Vincent Torre, who greatly supported me during this entire period of my PhD. I would like to thank him for all the guidance and support, academically and otherwise. He has taught me the right attitude towards science.

I am deeply grateful to Dr. Erika Ercolini without her support it was impossible to accomplish this work and I would like to thank her for her friendship.

I wish to express my sincere thanks to Dr. Rajesh Shahapure for introducing me to this new technique of optical tweezers and teaching me to prepare DRG neurons.

I would like to thank Dr. Jelena Ban for answering my queries related to biological part of this project and teaching me immunocytochemistry.

I would like to give special thanks to Giacomo and Walter and Hiba for their computational support, Alejandro and Elisa for their AFM experiments and Wasim for video imaging.

I would like to specially acknowledge Prof. Anders Carlsson for critical reading of my thesis and for his valuable comments and suggestions.

I would like to thank all my lab mates Giulietta, Elisabetta, Monica and Alessio, who were directly or indirectly helped me during four years of my stay in the lab and I would like to remember Diana, Jummy, Jacobo, Arin, Lin, Majid, Paolo, and the new arrivals- Akbar, Sourav and Manuel – and of course Manuela, who all made the Torre Lab a big happy family.

The early days of my Ph.D. would have been a nightmare if Sara had not been there to listen to my frustrated complaints.

I owe my loving thanks to my family whose patience and love enabled me to complete this work. Without their support, encouragement and understanding, I would have been a very different person.

At the end I would like to thank the most important person in my life, Houman, for his infinite kindness, support and love.